



**Michigan
Technological
University**

**Michigan Technological University
Digital Commons @ Michigan Tech**

Dissertations, Master's Theses and Master's Reports

2019

IMPROVED LOW-FREQUENCY IMPACT INSULATION CLASS MEASUREMENTS BASED ON COMPARISON TECHNIQUES

Sunit Girdhar

Michigan Technological University, sgirdhar@mtu.edu

Copyright 2019 Sunit Girdhar

Recommended Citation

Girdhar, Sunit, "IMPROVED LOW-FREQUENCY IMPACT INSULATION CLASS MEASUREMENTS BASED ON COMPARISON TECHNIQUES", Open Access Master's Report, Michigan Technological University, 2019.
<https://digitalcommons.mtu.edu/etdr/796>

Follow this and additional works at: <https://digitalcommons.mtu.edu/etdr>



Part of the [Acoustics, Dynamics, and Controls Commons](#)

IMPROVED LOW-FREQUENCY IMPACT INSULATION CLASS
MEASUREMENTS BASED ON COMPARISON TECHNIQUES

By
Sunit Girdhar

A REPORT

Submitted in partial fulfillment of the requirements for the degree of
MASTER OF SCIENCE

In Mechanical Engineering

MICHIGAN TECHNOLOGICAL UNIVERSITY

2019

© 2019 Sunit Girdhar

This report has been approved in partial fulfillment of the requirements for the Degree of MASTER OF SCIENCE in Mechanical Engineering.

Department of Mechanical Engineering – Engineering Mechanics

Report Advisor: *Andrew R. Barnard*
Committee Member: *Jason R. Blough*
Committee Member: *Darrell L. Robinette*

Department Chair: *William W. Predebon*

Table of Contents

List of figures	vi
List of tables.....	ix
Acknowledgements.....	x
Abstract.....	xi
1 Introduction.....	1
1.1 ASTM test standard for Impact Insulation Class	2
1.2 Limitations of the test method.....	4
1.2.1 Modal density.....	4
1.2.2 Measuring room absorption using room decay method.....	7
1.3 Proposed improvements for the current method	8
2 Details of the proposed method	9
2.1 Existing method.....	9
2.2 Proposed method	10
2.2.1 Mode Shapes	14
2.2.2 Mobility.....	15
2.2.2.1 Mobility of the test plate	15
2.2.2.2 Calculating damping for the test structure	16
2.2.2.3 Response of an infinite plate.....	17
2.2.3 Sound radiation	18
2.2.3.1 Analytical sound power radiation calculations	18
2.2.3.2 Sound intensity data to sound power radiation	19
3 Validation of the proposed method.....	20
3.1 Constructing a reference assembly and pre-test checks	20
3.1.1 Construction of the assembly.....	20
3.1.2 Pre-test checks	24
3.1.2.1 Tensile test for Young's modulus and Poisson's ratio....	25
3.1.2.2 Density measurement test	25
3.1.2.3 Variation in natural frequencies.....	25
3.1.2.4 Reciprocity check.....	27
3.2 Mode Shapes	28
3.2.1 Experimental modal analysis	28
3.2.1.1 Selection of hammer tip	30
3.2.1.2 Number of averages	31
3.2.2 Results.....	32

3.2.2.1	Modal analysis of the gypsum concrete base.....	33
3.2.2.2	Comparison of the mode shapes	34
3.2.2.3	Modal Assurance Criterion (MAC)	39
3.3	Mobility.....	39
3.3.1	Experimental mobility	40
3.3.2	Comparison of analytical and experimental mobility	40
3.4	Sound power radiation.....	44
3.4.1	Intensity probe testing.....	45
3.4.2	Input force participation.....	47
3.4.3	Comparison of results	47
3.4.3.1	Intensity heat maps	48
3.4.3.2	Sound power level comparison.....	52
3.5	Testing a new, unknown assembly.....	54
3.5.1	Details of the new assembly	55
3.5.2	True sound power measured in the anechoic chamber	55
3.5.3	Testing the assemblies in the reverberation chamber	56
3.5.4	Calculations and final remarks.....	57
4	Guidelines to implement the proposed method	60
4.1	Analytical method	60
4.2	Experimental method	60
4.3	Importance of modal density of the reference assembly.....	61
4.4	Common procedure – regardless of the basis of the method	62
4.5	Computing IIC rating with sound power.....	62
5	Conclusions and future scope	63
6	Reference List	64
A	Measurement uncertainty.....	66
A.1	Surface pressure-intensity indicator (F2)	66
A.2	Negative partial power indicator (F3)	67
A.3	Field non-uniformity indicator (F4)	68
B	Copyright documentation.....	70
B.1	Copyright permission for re-use of Figure 1-2.....	70
B.2	Copyright permission for Figure 1-3.....	71
B.3	Copyright permission for re-use of Figure 1-4.....	77
B.4	Copyright permission for re-use of Figure 1-5.....	79

B.5	Copyright permission for re-use of Figure 3-2.....	80
C	MATLAB codes for analytical calculations	83
C.1	Main body.....	83
C.2	Function: mode_shapes	85
C.3	Function: mobility_function.....	86
C.4	Function: sound_power	86

List of figures

Figure 1-1 Sources of sound radiation due to impact on floor/ceiling assemblies	2
Figure 1-2 A tapping machine (an example)	3
Figure 1-3 Positions of the tapping machine	3
Figure 1-4 Diffusers used for IIC test receiving rooms (an example)	6
Figure 1-5 100 Hz OTO band controls the IIC rating even when floor coverings are changed [10].....	7
Figure 1-6 A visual description of the proposed method.....	8
Figure 2-1 IIC reference contour (blue) modified for assembly with IIC rating 55 (red) .	10
Figure 2-2 Example of a basic Source-Path-Receiver model	11
Figure 2-3 Visualization of the step-by-step process for the proposed method	13
Figure 2-4 Auto-MAC for a 3DOF system (for reference).....	15
Figure 2-5 Effect of damping ratio (DR) on mobility.....	17
Figure 2-6 Spherical coordinate system for rectangular plate	18
Figure 3-1 Dimensions of the ABS plastic test plate	21
Figure 3-2 Test assembly built by Olivier et al [17].....	22
Figure 3-3 A model of the test assembly	23
Figure 3-4 A model of the test assembly (exploded view).....	23
Figure 3-5 A three-step process showing how the assembly was built	24
Figure 3-6 Tracking changes in natural frequency over forty-five days	26
Figure 3-7 Mean and standard deviation of natural frequencies over forty-five days.....	26
Figure 3-8 Reciprocity check for point 101 and 124 - 0 to 500 Hz	27
Figure 3-9 Reciprocity check for point 101 and 190 - 0 to 500 Hz	28
Figure 3-10 247 grid locations and four accelerometer locations.....	29

Figure 3-11 Reference signal for different hammer tips in the time domain.....	30
Figure 3-12 Reference signal for different hammer tips in the frequency domain.....	31
Figure 3-13 Coherence and FRFs for driving point measurements for three to seven averages (point 101).....	32
Figure 3-14 Stabilization diagram for mode picking - 250 Hz OTO.....	33
Figure 3-15 Mode shape of the gypsum concrete base at 232 Hz (approximately)	34
Figure 3-16 Mode shape comparison - 228.9 Hz.....	35
Figure 3-17 Mode shape comparison - 230.9 Hz.....	35
Figure 3-18 Mode shape comparison - 248 Hz.....	36
Figure 3-19 Mode shape comparison - 254.1 Hz.....	36
Figure 3-20 Mode shape comparison - 259.7 Hz.....	37
Figure 3-21 Mode shape comparison - 260.4 Hz.....	37
Figure 3-22 Mode shape comparison - 279.3 Hz.....	38
Figure 3-23 Mode shape comparison - 279.8 Hz.....	38
Figure 3-24 MAC for experimental and analytical mode shapes – 250 Hz OTO	39
Figure 3-25 Driving point mobility for response at point 101	40
Figure 3-26 Driving point mobility for response at point 124.....	41
Figure 3-27 Driving point mobility for response at point 190.....	41
Figure 3-28 Driving point mobility for response at point 212.....	42
Figure 3-29 Driving point mobility for all response locations for 250 Hz OTO	43
Figure 3-30 Surface averaged mobility for all response locations for 250 Hz OTO	44
Figure 3-31 Measurement area for intensity test shown.....	45
Figure 3-32 Intensity probe and the grid used for Intensity measurement test.....	46
Figure 3-33 GRAS Intensity probe with 25 mm spacer	46
Figure 3-34 Intensity heat map - 160 Hz OTO	48

Figure 3-35 Intensity heat map - 200 Hz OTO	49
Figure 3-36 Intensity heat map - 250 Hz OTO	49
Figure 3-37 Intensity heat map - 315 Hz OTO	50
Figure 3-38 Intensity heat map - 400 Hz OTO	50
Figure 3-39 Intensity heat map - 500 Hz OTO	51
Figure 3-40 Intensity heat map - 630 Hz OTO	51
Figure 3-41 Intensity heat map - 800 Hz OTO	52
Figure 3-42 The portion of wavelength covered over the length of the test grid for 160 Hz and 800 Hz	53
Figure 3-43 Comparison of analytical and experimental sound power radiation	54
Figure 3-44 Discrete point intensity test for the new assembly	55
Figure 3-45 Test of ABS assembly in the reverberation room	56
Figure 3-46 Comparison of the proposed method with the actual sound power of the test assembly	58
Figure 3-47 Difference in results due to imperfect shaker mounting	59
Figure A-1 F2 field indicator is lesser than the dynamic capability index (L_d)	66
Figure A-2 F3 field indicator compared with dynamic capability index (L_d) for all OTO bands under consideration	67
Figure A-3 F3-F2 less than 3dB for OTO bands higher than 100 Hz	68
Figure A-4 Value of factor C calculated using F4 field indicator compared with standard deviation grades	69

List of tables

Table 3-1 Material properties for ABS plastic.....	21
Table 3-2 Model numbers for PCB transducers used	29
Table 3-3 Data acquisition parameters for modal analysis.....	29
Table 3-4 Details of data acquisition parameters and the input signal for shaker	47
Table 4-1 Number of modes in OTO bands ranging from 40 Hz to 125 Hz for a 12.5 ft. X 10 ft. X 0.03 ft. Aluminum panel with SS boundary conditions	61

Acknowledgements

I would like to acknowledge our corporate sponsor, Mr. Carey Widder, President of GrassWorx LLC for funding this project. I would also like to express my appreciation for my advisor Dr. Andrew Barnard, for his constant guidance throughout the project, and general support related to data interpretation and manufacturing the test assembly. I would also like to thank the rest of my committee, Dr. Jason R. Blough, and Dr. Darrell L. Robinette for their support, along with Dr. James DeClerck, and Professor Charles D. VanKarsen for their academic teachings filled with their valuable anecdotes and comedic respites. I also want to acknowledge all the Dynamic Systems Lab students for their support for data acquisition, test assembly setup, and general brainstorming sessions. Moreover, I would like to thank my family and friends for their constant love, support, and encouragement throughout my years of studies.

Abstract

In today's world, noise pollution is growing as a major concern and it is becoming more and more difficult to find quiet places. But when the problem escalates to the extent that people are annoyed with loud noises even in their apartments, it becomes an alarming issue for engineers. Around the world, cities have defined some basic performance requirements for buildings, and isolation of residents from noise is one of the cardinal performance requirements.

In the United States, building codes use the Impact Insulation Class (IIC) rating to characterize the performance of floor/ceiling assemblies. This method uses the response measured in one-third octave (OTO) bands from 100 Hz to 3150 Hz and compares it with a reference curve to obtain the rating. However, this standard suffers from some limitations. The standard assumes the receiving rooms in the testing labs to be modally dense for all frequency OTO bands under consideration but the labs usually have a non-modally dense acoustic environment for low-frequency bands. Due to this, different labs give different results for the same assembly, thereby making it difficult to get reproducible IIC measurements.

With the method proposed in this report, the room contribution for these low-frequency OTO bands could be removed, paving a way to obtain more reproducible IIC measurements. This room contribution is removed by using a reference calibration assembly with a known sound power and employing the comparison technique. The comparison of measurements of the reference assembly in the test labs with the known sound power gives a calibration factor, defining how the room contribution affects the measurement data. These calibration factors are then used for the actual assemblies to get to the "true" sound power, unbiased by the effects of room contribution.

This report uses a simply supported rectangular plate as a reference assembly and analytically calculates the mode shapes, mobility, and sound power radiation. These analytical predictions are compared with the experimentally obtained values. This reference assembly is then used in a reverberation room to characterize the room contribution in one-third octave bands. The reference assembly is then replaced by a new, unknown assembly, and the "true" sound power information is predicted using the proposed method.

1 Introduction

Multiple-story buildings are the norm of all the major cities in today's world. In such times, it is important to make sure that these buildings are constructed with quality materials and sensible engineering choices. If not, these buildings may potentially cause harm to the residents. Therefore, more and more cities around the world are establishing building standards and codes to ensure three main things: safety of life and property, affordability, and general health and welfare of the residents. These building codes depend upon the type and usage of the building. For example, hospitals and schools have stricter requirements as compared to say, an office building or a mechanical workshop.

The building codes specify some performance requirements that the buildings should meet. One such requirement is the isolation of the residents from the noise generated outside the room. This noise is typically generated due to two major sources: noise generated by the residents in the neighboring space that passes through the walls and partitions, and the noise generated from the space above due to impact on the floor/ceiling assembly. In this report, the author studied the latter kind of noise.

The noise from floor/ceiling assemblies may create annoyance for the residents living in the space below. If the problem is more pronounced, it may even lead to hearing damage and speech intelligibility problems. Therefore, it is important to isolate the residents from the noise generated from impacts on floors in the buildings. Some of the possible sources of such impacts are footsteps, dragging furniture, or jumping on the floors. Out of these sources, annoyance due to footsteps is becoming a major cause of concern among residents [1] and in some cases, these issues have motivated the residents to file lawsuits against the developers [2]. This makes the dynamics of the floor/ceiling assembly due to footsteps an important field to study.

As the floor/ceiling assembly is impacted by a force, it generates vibration in the entire assembly, as shown in Figure 1-1. This vibrational energy may be directly radiated as acoustical energy into space down below, known as the direct path, or it may lead to a vibration in the side walls or columns attached to it. This vibration in the side walls or columns may further lead to sound radiation. This latter path that sound takes to travel is known as flanking path and it has been ignored for the purposes of this study.

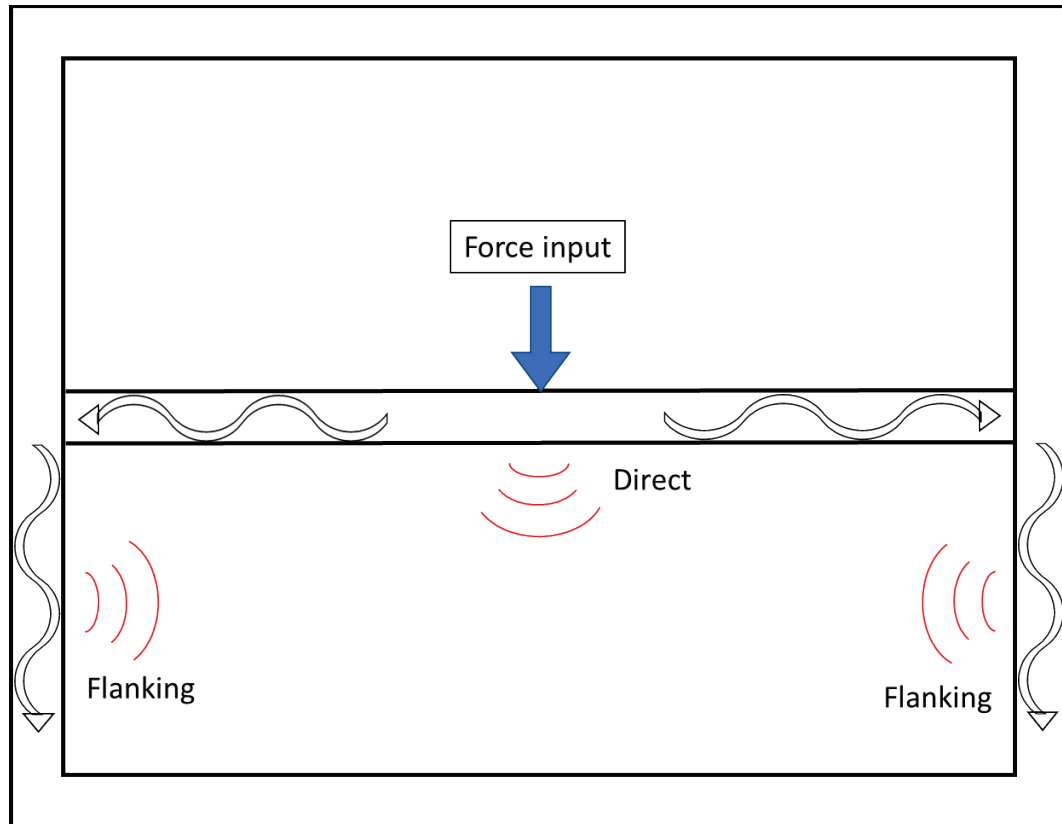


Figure 1-1 Sources of sound radiation due to impact on floor/ceiling assemblies

In the United States, the performance of a floor/ceiling assembly under footstep impacts is characterized by an Impact Insulation Class (IIC) rating. The process involved in obtaining this IIC rating for an assembly is defined by ASTM E989 standard [3] and this method suffers from some reproducibility issues due to the measurement methodology. The following sections discuss this ASTM standard and its limitations in detail.

1.1 ASTM test standard for Impact Insulation Class

The floor/ceiling assemblies are tested in a set of two rooms stacked vertically. To simulate the impact of footsteps, a standard tapping machine, as shown in Figure 1-2, is used on the floor side to generate an input force. This machine excites the structure at five different locations shown in Figure 1-3, and the averaged sound pressure level response is measured in the space below (also known as the receiving room) in one-third octave (OTO) frequency bands ranging from 100 Hz to 3150 Hz. This response is measured either with multiple stationary microphones or a single microphone mounted on a rotating beam.

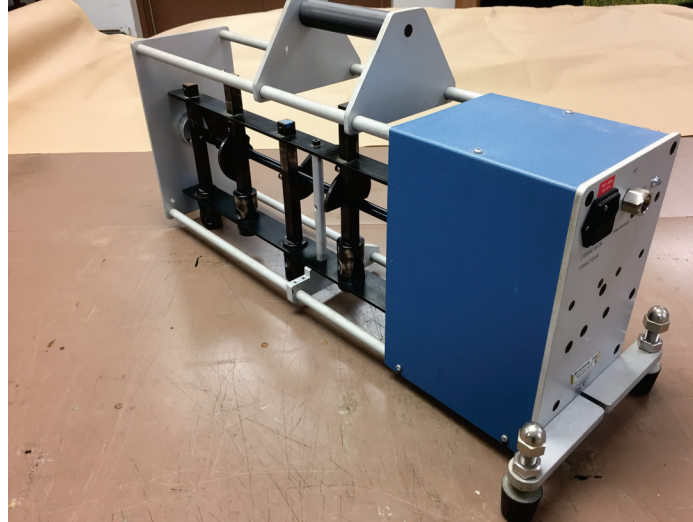


Figure 1-2 A tapping machine (an example) reprinted with the permission of Carey Widder, see Appendix B.1

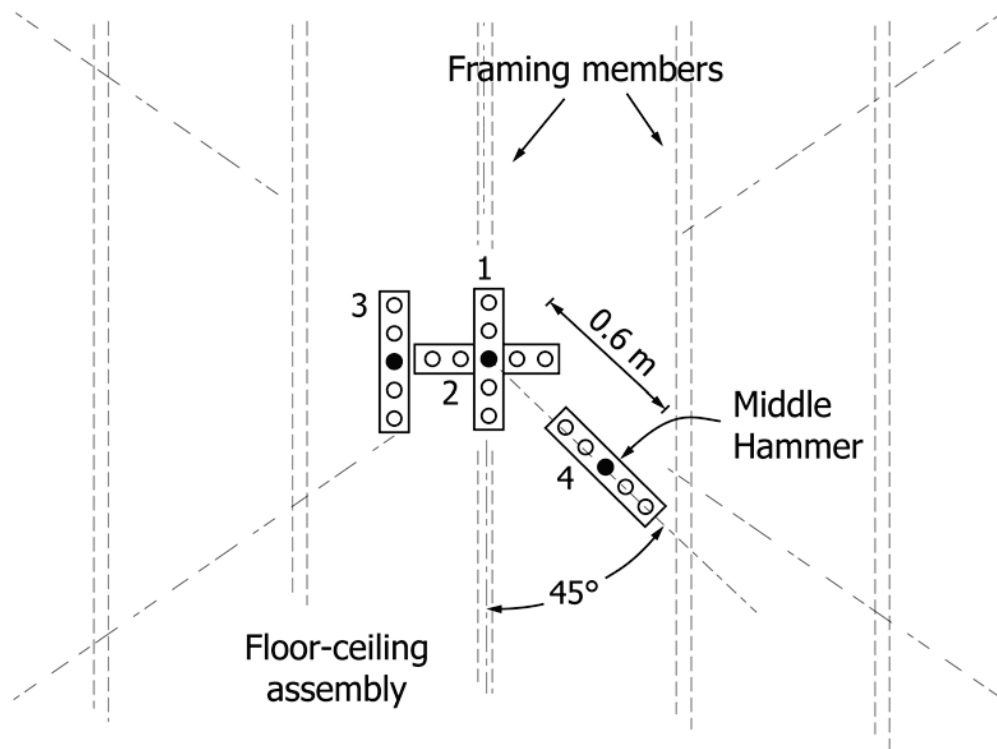


Figure 1-3 Positions of the tapping machine, reproduced, with permission from [4], copyright ASTM International, 100 Barr Harbor Drive, West Conshohocken, PA 19428, see Appendix B.2

The receiving room for the IIC test is usually a reverberation room and the minimum room volume requirement specified in the standard is 125 m³. The standard also states that it is important to ensure that the sound absorption in the room is below a defined level so that a diffuse sound field could be achieved. Testing labs generally use the room decay method to measure this absorption. Speakers are placed in the corners of the room and a random noise signal is played through them. These speakers are then turned off and the time required for the sound in the room to decay by 60 dB is measured, which is used to calculate the room absorption.

Several studies have been done in the past to highlight the drawbacks of the IIC test method [1, 2, 5-8] and the focus of this report is on the limitations of measurement methodology specified in the standard, further discussed in the next section.

1.2 Limitations of the test method

The test method, although a mandatory part of the building codes, has certain limitations, and several acousticians in the industry are working on these issues [1, 2, 6-9]. In this section, the discussion is limited to the measurement methodology specified in the standard with the partly incorrect assumption of the modal density of the receiving room and the issues with the room decay method while measuring room absorption.

1.2.1 Modal density

The ASTM test method [3, 4] assumes that the measured averaged Sound Pressure Level (SPL) does not change, irrespective of the measurement location, or, the microphone location, in the receiving room. This is to ensure good repeatability and reproducibility of test results. Although, this assumption is true only if the sound field in the room is truly “reverberant” for the OTO bands under consideration. If that is not the case, then the measured response is greatly affected by the acoustic modes in the room. Barnard et al [10] measured the response of a floor/ceiling assembly in a receiving room using six microphones, along with measuring the vibrational response of the under test using accelerometers. The authors showed that a mode recorded by the microphones in the receiving room was not present in the data recorded by the accelerometers on the test structure. This means that the source of the high sound levels picked up by the test microphone for that frequency is not the structure, but the room itself. Due to this modal behavior, different microphone locations would measure different response, therefore, the room is non-reverberant for this frequency. Using this measured data for IIC calculations would give erroneous results. Thus, for the IIC method to give satisfactory results, it is important to make sure that the test field is truly “reverberant” for the entire frequency bandwidth under study.

Any OTO band in a given room is reverberant if there are three or more modes in the frequency bandwidth. As we go higher in frequency, both, the bandwidth of the OTO band and the number of modes in the band increases, but at low frequencies, obtaining a reverberant OTO band is always a challenge. A cross-over frequency over which the OTO bands in the room are reverberant is defined based on the room dimensions. This cross-over frequency was defined by Schroeder as

$$f_{co} = 2000 \sqrt{\frac{T_{60}}{V}}, \quad (1-1)$$

where, f_{co} is the Schroeder cross-over frequency in Hz, over which the room is reverberant, T_{60} is the time in seconds for the sound energy in the room to decay by 60 dB, and V is the volume of the room in m^3 . To ensure that the IIC measurements are made in a diffuse field, the receiving rooms should be very large but the cost of construction and maintenance of these very large rooms would be very high. Barnard et al [10] show that the cut-off frequency lies for the IIC receiving rooms in the US lies in the range of 170 – 250 Hz. Therefore, the measurements made in 100 Hz and 125 Hz are in a non-diffuse sound field.

It could be argued that some of the IIC test receiving rooms have diffusers (Figure 1-4) which help in creating a more diffuse sound field. However, it is important to note that for a diffuser to be effective at any given frequency, it should be at least a few wavelengths long. Generally, the diffusers used in reverberations rooms are close to 5-6 ft. (1.5 – 1.8 m) long but the wavelength for 100 Hz, the lowest OTO band used for IIC test, is close to 11 ft. (3.4 m). This means that diffusers are not even one wavelength long for 100 Hz OTO band and therefore, they are ineffective for such low-frequency bands.



Figure 1-4 Diffusers used for IIC test receiving rooms (an example) reprinted with the permission of Eric Wolfram, see Appendix B.3

The low-frequency response of the floor-ceiling assembly generally controls the final IIC rating (more information on how the rating is calculated is available in Section 2.1) and these low-frequency measurements in the non-diffuse field leads to non-reproducible readings in different IIC labs. These low-frequency measurements also limit how good the rating of the floor-ceiling assembly can be. Figure 1-5 shows the recorded response of a floor-ceiling assembly and it can be seen that the deficiencies are highest in the 100 Hz band (shown on the right, for more information on the deficiencies, refer Section 2.1). These high deficiencies control how good the results of the test can get and even when the floor coverings are changed on this assembly, the response in 100 Hz band remains unchanged. Therefore, it becomes vital to measure good data in the low-frequency bands and non-diffuse field in receiving rooms creates difficulties in doing that.

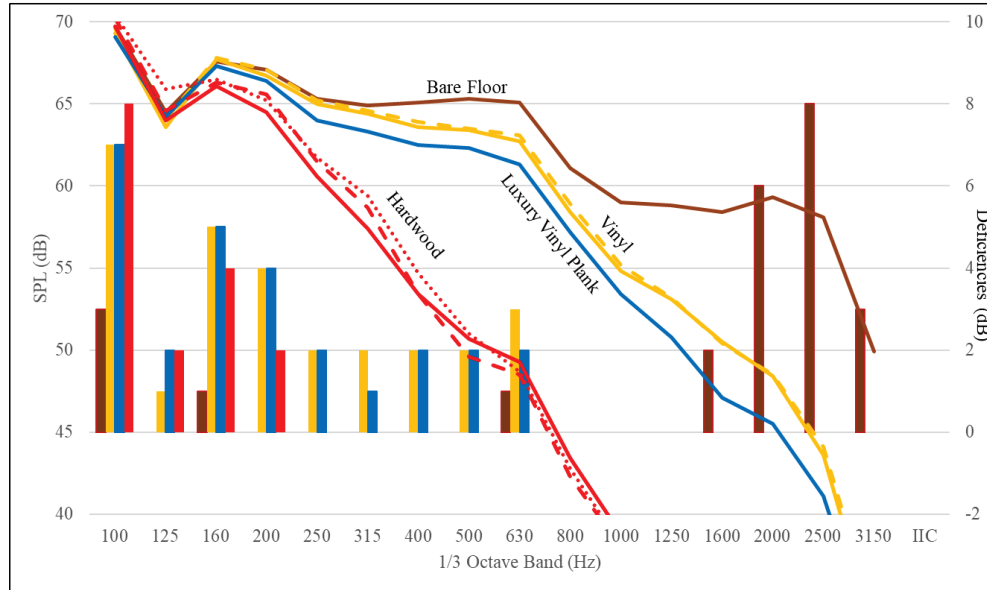


Figure 1-5 100 Hz OTO band controls the IIC rating even when floor coverings are changed [10], reprinted with permission of Gordon Ebbitt, see Appendix B.4

1.2.2 Measuring room absorption using room decay method

The IIC test method specifies the room decay method for measurement of room absorption, along with the minimum required room absorption, but the specified process suffers from some disadvantages. The room decay method works well when the sound field is reverberant, but at low-frequencies, the room is non-modally dense and therefore, the room decay method does not give good results for room absorption values in low-frequency OTO bands.

For IIC tests, the required room absorption is defined only for frequencies ranging from $2000/(V^{1/3})$ to 2000 Hz, where V is the volume of the room in m^3 [4]. For a room fulfilling the minimum volume requirement of $125 m^3$, this frequency range is 400 Hz to 2000 Hz. For OTO bands lower than 400 Hz, absorption is not measured.

In addition to this, the test speakers used for the room decay method are not a true representation of the floor/ceiling assembly. The test speakers are placed at the corner of the room while the actual test assembly (floor/ceiling assembly) is mounted on the top, as viewed from the receiver room.

Overall, this goes on to show that the receiving room clearly has an effect on measured data. Therefore, the same assembly will give non-reproducible IIC results when tested in different test labs. The proposed solution gets rid of this effect of the room on the data, and therefore, paves the way for a more reproducible IIC test method.

1.3 Proposed improvements for the current method

If the room contribution while performing the IIC test were somehow known, it could be easily subtracted from the measured data. Unfortunately, these effects are hard to calculate in advance, but could be measured using a “calibration source”. Consider Figure 1-6. If a calibration source is tested in the IIC receiving room, it is expected that the data would be skewed because of the room contribution and the measurement location. However, if the sound power response of this calibration source is known in advance, the room error correction could be calculated (Figure 1-6 left). With this new-found information about the room effects, the true sound power of the test assembly can be obtained instead of the biased sound power (Figure 1-6 right).

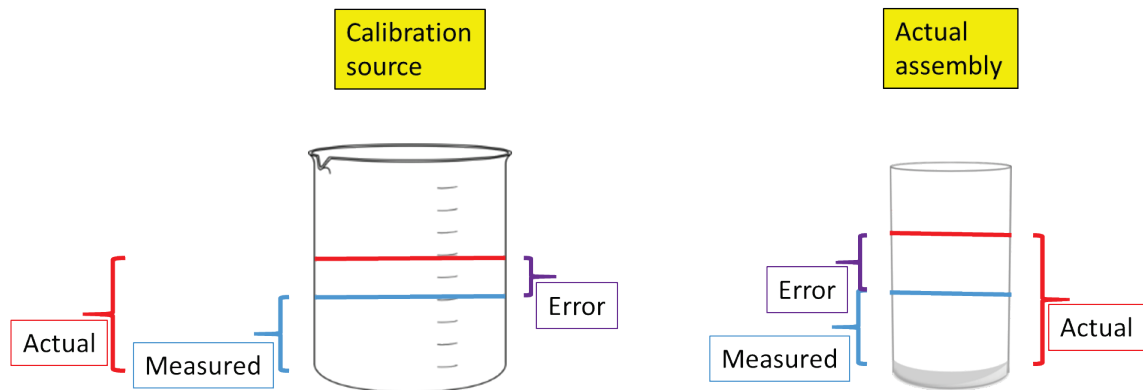


Figure 1-6 A visual description of the proposed method

The proposed method draws similarities from the SAE J1400 test method [11] used in the automotive industry to assess the acoustic transmission loss (TL) of automotive assemblies and materials. A reference sample with known TL is used to obtain the calibration factor of the test room. This factor is then used to obtain the true TL of the test assembly from the measured data. The next chapter discusses the proposed method and the background math in detail.

2 Details of the proposed method

This chapter contains a discussion on the existing test methodology for IIC test method and the proposed method, along with their background math.

2.1 Existing method

For the IIC test, the measured averaged Sound Pressure Level (SPL) response using microphones in the receiving room is compared with a reference curve defined in the standard [3] by following these steps:

1. Create a reference contour, as shown in Figure 2-1 with a blue curve.
2. Add a constant value “T” to the reference contour while obeying these two rules:
 - a. Sum of all the positive differences between the measured SPL data and the reference contour is less than 32.
 - b. The positive difference between measured SPL data and the contour in any single one-third octave (OTO) band is less than 8.
3. $(110 - T)$ gives the IIC rating of the test assembly.

Figure 2-1 shows the reference data (as an example) for a floor/ceiling assembly with IIC rating 55, with the dashed red curve shown as the modified reference contour for this assembly. For this example, the maximum positive difference between SPL data and reference curve is less than 8 dB in any given OTO and sum of all positive differences is less than 32 dB. The dotted black lines show the level of the original curve as zero, and the modified curve as 55, thus giving an IIC rating of 55. For more details on the IIC rating calculations, please refer the standard [3].

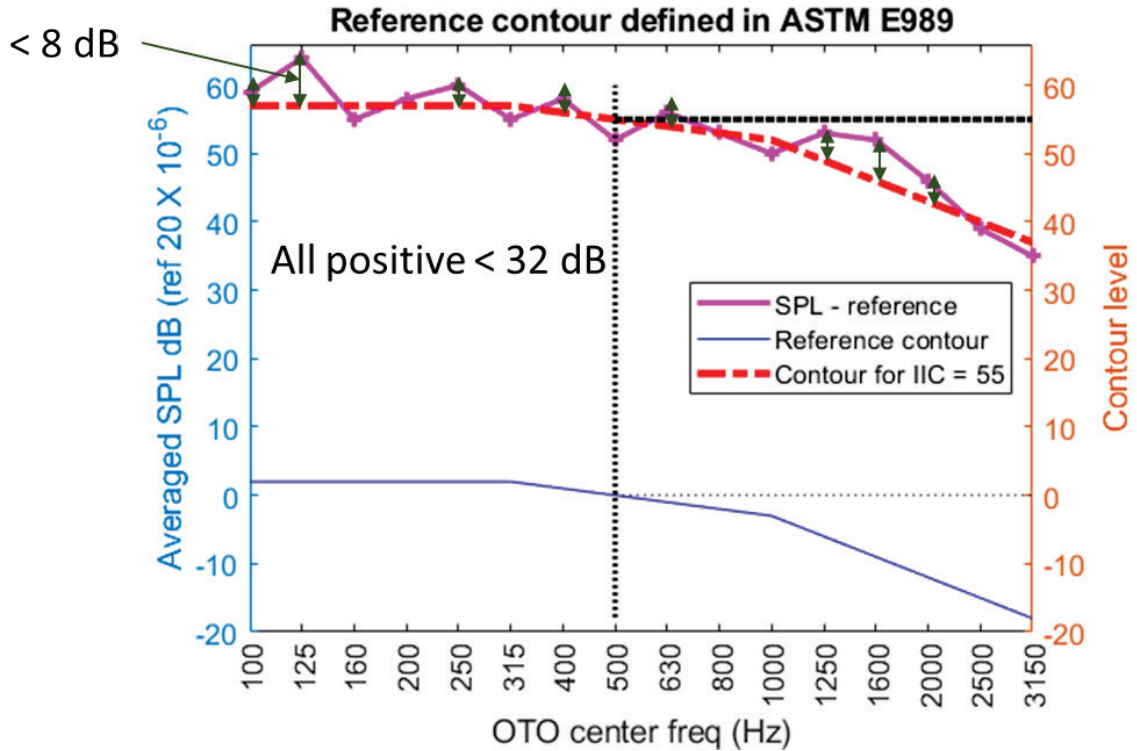


Figure 2-1 IIC reference contour (blue) modified for assembly with IIC rating 55 (red)

2.2 Proposed method

The standard ASTM test method uses the averaged SPL data for the curve-fitting process to obtain the IIC rating. This SPL data are biased with the room contribution and in order to remove this contribution, we need to study the fundamentals of this acoustics problem.

Fundamentally, every noise and vibration problem could be broken down into the Source-Path-Receiver (SPR) domain. As the name suggests, the source is what generates the noise and/or the vibration, the receiver is the person or object facing the problem, and the path would be how the noise and/or vibration reached the receiver from the source. To use a very simple example of passengers in a car complaining about the loud engine noise, the source would be the car engine, the receiver would be the passengers and the path would be everything in between, including the air, car chassis, etc. Another basic example of this SPR domain is the noise from a loudspeaker inside a room, presented in Figure 2-2. In the case of annoyance to the residents in a building due to impact on the floor/ceiling assembly, the source is the floor/ceiling assembly excited by the input force generated by the upstairs' residents, the receiver is the residents in the room under consideration and the path is the air (recall that we ignored the flanking path for this study).

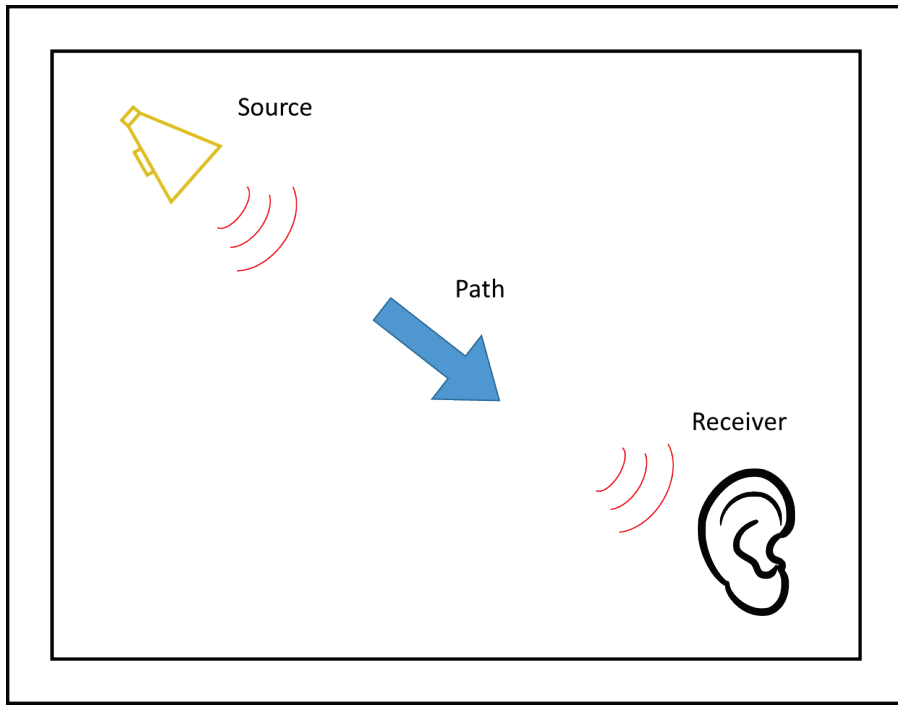


Figure 2-2 Example of a basic Source-Path-Receiver model

Sound Pressure Level (SPL) used for the IIC test depends upon how loud the floor/ceiling assembly is (the source), and how the sound travels from the source to the microphone (the path). The room contribution observed in IIC data is due to this path content of SPL. To get rid of this room contribution, a path-independent measurement quantity should be used, such as sound power level. Sound power level (L_w) depends only on the source, and not the path. Therefore, reproducibility of the IIC test results could be improved if L_w is used to characterize the response of floor/ceiling assemblies, instead of SPL.

The sound power of a test assembly could easily be calculated using the measured sound pressure level using

$$\bar{L}_p = L_w + 10\log(4/\bar{\alpha}S), \quad (2-1)$$

where \bar{L}_p is the averaged sound pressure level (dB ref 20×10^{-6} Pa), L_w is the sound power level (dB ref 10^{-12} W), $\bar{\alpha}$ is the averaged room absorption coefficient, and S is the total surface area of the room in m^2 .

With the current method, using the averaged sound pressure level measurements to calculate the sound power levels has two disadvantages:

1. The room absorption coefficient is not measured for the low-frequency bands, recall 1.2.2.
2. The averaged sound pressure level response is not truly an averaged response in the room at low-frequencies because of the acoustic room modes.

Therefore, with the existing measurement methodology, sound power of the test assembly cannot be obtained reliably. Several methods were considered to measure the sound power of the floor/ceiling assemblies and the details of these methods are listed below:

1. Nearfield Acoustic Holography (NAH): The sound power of the test assembly is calculated by making measurements in the nearfield of the test structure using an array of microphones. The method requires a cost and time investment.
2. Hemi-anechoic chamber: The sound power of the test assembly is measured using a microphone array set-up as a hemisphere in a hemi-anechoic chamber. The method requires construction of hemi-anechoic chambers as receiving rooms.
3. Intensity measurements: The sound power of the test assembly is calculated using intensity probe measurements, either in an anechoic chamber, or in a reverberation chamber using the concepts of signal separation. The method requires construction of anechoic chambers as receiving rooms, or development of signal separation algorithm for reverberation rooms.
4. Acoustic camera: The sound power of the test assembly can be calculated using an acoustic camera. The method requires an expensive acoustic camera and the supporting software.
5. Comparison method: The reverberation room is calibrated using a reference source with known sound power values and these calibrated values are used to obtain the sound power of the test assembly. The method requires construction of a reference assembly with known sound power values.

The comparison method does not involve very high cost or time investment, therefore, a decision was made to use the comparison method to obtain sound power values of the floor/ceiling assemblies. The basic concepts of this method are explained in Section 1.3. A “calibration source” could be used to gauge the room contribution and the two-step process is shown in Figure 2-3:

- Step 1: Test a source with known sound power in the IIC receiving room and calculate the (room) calibration factor using

$$L_w(\text{known}) = L_p(\text{measured, known}) + CF, \quad (2-2)$$

where CF is the (room) calibration factor

- Step2: Replace the calibration source with actual test assembly, record the sound pressure level, and use the calibration factor to get the actual sound power level of the test assembly.

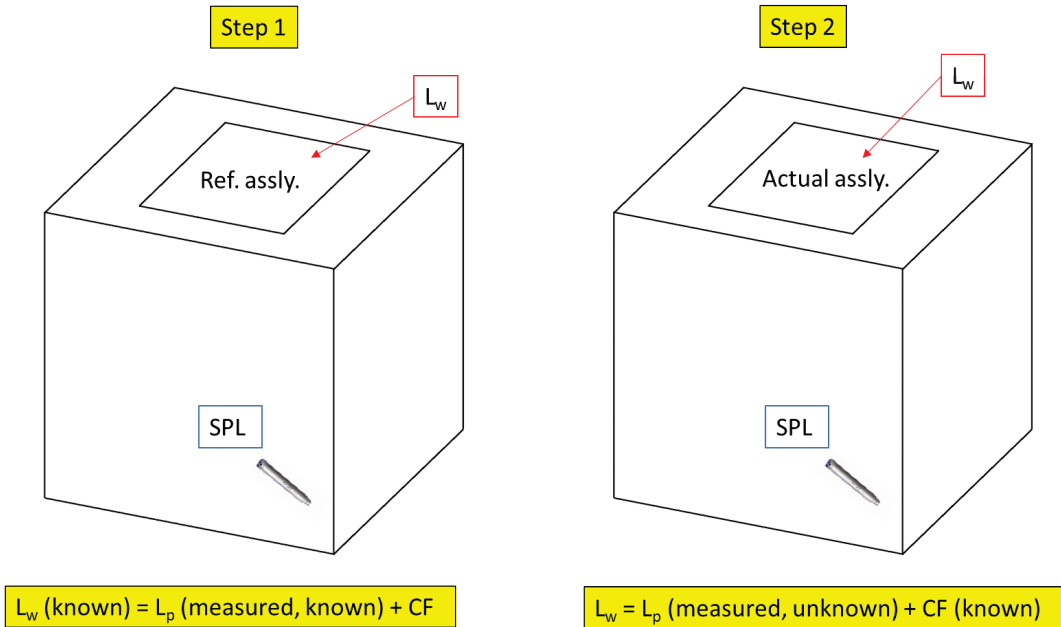


Figure 2-3 Visualization of the step-by-step process for the proposed method

As a reminder, the room is not modally dense at lower frequencies, and it is imperative to make sure that the microphone location is unchanged between the two steps of the process. As long as this is ensured, the test engineer is only required to calibrate the room once and the same CF numbers could be used to test multiple floor/ceiling assemblies. Any change in the microphone location would cause the calibration factors to change and would, therefore, call for a re-calibration of the room with new response locations.

This method also targets the second limitation of the existing method (Section 1.2.2), as the absorption values are no longer needed to get to the true sound power response of the test assembly, so the room decay method to calculate absorption is no longer required.

It is important to note that this method heavily depends upon the “known” sound power of the calibration source. This known sound power can either be obtained analytically or experimentally. Analytical predictions can only be done for simple structures with controlled boundary conditions using well-known, textbook formulas for bending theory and sound radiation. In contrast, experimentally, the sound power can be obtained for any calibration source if it had previously been tested in acoustic free-field conditions. Even though the experimental method works great for any reference assembly, for large assemblies such as those used in IIC tests, this method may be expensive.

For this study, both analytical and experimental methods were used for a rectangular plate with simply supported (SS) boundary conditions, selected as the reference assembly (more details in Section 3.1). In the following sections, well-defined, textbook formulas for mode shape, mobility, and sound power radiation predictions for rectangular plates with SS boundary conditions are discussed.

2.2.1 Mode Shapes

The formula for analytical prediction of mode shape of a simply supported rectangular plate is given by [12]

$$w_{mn}(x, y) = \sin\left(\frac{m\pi x}{l}\right) \sin\left(\frac{n\pi y}{b}\right), \quad (2-3)$$

where $w_{mn}(x, y)$ is the mode shape at location x, y on the plate, (m, n) is the order of the mode shape, and l, b is the length and width of the plate in meters, that relates to m and n , respectively.

This analytical mode shape is compared to the experimental measurements in Section 3.2.2.2. Another widely used mode shape comparison tool is the Modal Assurance Criterion (MAC). If the mode shapes are highly similar, the MAC values are close to one. On the other hand, if the mode shapes are very different, the MAC value obtained would be close to zero.

The expression used to calculate these MAC values is

$$MAC(\{\varphi_1\}, \{\varphi_2\}) = \frac{|\{\varphi_1\}^{*t}\{\varphi_2\}|^2}{(\{\varphi_1\}^{*t}\{\varphi_1\})(\{\varphi_2\}^{*t}\{\varphi_2\})} \quad (2-4)$$

Where $(\{\varphi_1\}, \{\varphi_2\})$ are the two mode shape vectors being compared, and “* t ” is the complex conjugate transpose of the matrix.

A typical MAC matrix contains the MAC values for all combinations of mode shape vectors as matrix elements. An example of Auto – MAC (MAC for a mode shape vector with itself) for a 3 degree of freedom (DOF) system is presented in Figure 2-4. It could be observed that for such a system, the MAC values at the diagonal elements are the MAC of a mode with itself. For a system with unique modes, it is expected for the diagonal elements would be close to one and all the off-diagonal elements would be close to zero.

Auto - MAC	Mode 1 (A1)	Mode 2 (A2)	Mode 3 (A3)
Mode 1 (A1)	MAC (A1,A1)	MAC (A1,A2)	MAC (A1,A3)
Mode 2 (A2)	MAC (A2,A1)	MAC (A2,A2)	MAC (A2,A3)
Mode 3 (A3)	MAC (A3,A1)	MAC (A3,A2)	MAC (A3,A3)

Figure 2-4 Auto-MAC for a 3DOF system (for reference)

2.2.2 Mobility

In this section, we discuss the formulas used for mobility calculations for a test plate, calculating damping of the test structure for mobility calculations, and response of an infinite plate calculated for a sanity check.

2.2.2.1 Mobility of the test plate

It is well established that the sound radiation by a structure depends upon the surface velocity. Mobility is simply this velocity response divided by the force for a given structure. The well-established, textbook formula [12] for mobility calculations is represented as

$$mob = \frac{v(x_r, y_r)}{F(x_f, y_f)}(\omega) = \sum_{m=1}^{\infty} \sum_{n=1}^{\infty} \frac{i\omega}{MM} \frac{A_{mn}(x_r, y_r, x_f, y_f)}{\omega_{mn}^2 - \omega^2}, \quad (2-5)$$

where mob is the mobility, (x_r, y_r) is the response location, (x_f, y_f) is the input force location, ω is the angular frequency in radian/sec, MM is the modal mass, ω_{mn} is the angular frequency of the mode in radian/sec, and $A_{mn}(x_r, y_r, x_f, y_f)$ is the modal coefficient.

The modal mass is given by

$$MM = \frac{lbh\rho}{4}, \quad (2-6)$$

where h is the thickness of the plate in meter and ρ is the density of the plate in kg/m^3 .

The modal coefficient for a simply supported rectangular plate is given as

$$A_{mn}(x_r, y_r, x_f, y_f) = \left[\left(\sin\left(m\pi \frac{x_r}{l}\right) \sin\left(n\pi \frac{y_r}{b}\right) \right) \left(\sin\left(m\pi \frac{x_f}{l}\right) \sin\left(n\pi \frac{y_f}{b}\right) \right) \right], \quad (2-7)$$

Substituting the values for modal coefficients (Equation 2-7) and modal mass (Equation 2-6) back in Equation 2-5, it is easy to calculate the mobility of the test plate.

2.2.2.2 Calculating damping for the test structure

It is interesting to note that damping plays an important role in calculating the mobility of a structure. As shown in Figure 2-5, low damping gives rise to sharp peaks in the frequency domain at resonance, and vice versa.

In general, assumed damping values are used to generate the analytical model and these values are later fine-tuned to match with the experimental data. A disadvantage to this method is that any error in the analytical prediction process may disguise as a damping error and the test engineer runs the risk of tuning the damping to an incorrect value. To get rid of this potential variability, the damping values used in the analytical mobility prediction of the test structure were directly extracted from the experimental data.

To obtain the damping, the frequency response for all the modes in the bandwidth excited by the hammer tip (Section 3.2.1.1) was filtered and the damping was calculated through the time domain decay method. The decay rate of time-domain response is used to calculate the loss factor using

$$loss = \frac{2.2}{f_m * T_{60}}, \quad (2-8)$$

where T_{60} is the time required in seconds for the signal to decay by 60 dB and f_m is the frequency of the mode in Hz. The calculated loss factor values (twice the damping ratio) are averaged to calculate the average damping across the entire frequency bandwidth.

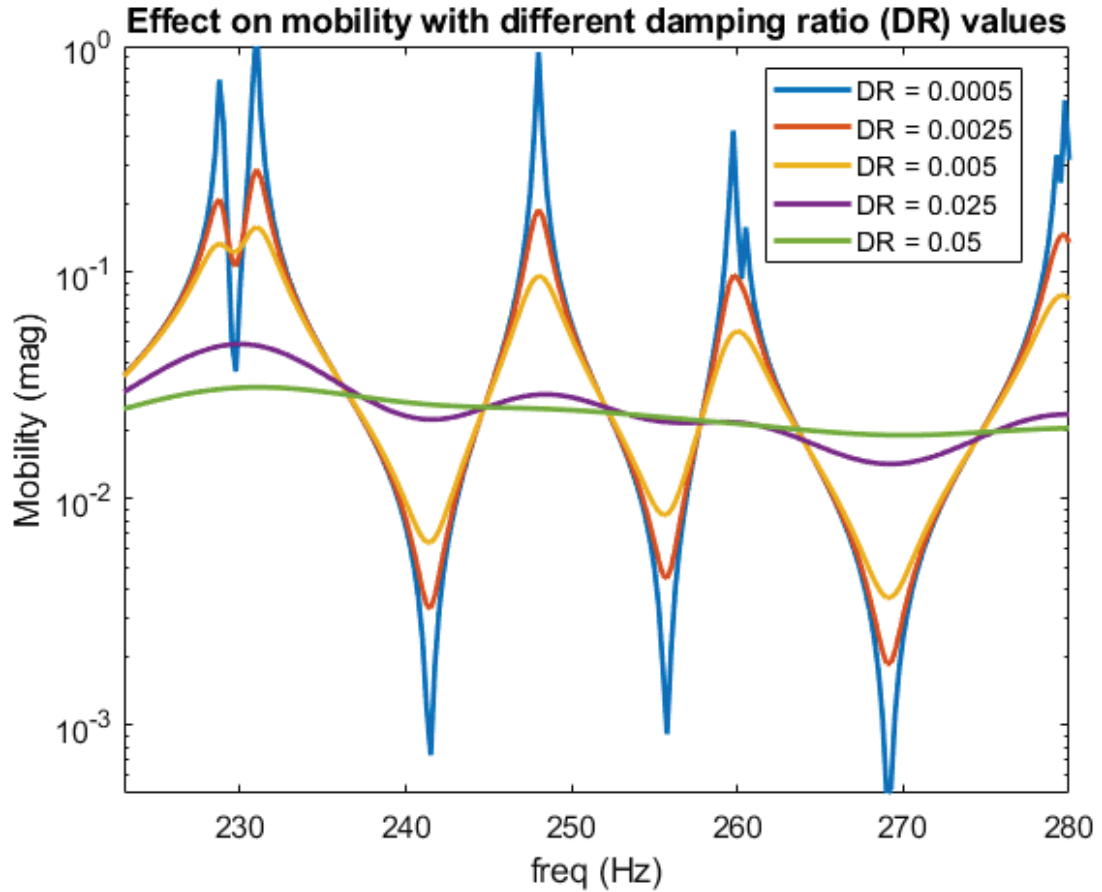


Figure 2-5 Effect of damping ratio (DR) on mobility

2.2.2.3 Response of an infinite plate

For an infinite plate, the shock waves due to the input force would keep on traveling outwards from the input location in the absence of any boundary reflections. Therefore, standing waves would not exist and hence, this infinite plate would not have any modes.

The response of an infinite plate is often used as a sanity check as its response should just be a mean of the response of the actual test plate [12]. The mobility of an infinite plate is given as

$$mob_{inf} = \frac{1}{8\sqrt{D\rho h^3}} \quad (2-9)$$

where D is the flexural rigidity, given by

$$D = \frac{Eh^3}{12(1-\nu^2)}, \quad (2-10)$$

where E is the Young's modulus in Pa and ν is the Poisson's ratio of the test material.

2.2.3 Sound radiation

In this section, we discuss the background math for sound radiation for simply supported rectangular plates and converting sound intensity measurement data to sound power values.

2.2.3.1 Analytical sound power radiation calculations

The sound radiation from a rectangular plate with simply supported boundary conditions can be calculated using formulas provided in several references [12-15]. For simplicity, these calculations are typically done in a spherical coordinate system, defined in Figure 2-6.

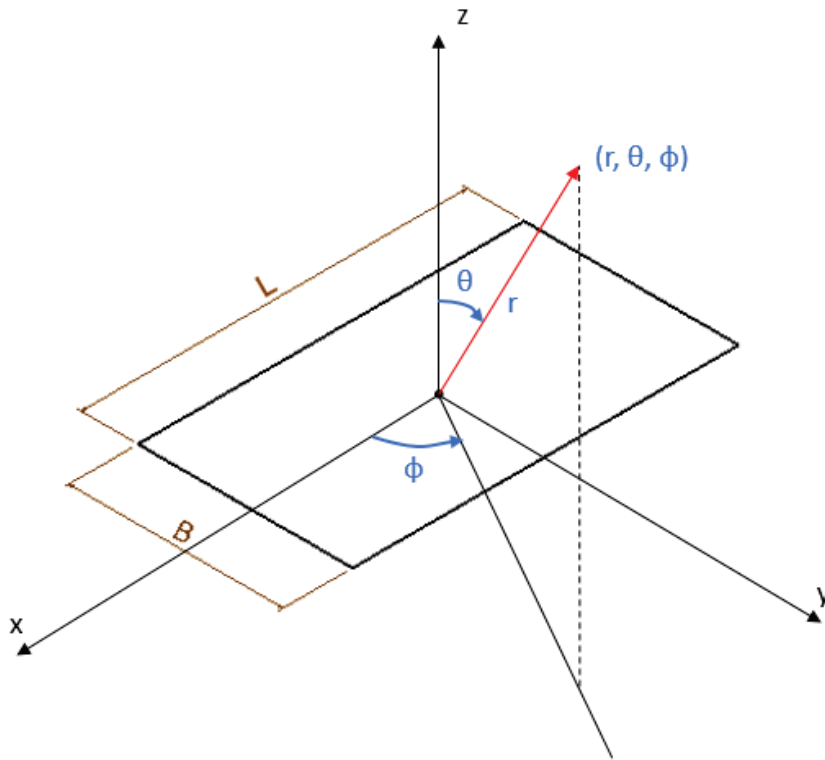


Figure 2-6 Spherical coordinate system for rectangular plate

The sound power radiated for a rectangular plate with SS BC for 1/8th of a sphere (quadrant) is given by

$$P = 8\rho_0 c_0 \left(\frac{u_m k_0 l b}{\pi^3 m n} \right)^2 \int_0^{\frac{\pi}{2}} \int_0^{\frac{\pi}{2}} \left\{ \frac{\sin(\frac{\alpha}{2}) \sin(\frac{\beta}{2})}{[(\alpha/m\pi)^2 - 1][(\beta/n\pi)^2 - 1]} \right\}^2 \sin \theta d\theta d\varphi, \quad (2-11)$$

where sin is used for even values of m and n , and cos is used for odd values of m and n , P is the sound power in Watts, ρ_0 is the density of air in kg/m³, c_0 is the speed of sound in air in m/s, k_0 is the wavenumber in air in meter⁻¹, and (α, β) are given by

$$\alpha = k_0 l \sin \theta \cos \varphi, \quad (2-12)$$

$$\beta = k_0 b \sin \theta \sin \varphi, \quad (2-13)$$

u_m is given by

$$\frac{u_m^2}{8} = \langle u_w \rangle^2 = \frac{1}{lb} \int_0^l \int_0^b \frac{1}{2} u_w^2 dx dy, \quad (2-14)$$

where $\langle u_w \rangle^2$ = temporal and spatial average of the square of surface velocity.

2.2.3.2 Sound intensity data to sound power radiation

The experimental sound power was obtained through an intensity measurement test (details available in Section 3.4.1) and the measured SPL values by the intensity probe microphones are converted to intensity probe values using [16].

$$I(\omega) = \frac{\text{imag}(G_{12})}{\omega \rho_0 \Delta r}, \quad (2-15)$$

where $I(\omega)$ is the intensity in W/m², $\text{imag}(G_{12})$ is the imaginary part of the cross-spectrum of the two microphones on the intensity probe, and Δr is the microphone spacer length in meters. This intensity data, multiplied by the area of the measurement grid gives the sound power radiated from the grid, in Watts.

3 Validation of the proposed method

The end goal of the proposed method is to characterize the room contribution in the measured data and remove its effects during post-processing. Given the limitations of the test chambers available, a relatively small-sized assembly was used for validation, as compared to the actual floor/ceiling assembly used for IIC test.

The following five steps are a break-down of the process followed as a proof of concept for the proposed method:

1. Construct a test assembly with controlled boundary conditions which would act as a reference assembly and run some pre-test checks.
2. Obtain experimental mode shapes from test data and compare it with analytical mode shapes.
3. Compare experimentally obtained mobility with analytical predictions.
4. Measure the sound power radiation from the test structure and compare with analytically obtained data. A good comparison means that we can analytically predict sound power radiation of any given structure within reason.
5. Test the reference assembly in the reverberation chamber, along with a new, unknown assembly and characterize the room contribution.

In this chapter, we discuss this step-by-step approach to verify the validity of the proposed method and to remove the room contribution from the measured data.

3.1 Constructing a reference assembly and pre-test checks

In this section, we discuss the rationale behind the construction of the test assembly, and results of some pre-tests checks performed to ensure that the assembly is performing the way it should.

3.1.1 Construction of the assembly

The reference test assembly was made with a 30 in X 19 in X 0.125 in (762 mm X 482.6 mm X 3.18 mm) ABS plastic panel (McMaster – Carr number: 8586K561). Figure 3-1 shows the dimensions and Table 3-1 presents the material properties of the test plate.

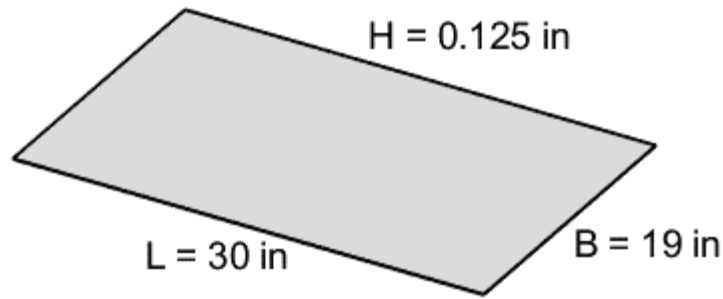


Figure 3-1 Dimensions of the ABS plastic test plate

Table 3-1 Material properties for ABS plastic

Material property	Value	Units
Young's modulus	2.25×10^9	Pa
Density	1030	Kg/m ³
Poisson's ratio	0.35	No units
Loss factor	0.0137	No units

The test plate has simply supported (SS) boundary conditions (BC). These BCs are widely studied and the analytical estimation of mobility and sound power radiation for thin plates with this boundary condition is well documented. To reduce unnecessary complications with the test assembly, the same SS boundary conditions were used on all four sides of the plate.

It is important to note that until recently, it was tough to obtain and control simply supported boundary conditions for thin plates in lab settings, but Olivier et al [17] presented an innovative way of mounting rectangular test plates to simulate SS BC, shown in Figure 3-2. The authors used glue to mount the aluminum test plate to thin aluminum blades on all four sides and bolted these side blades to a heavy, rigid aluminum base frame. They showed that the test data obtained was within 4% of the analytical predictions for the first ten natural frequencies. This study shows a lot of promise in developing thin, rectangular lab test structures with simply supported boundary conditions.

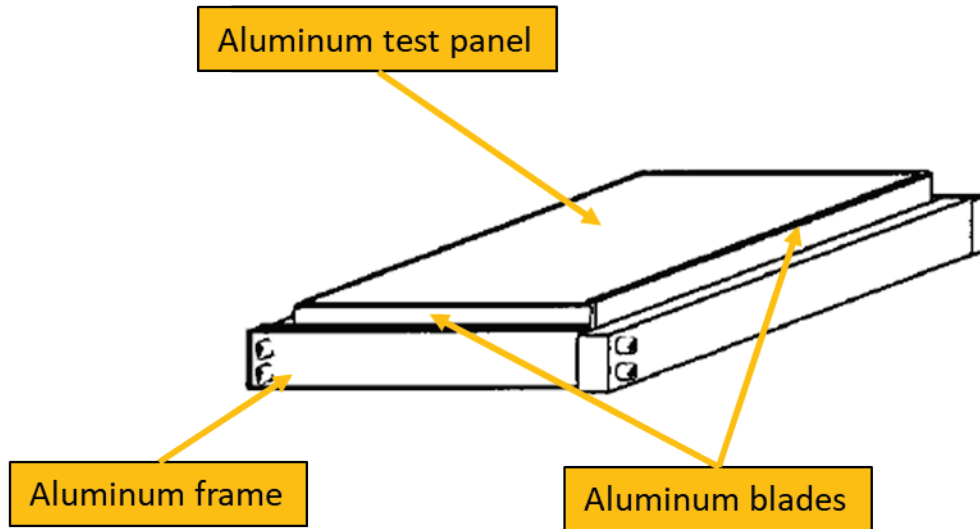


Figure 3-2 Test assembly built by Olivier et al [17] reprinted with the permission of the journal, see Appendix B.5

Considering the budget constraints, the assembly for this report was made with cost-effective materials instead of aluminum used by Olivier et al [17]. The test plate and side blades were replaced with ABS plastic, and the aluminum base which served as a heavy, rigid base for the test plate, was replaced with gypsum concrete. The gypsum concrete assembly was designed in compliance with the weight requirements set forth by Olivier et al.

A model of the proposed test assembly is shown in Figure 3-3. The test panel is highlighted with grey, the side blades are highlighted with red and blue (based on their different lengths), and the concrete base is highlighted with green. The length of the side blades is equal to the size of the side of the plate they would be glued to, with a uniform width and thickness of 4" X 0.02" (101 mm X 0.5 mm). The concrete base is a 3" wide by 3" thick block going the entire perimeter of the test plate. Figure 3-4 shows the exploded view of the assembly, along with the steps for construction.

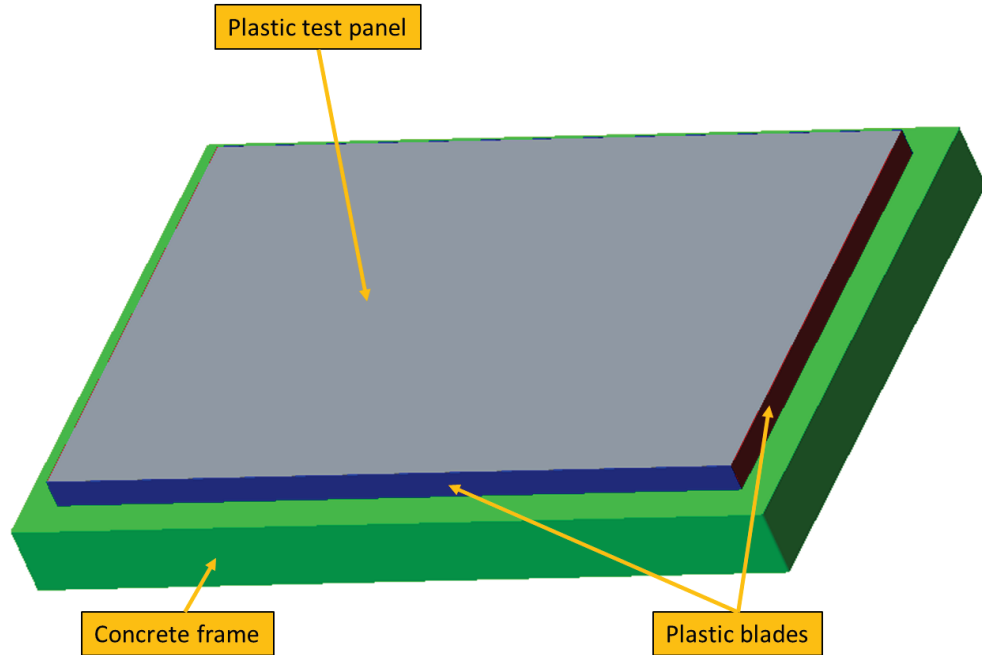


Figure 3-3 A model of the test assembly

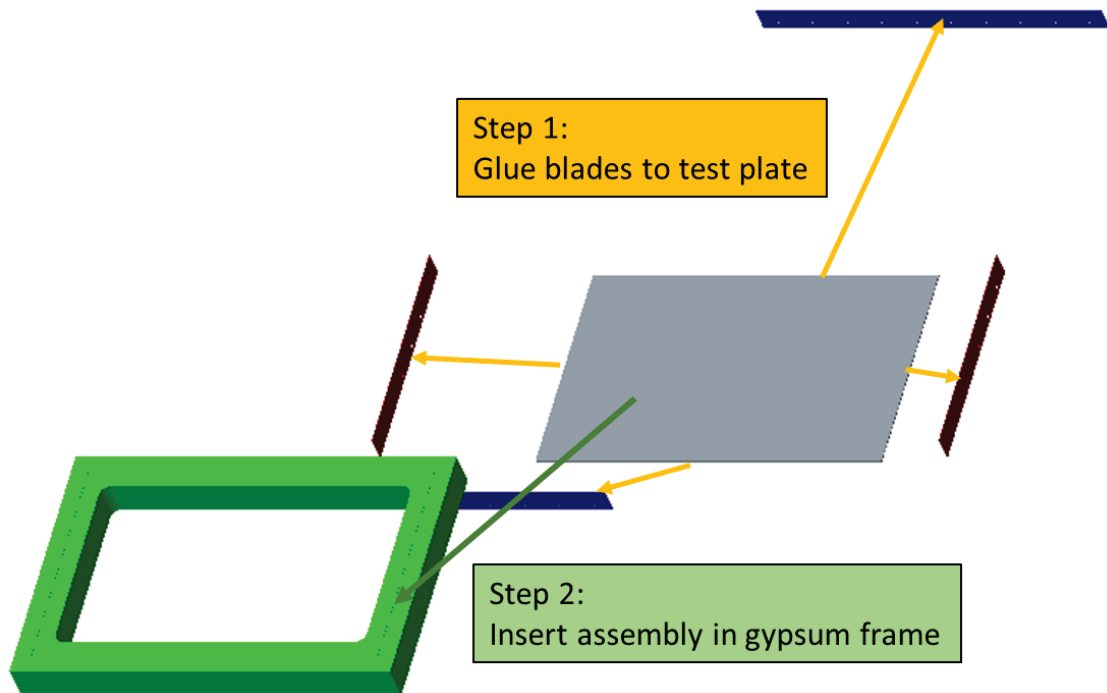


Figure 3-4 A model of the test assembly (exploded view)

The side blades were glued to the test plate, using Loctite 444 as a sealant and Loctite 7452 as an adhesive accelerator. As the glue sets in, the gypsum concrete was prepared, per supplier's recommendations, and poured into a wooden mold. The plate assembly was then pushed into the gypsum, in-keeping with the requirement of the height of the blade above the frame level, mentioned in the work done by Olivier et al [17].

A three-step process used to build the physical assembly is shown in Figure 3-5. Step 1a shows the preparation of wooden mold and step 2a show the base after the gypsum was poured. Step 1b and 2b shows the test plate and the gluing of the side blades on all four sides. The result of the final step is shown in step 3 as the test assembly now sits inside the gypsum concrete base. Once the gypsum dries, the side wooden molds were removed.

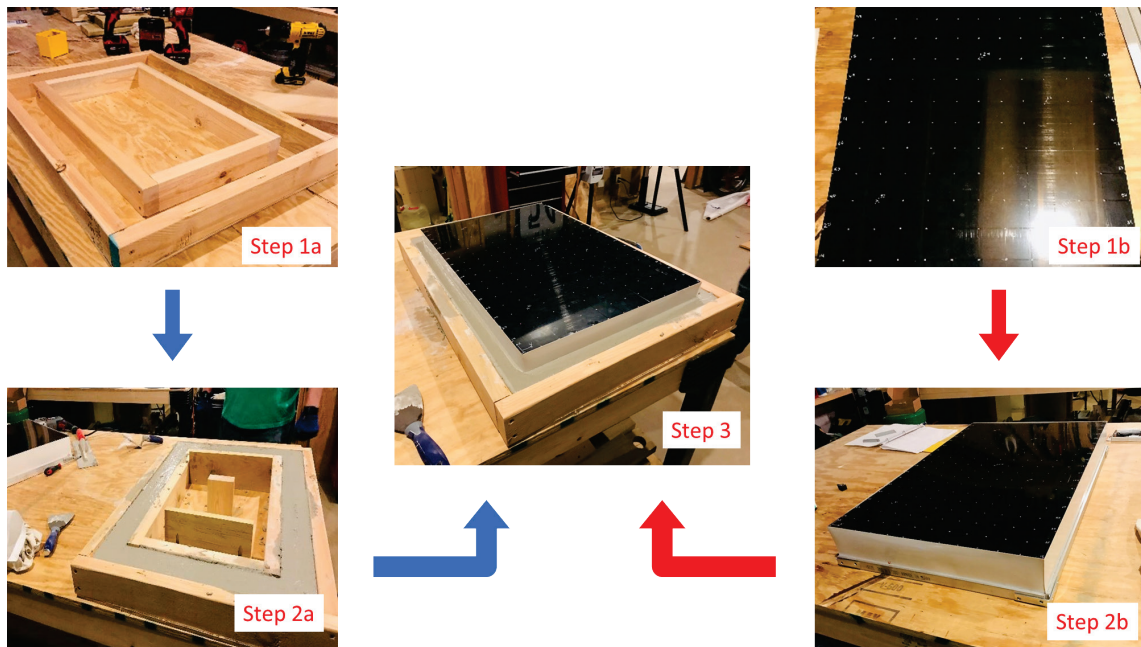


Figure 3-5 A three-step process showing how the assembly was built

3.1.2 Pre-test checks

Before beginning the final tests, it is advisable to run some pre-test checks to understand more about the test structure and to verify that it is behaving the way it is supposed to. In this section, we discuss the tensile test performed to obtain Young's modulus and Poisson's ratio, density measurement test, variation in the natural frequencies of the test assembly, and a reciprocity check for linearity.

3.1.2.1 Tensile test for Young's modulus and Poisson's ratio

The experimental Young's modulus and Poisson's ratio values for the test material were obtained by performing a tensile test. Six samples were cut to the recommended test sizes and the average Young's modulus and Poisson's ratio values obtained were 1.88×10^9 Pa and 0.41 respectively.

When these values were used to compute the analytical mobility, the comparison with experimental data was poor, so the values were modified by approximately 19.6% and 14.6%, to 2.25×10^9 Pa and 0.35, respectively. This difference in properties could potentially be caused due to the additional edge stiffness in the test assembly because of gluing of the blades on all four sides but further analysis is required to validate this assumption.

3.1.2.2 Density measurement test

The density of the test material was measured and compared with the values provided by the supplier. Ten samples of different sizes were cut from the material and their mass and volume were measured. The mean density obtained was 1028 (approximately 1030) kg/m^3 . These compare well with the density values provided by the supplier (1030 kg/m^3).

3.1.2.3 Variation in natural frequencies

The rigid and heavy gypsum concrete base frame takes some time to dry and as that happens, it changes its interactions with the plastic blades. This could potentially lead to a change in the dynamics of the test plate and it is important to understand this change. Driving point measurements for the test plate were recorded eight times over a total span of forty-five days to obtain the natural frequencies. Figure 3-6 tracks this change for five natural frequencies ranging from 200 – 300 Hz for one point on the test plate, and shows that the variation is within reason. This variation is due to the experimental error and not the variation in gypsum frame and its interaction with the plastic side blades. Figure 3-7 shows the mean and one standard deviation values for the same data and again concludes that the variation in the frequencies over different days does not raise any major concerns.

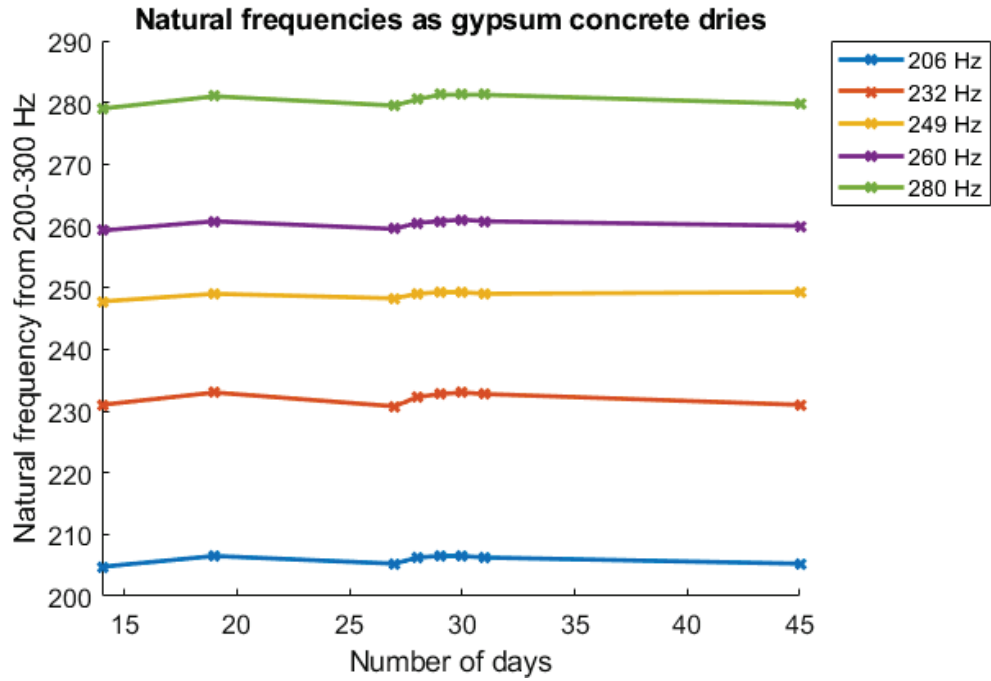


Figure 3-6 Tracking changes in natural frequency over forty-five days

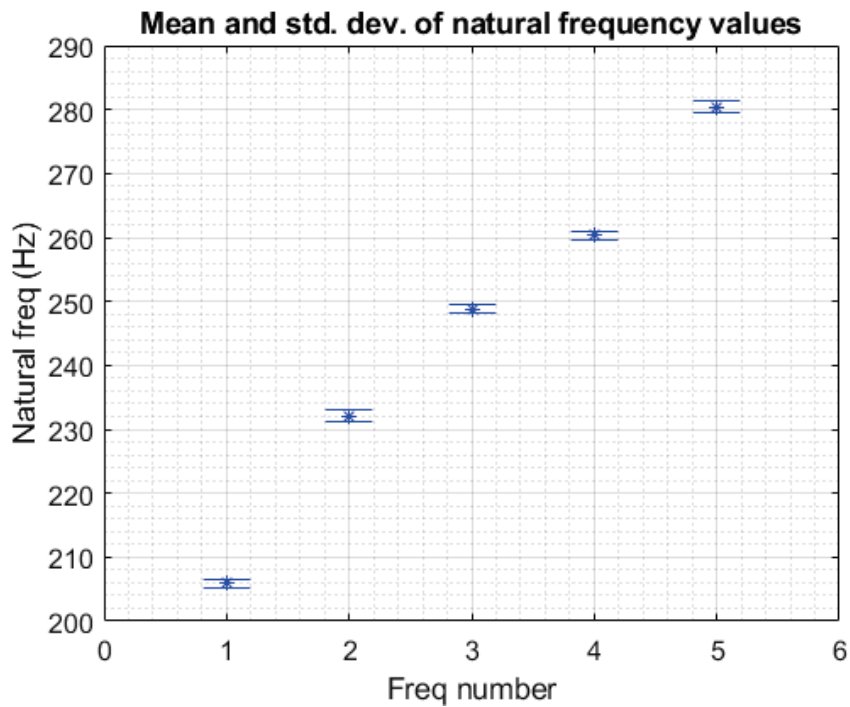


Figure 3-7 Mean and standard deviation of natural frequencies over forty-five days

3.1.2.4 Reciprocity check

If a structure is linear, the interchanging of response and reference (force input) location should not affect the measured Frequency Response Function (FRF). To verify this, a reciprocity check was done for two sets of points on the plate (points 101 and 124, and points 101 and 190, refer Section 3.2.1 for details on the points chosen). Figure 3-8 and Figure 3-9 presents this comparison, respectively. It can be observed that the two responses match fairly well and the structure shows good reciprocity in the frequency bandwidth. It is worth noting that the comparison is shown only below 500 Hz. The hammer tip used for the experiment can excite the structure only for frequencies lower than 500 Hz. More information on the hammer tip is provided in Section 3.2.1.1.

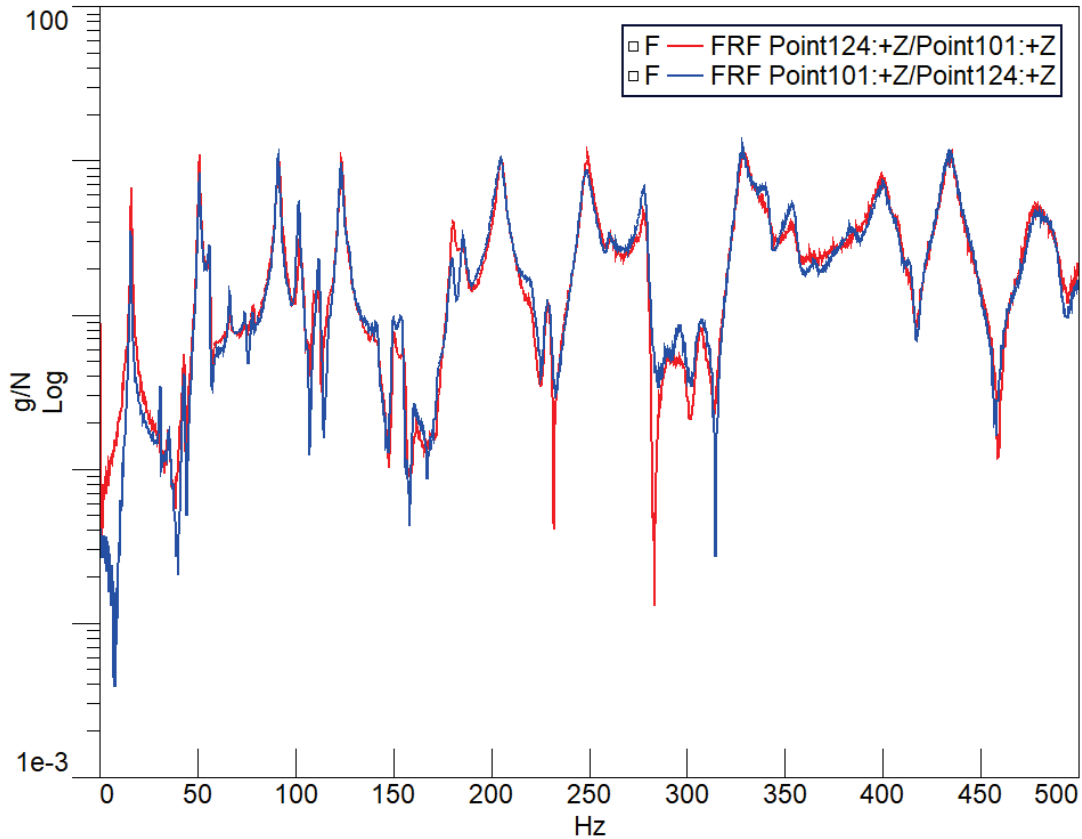


Figure 3-8 Reciprocity check for point 101 and 124 - 0 to 500 Hz

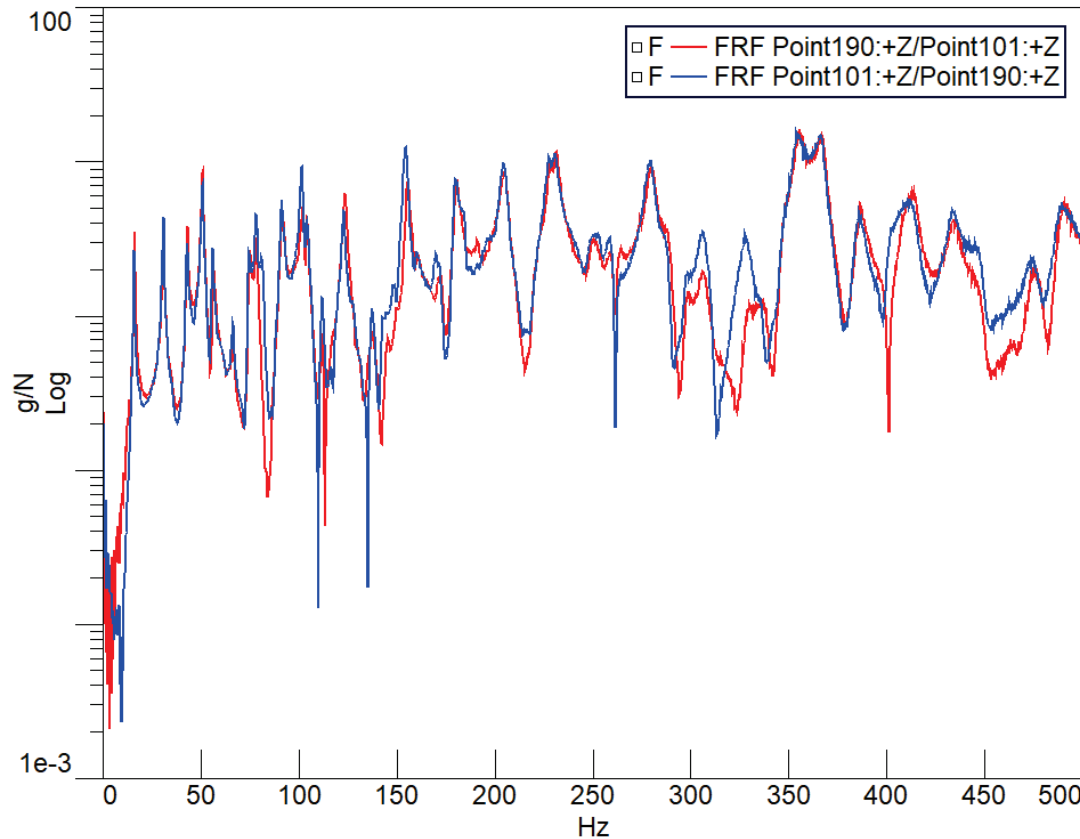


Figure 3-9 Reciprocity check for point 101 and 190 - 0 to 500 Hz

3.2 Mode Shapes

In this section, the experimental modal analysis and the comparison of experimental and analytical mode shapes are presented.

3.2.1 Experimental modal analysis

The experimental mode shapes were extracted through a modal analysis conducted using a roving hammer test. The test plate was distributed in 247 equally spaced grid points, 19 on the longer side and 13 on the shorter side (approximately 1.67 in (4.23 mm) and 1.58 in (4.02 mm) apart, respectively), as shown in Figure 3-10 (left). Note that the grid points are located at the edges of the plate too. This was done to ensure that any displacement in the edges of the test plate is zero, as would be expected from a simply supported structure. Figure 3-10 (right) shows the four accelerometer locations on the plate, highlighted with red dots. The number written next to these four locations is the point

number and these will be referred to in the upcoming sections while discussing the results.

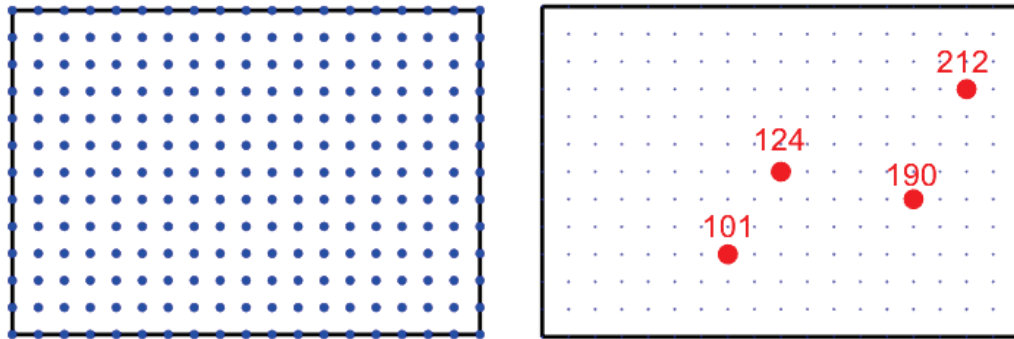


Figure 3-10 247 grid locations shown with blue dots (left) and four accelerometer locations (right)

The serial number of all the transducers used and the data acquisition parameters for the experiment are presented in Table 3-2 and Table 3-3 respectively.

Table 3-2 Model numbers for PCB transducers used

Transducer type	Model number
Impact hammer	086C03 SN22890
Accelerometer on pt. 101	352A21 SN LW200991
Accelerometer on pt. 124	352A21 SN LW240952
Accelerometer on pt. 190	352A21 SN LW240953
Accelerometer on pt. 212	352A21 SN LW202124

Table 3-3 Data acquisition parameters for modal analysis

Parameter	Value
Software used	LMS Test.Lab Spectral Testing
Frequency resolution (Δf)	0.25 Hz
Acquisition time	4 seconds
Bandwidth	1024 Hz
Window on reference channel	Uniform
Window on response channels	Uniform

In the upcoming sub-sections, we discuss the selection of an appropriate hammer tip and number of averages for the impact test.

3.2.1.1 Selection of hammer tip

The frequency bandwidth excitation due to an impact hammer depends upon the type of the hammer tip used. Three different types of tips were considered for the experiment: steel tip (hard), white vinyl tip (medium), and red tip (soft). With some initial data, the steel tip and white vinyl tip showed considerable effects of a double hit phenomenon (Figure 3-11). This double hit impact means that the hammer was impacting the structure twice in the same measurement period, which affected the overall response of the test structure. The most probable reason for this may be that the plastic plate is very responsive and it is difficult to pull the hammer away from the structure fast enough to ensure a single hit. The problem was intensified when the input force to the structure was high because of the harder hammer tips, such as steel and white vinyl. To get rid of this complication, the soft red tip was chosen for the rest of the experiment. The red tip does not show considerable effects of double hits in the time domain in Figure 3-11.

On the downside, with the red tip, the frequency bandwidth excited was limited to about 500 Hz (Figure 3-12) and this limits the frequency bandwidth for comparison of the modal test with the analytical data.

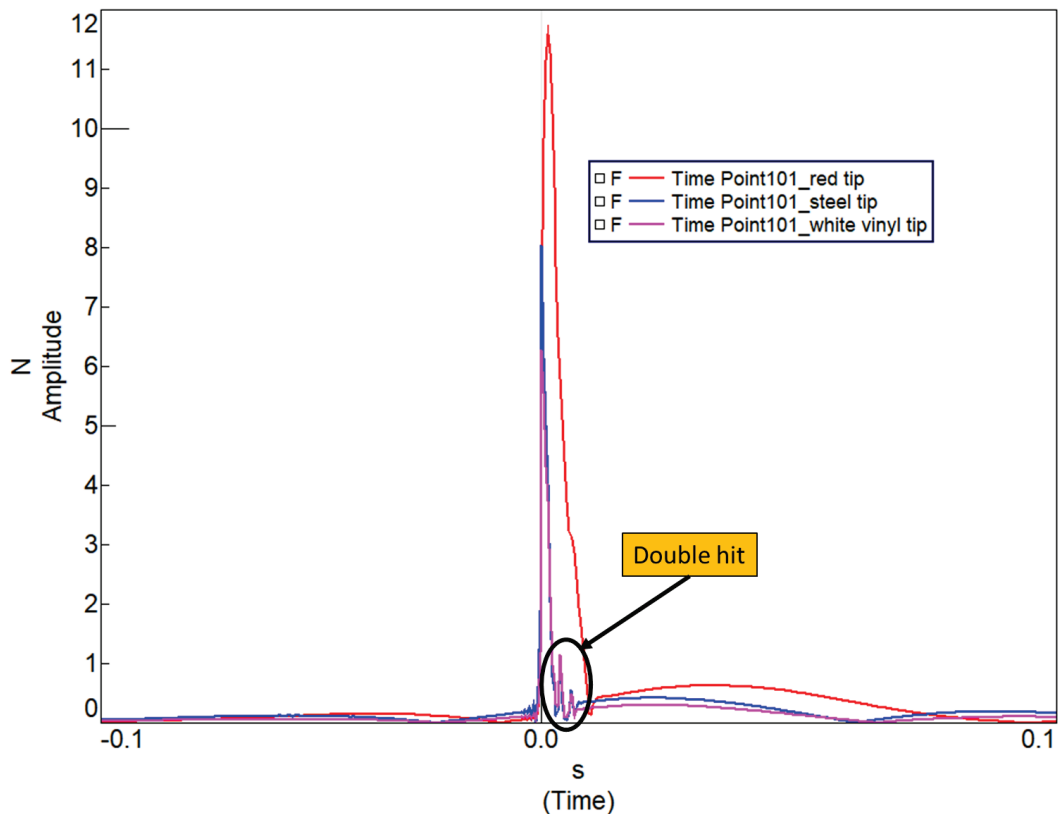


Figure 3-11 Reference signal for different hammer tips in the time domain

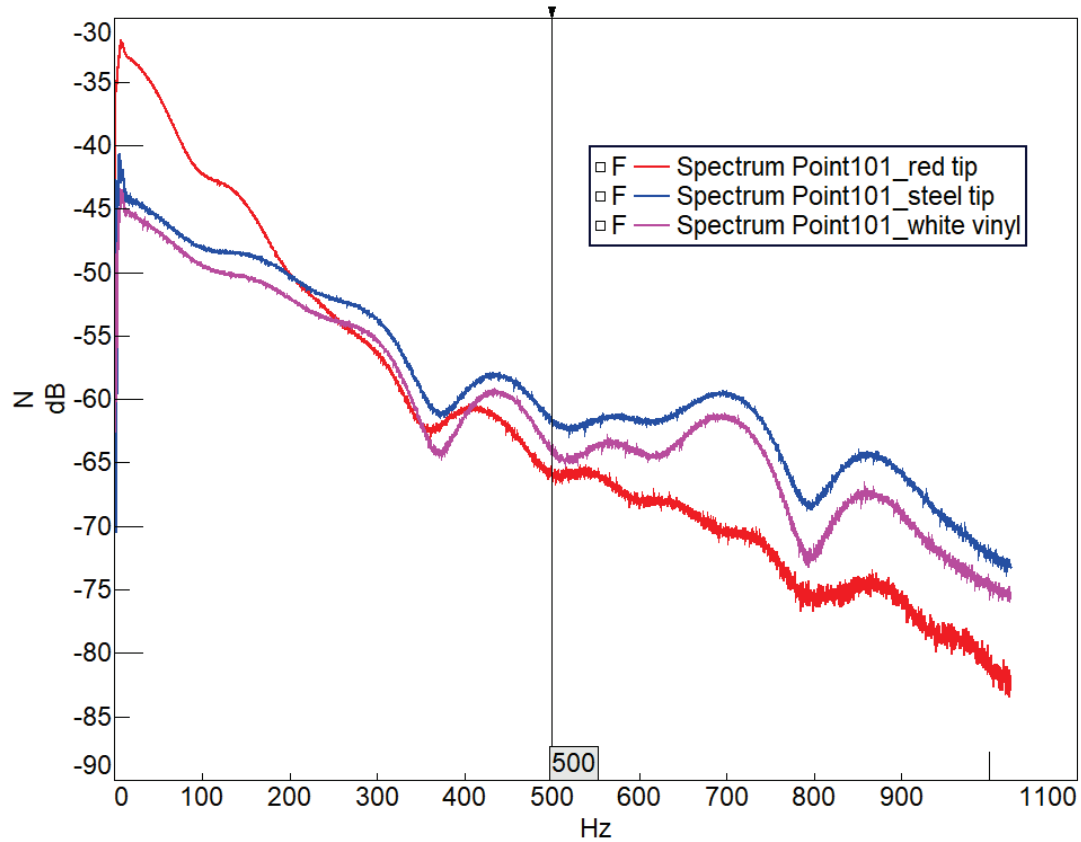


Figure 3-12 Reference signal for different hammer tips in the frequency domain

3.2.1.2 Number of averages

Measured data were averaged from three to seven times for a driving point (point 101) and the coherence and FRFs are represented in the top and bottom plots in Figure 3-13, respectively. All the FRFs line up well and seven averages were used for the rest of the impact test.

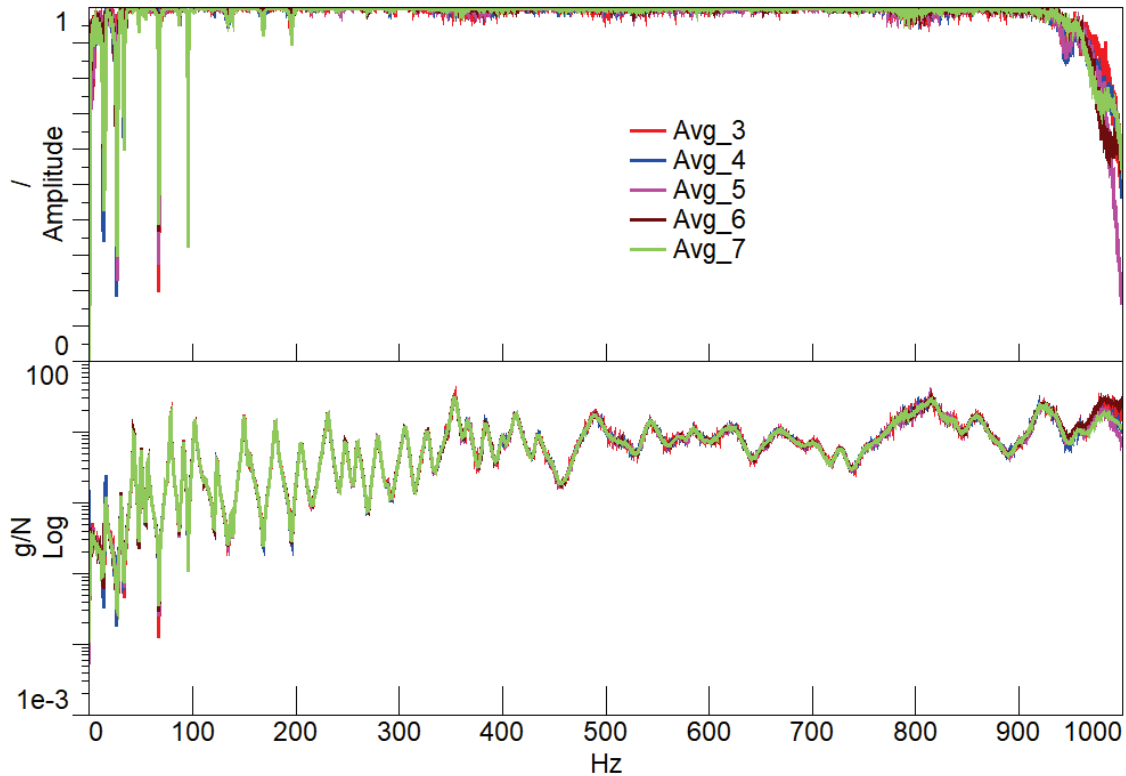


Figure 3-13 Coherence (top) and FRFs (bottom) for driving point measurements for three to seven averages (point 101)

3.2.2 Results

The FRFs recorded from the impact hammer test were solved for poles and residues using the PolyMAX algorithm available in the software package. The stabilization diagram (for mode picking) for one of the OTO bands (250 Hz) is shown in Figure 3-14 as an example, with the stable modes highlighted. This stabilization diagram was obtained by solving the model with an order of “80” in PolyMAX.

The experimental data shows nine stable modes in the stabilization diagram but only eight of those nine were observed in the analytical data for this frequency band. Our assumption is that eight out of these nine experimental modes (highlighted in red) are plate modes and the one additional mode (231 Hz - highlighted in blue) is the mode of the gypsum concrete base. To verify this assumption, a modal analysis of the gypsum concrete structure was performed and the results are presented in Section 3.2.2.1.

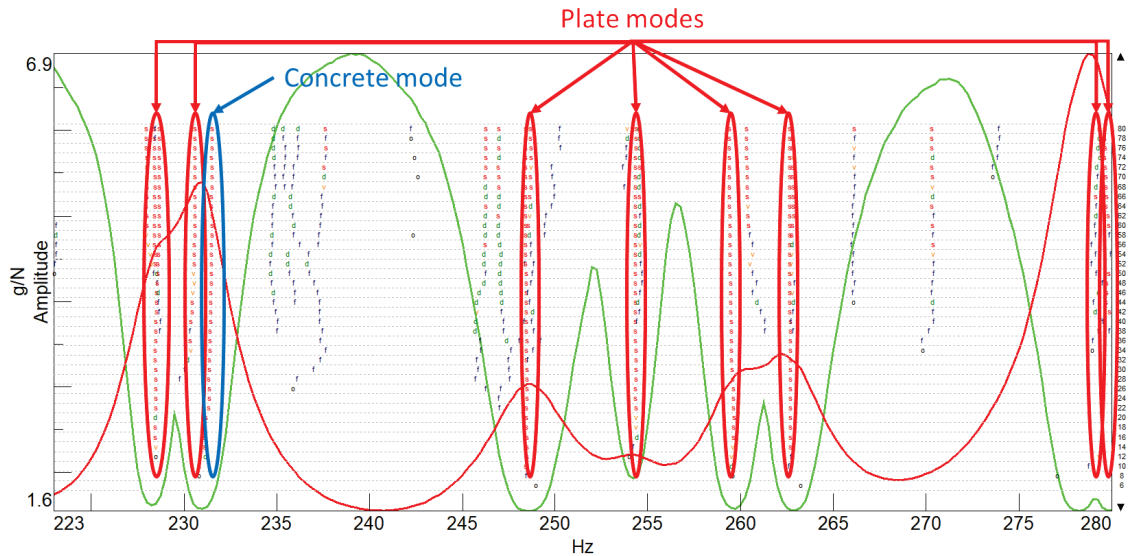


Figure 3-14 Stabilization diagram for mode picking - 250 Hz OTO

One of the major reasons for using a heavy, rigid base for the simply supported assembly was that this base assembly should not affect the modes of the test plate in the frequency range of interest. In this case, the base assembly is affecting the results even at low frequencies. This unwanted effect could be removed from the data by constructing an even heavier, more rigid assembly but this assertion needs further analysis. For the case of this study, the effect of the gypsum concrete base was ignored. The test plate modes were intelligently selected from the stabilization diagram based on the expectations from analytical predictions.

3.2.2.1 Modal analysis of the gypsum concrete base

A roving accelerometer modal analysis test was performed for the concrete structure for a total of twenty points in all three directions (x, y, and z – directions of the plate). Repeating the PolyMAX process for the experimental data, one of the modes of the concrete base was observed at approximately 232 Hz, shown in Figure 3-15. This proves that the earlier assumption for the additional mode showing up in the stabilization diagram for 250 Hz OTO (Figure 3-14) is a gypsum concrete base mode instead of a test plate mode.

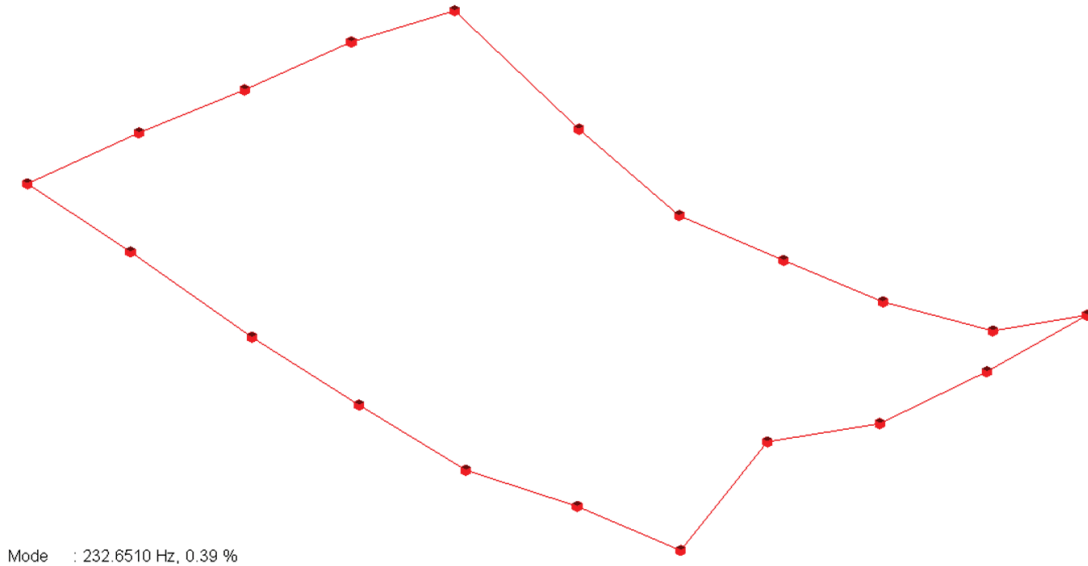


Figure 3-15 Mode shape of the gypsum concrete base at 232 Hz (approximately)

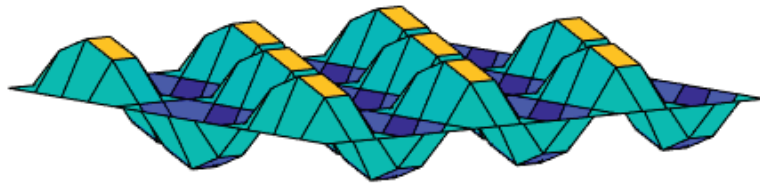
3.2.2.2 Comparison of the mode shapes

Figure 3-16 to Figure 3-23 show the comparison of experimental and analytical mode shapes for the modes in 250 Hz OTO band, along with the mode order (m , and n), as an example. An important thing to be noted here is that for the experimental mode shapes, the boundaries of the plate have non-zero displacement, even with the simply supported boundary conditions. This is due to the fact that the impact location of the hammer was not on the exact edge of the plate, but a few millimeters farther inside from the edge. This is why this displacement shown here for the edges is the experimental error.

Overall, Figure 3-16 to Figure 3-23 show a good comparison of experimental and analytical mode shapes. A similar level of comparison is also observed for mode shapes in the other OTO bands in the frequency bandwidth (not presented in this report).

228.9 Hz mode, $m = 6, n = 3$

Analytical



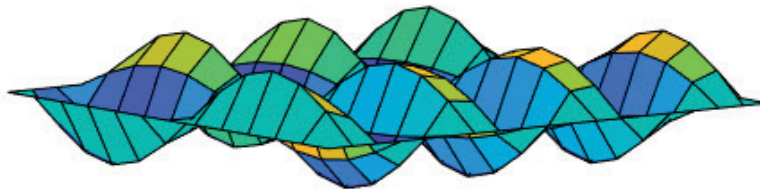
Experimental



Figure 3-16 Mode shape comparison - 228.9 Hz

230.9 Hz mode, $m = 7, n = 2$

Analytical

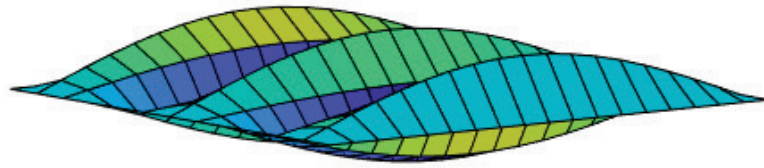


Experimental



Figure 3-17 Mode shape comparison - 230.9 Hz

248.0 Hz mode, $m = 1, n = 5$
Analytical



Experimental

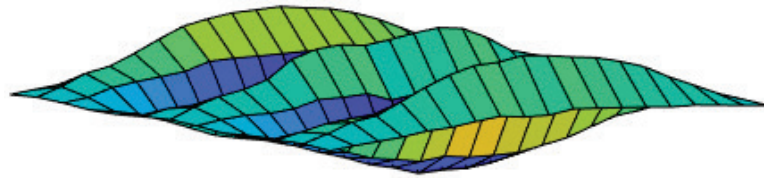


Figure 3-18 Mode shape comparison - 248 Hz

254.1 Hz mode, $m = 5, n = 4$
Analytical



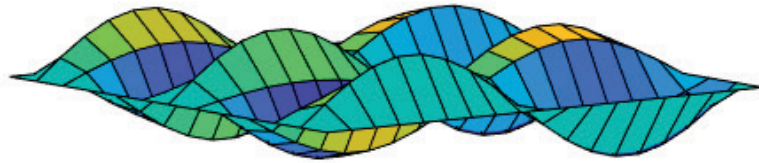
Experimental



Figure 3-19 Mode shape comparison - 254.1 Hz

259.7 Hz mode, $m = 2, n = 5$

Analytical



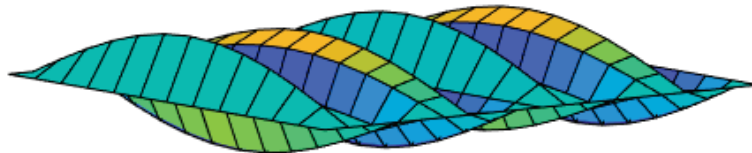
Experimental



Figure 3-20 Mode shape comparison - 259.7 Hz

260.4 Hz mode, $m = 8, n = 1$

Analytical



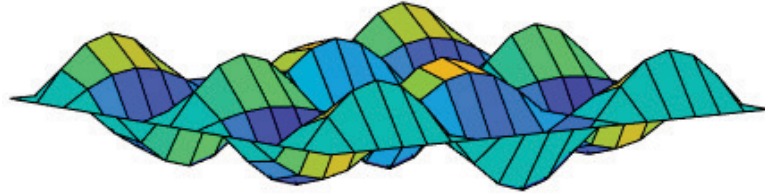
Experimental



Figure 3-21 Mode shape comparison - 260.4 Hz

279.3 Hz mode, $m = 3, n = 5$

Analytical



Experimental

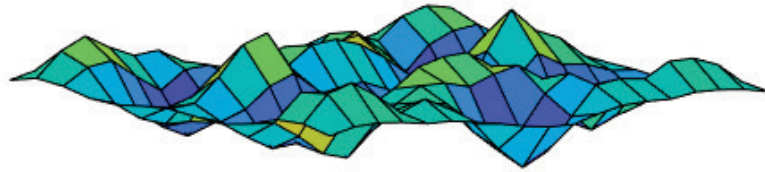
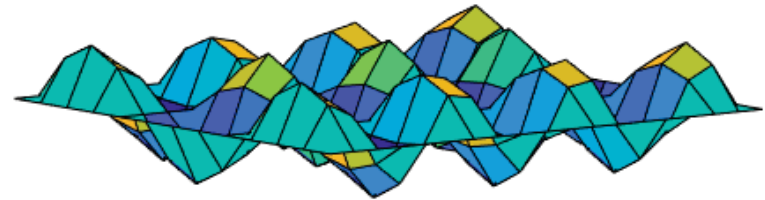


Figure 3-22 Mode shape comparison - 279.3 Hz

279.8 Hz mode, $m = 7, n = 3$

Analytical



Experimental



Figure 3-23 Mode shape comparison - 279.8 Hz

3.2.2.3 Modal Assurance Criterion (MAC)

The MAC matrix obtained through comparison between analytical and experimental data has several similarities to the Auto-MAC discussed in Section 2.2.1. If the analytical and experimental data compare well, the MAC values at the diagonal elements of the MAC matrix will be closer to one and off-diagonal elements will be closer to zero. Figure 3-24 shows the MAC correlation between the analytical and experimental mode shapes for the 250 Hz OTO band. As expected, the diagonal elements are close to one and all the off-diagonal elements are close to zero. This shows a good correlation between the analytical and experimental mode shapes.

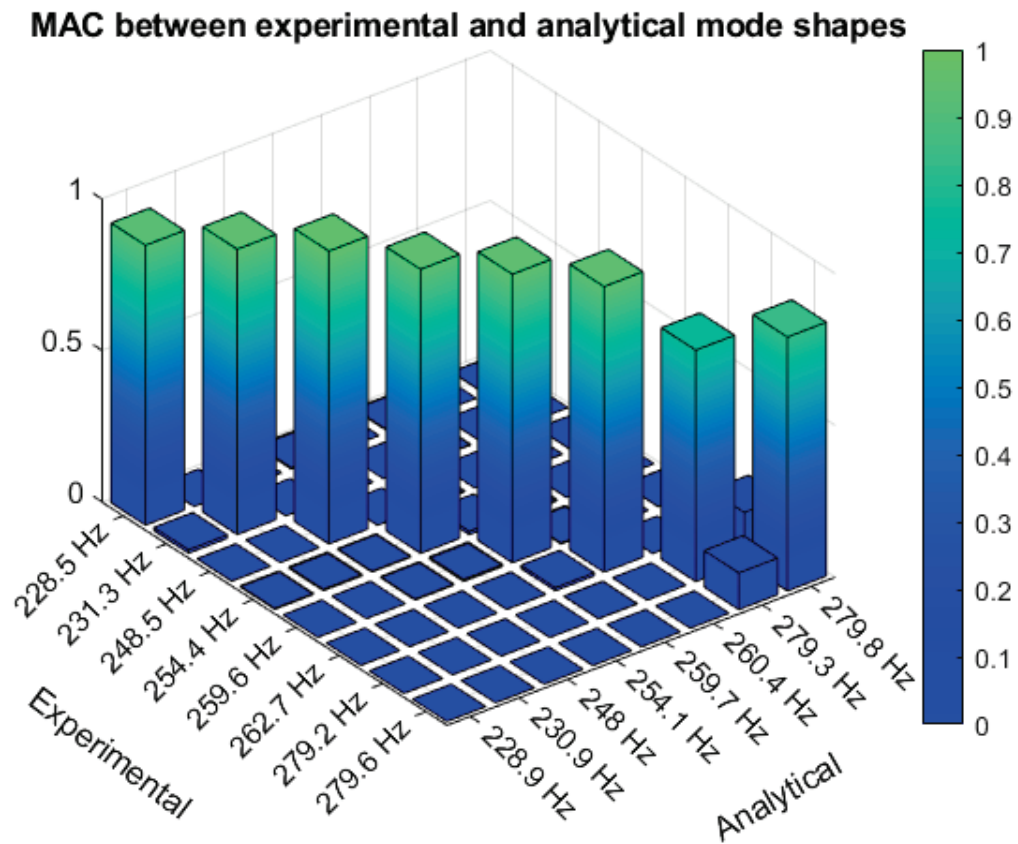


Figure 3-24 MAC for experimental and analytical mode shapes – 250 Hz OTO

3.3 Mobility

This section discusses the process to obtain experimental mobility and comparison with analytical predictions.

3.3.1 Experimental mobility

The data recorded for the modal analysis were used to obtain experimental mobility of the test plate, by converting acceleration-based FRFs (accelerance) to velocity-based FRFs (mobility) using

$$mobility = \frac{accelerance}{i\omega} \quad (3-1)$$

3.3.2 Comparison of analytical and experimental mobility

The experimental driving point mobility for the four response locations for frequencies ranging from 100 Hz to 500 Hz is compared with the analytical predictions from Figure 3-25 to Figure 3-28. Since the impact hammer was unable to excite frequencies higher than 500 Hz, data higher than 500 Hz is not presented.

In general, the analytical and the experimental data match fairly well but some additional peaks show up in the experimental data. These additional peaks correspond to the modes of gypsum concrete (as discussed in Section 3.2.2). It is also important to note that the response of the infinite plate is approximately the mean of the test plate's response over the entire frequency bandwidth presented.

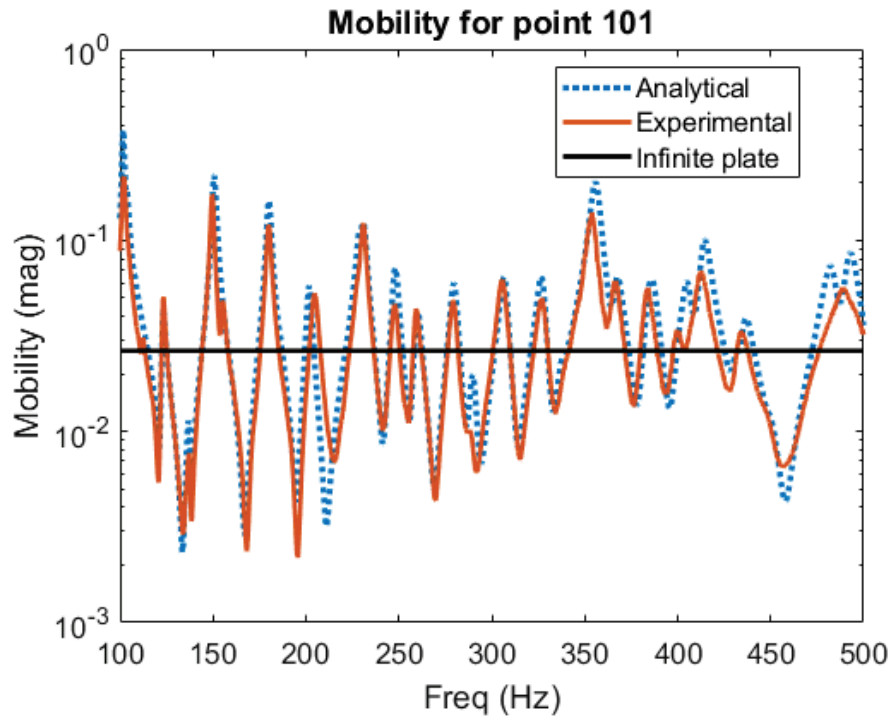


Figure 3-25 Driving point mobility for response at point 101

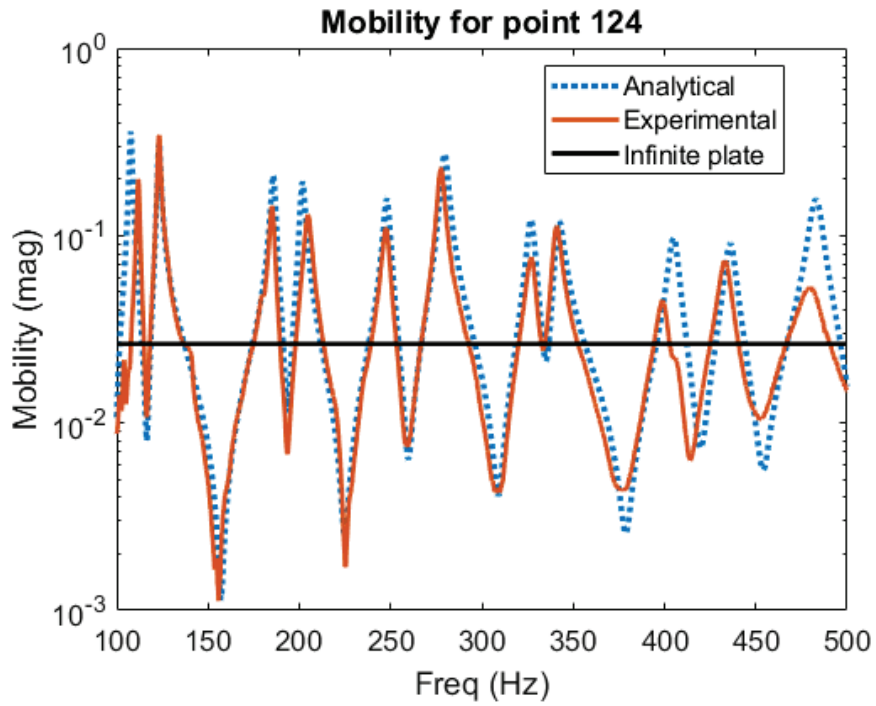


Figure 3-26 Driving point mobility for response at point 124

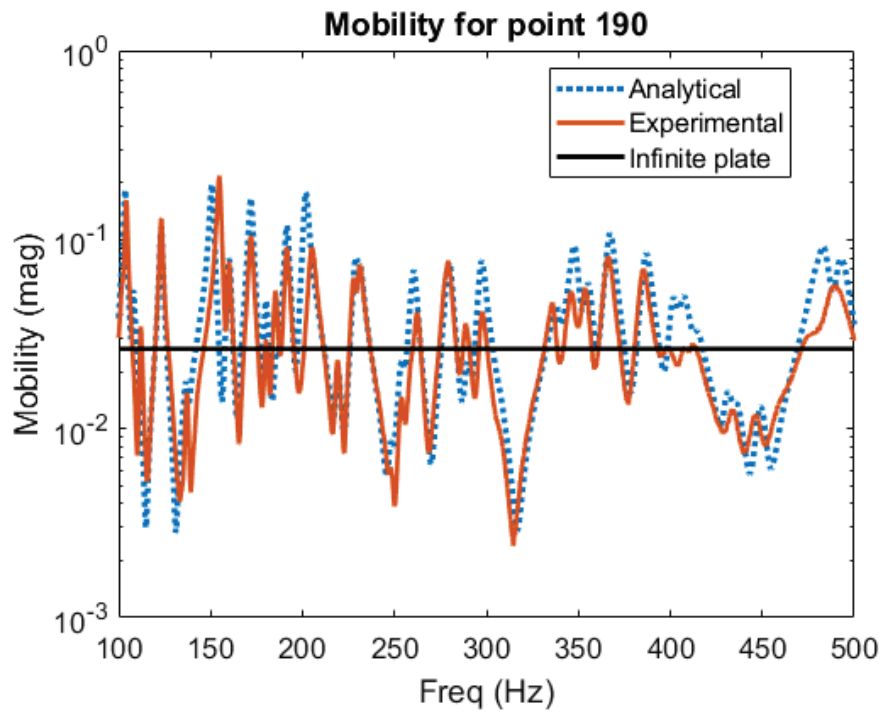


Figure 3-27 Driving point mobility for response at point 190

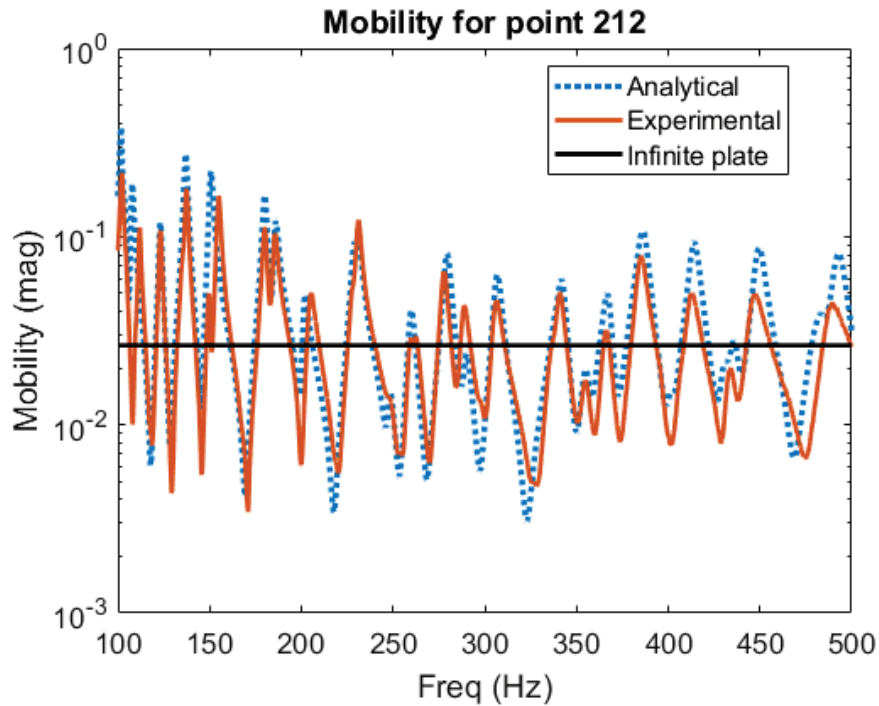


Figure 3-28 Driving point mobility for response at point 212

For one of the OTO bands, 250 Hz, the driving point mobility for all four response points are presented in Figure 3-29, where the blue dotted line represents the analytical data (denoted by An.), the orange line is the experimental data (denoted by Exp.) and the black line is the response of an infinite plate (denoted by Inf.).

It could be observed that the experimental data compare well with the analytical predictions and the response of the infinite plate is the approximate mean of the response of the test plate.

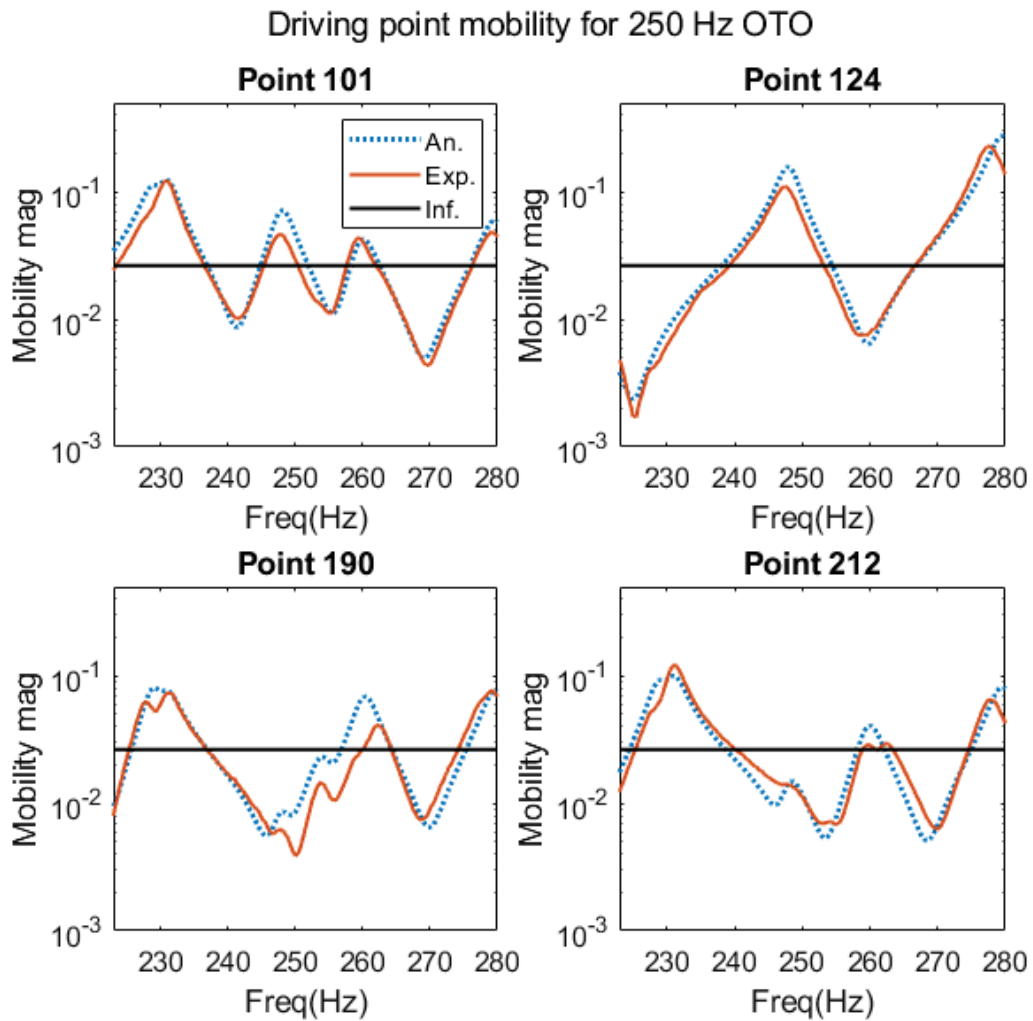


Figure 3-29 Driving point mobility for all response locations for 250 Hz OTO

Figure 3-25 to Figure 3-29 present only the drive point mobilities but the sound radiation depends upon the averaged surface mobility for all the points. The analytical and experimental results for surface averaged mobility for 250 Hz OTO band are represented in Figure 3-30 and it shows that the analytical predictions match well with experimental data. This means that the mobility of any point on the plate could be reliably predicted using some analytical calculations. Multiplying this mobility with the input force gives the surface velocity and sound radiated from the structure depends upon this surface velocity. A good comparison of analytical and experimental mobility instills some confidence in showing that sound radiation could be reliably predicted. In the next section, we discuss the experimental methods used to measure sound power and compare it with the analytical sound power levels.

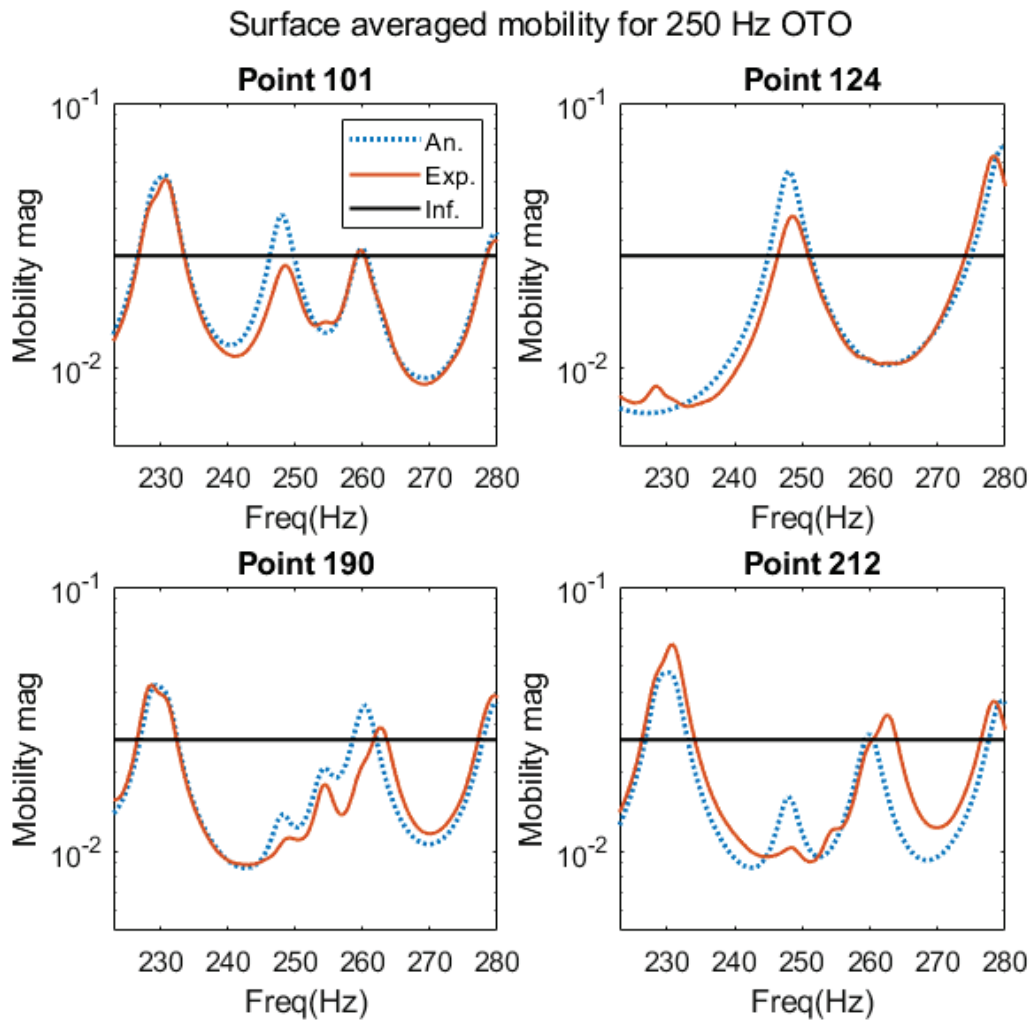


Figure 3-30 Surface averaged mobility for all response locations for 250 Hz OTO

3.4 Sound power radiation

The experimental sound power of the test structure was obtained through a discrete point intensity test performed in the anechoic chamber. In this section, we discuss the details of this intensity test, the participation of the input force, and compare the analytical and experimental results of sound power radiation.

3.4.1 Intensity probe testing

To closely simulate the sound radiation in an infinite baffle, the test plate was mounted on foam to reduce the effect of sound radiated from the bottom surface. This foam mounting is shown in Figure 3-32. The sound intensity values were measured on 56 grid points and these grids were distributed such that they all have the same surface area ($0.25 \times 0.25 \text{ m}^2$). Figure 3-31 shows the 56 measurement areas with red squares and the measurement locations are highlighted with black-colored dots. These measurement locations give the average intensity value over one measurement area (one red square).

Measurement locations for the intensity test grid

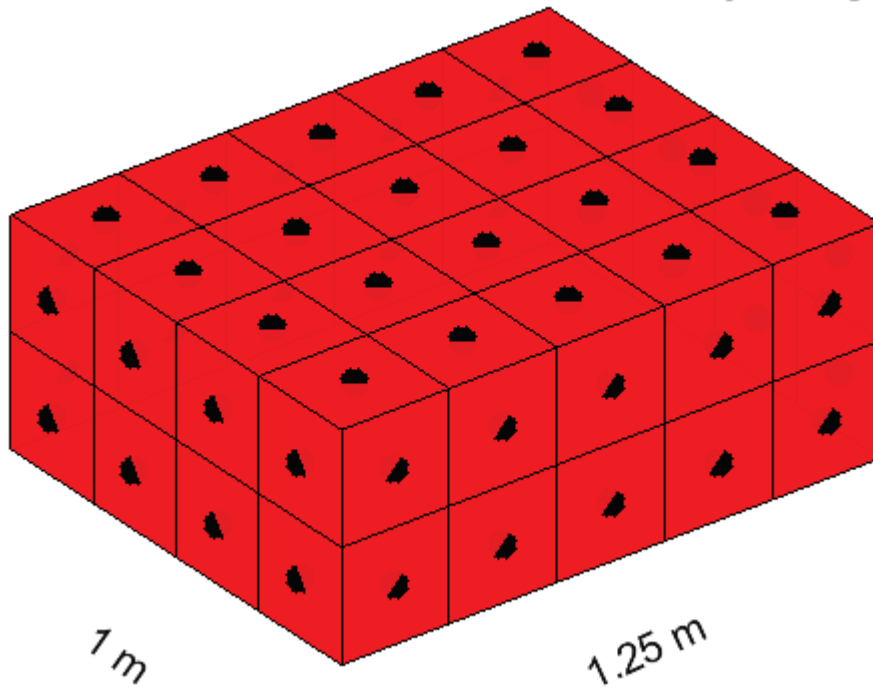


Figure 3-31 Measurement area for intensity test shown with red squares and measurement locations shown with black dots

The assembly was tested in an anechoic chamber to simulate acoustic free-field conditions. Force input was provided using a TMS shaker (K2007E01 SN 1738), controlled remotely from outside the test chamber. The response was measured using a GRAS Intensity probe (microphones: 40AI SN 6934 and 6948), shown in Figure 3-33 and highlighted in Figure 3-32. The measurement uncertainty was characterized using field indicators, as explained in Appendix A.

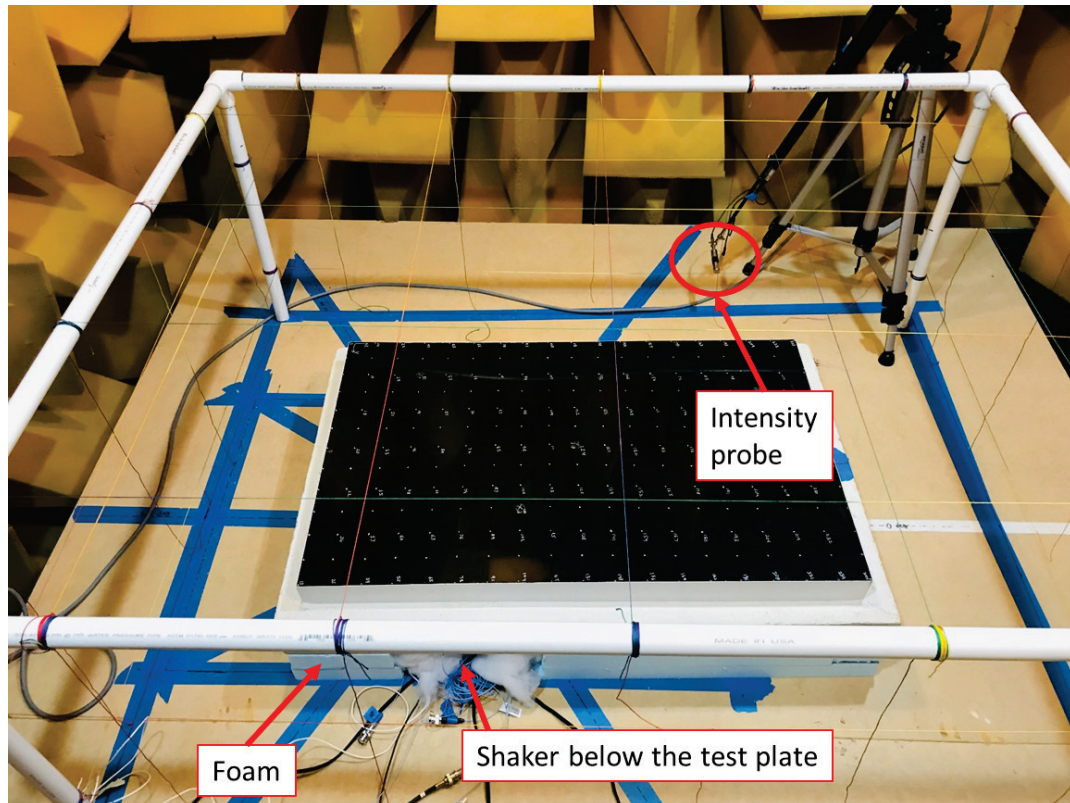


Figure 3-32 Intensity probe and the grid used for Intensity measurement test. Input shaker is below the structure, cannot be seen in the picture

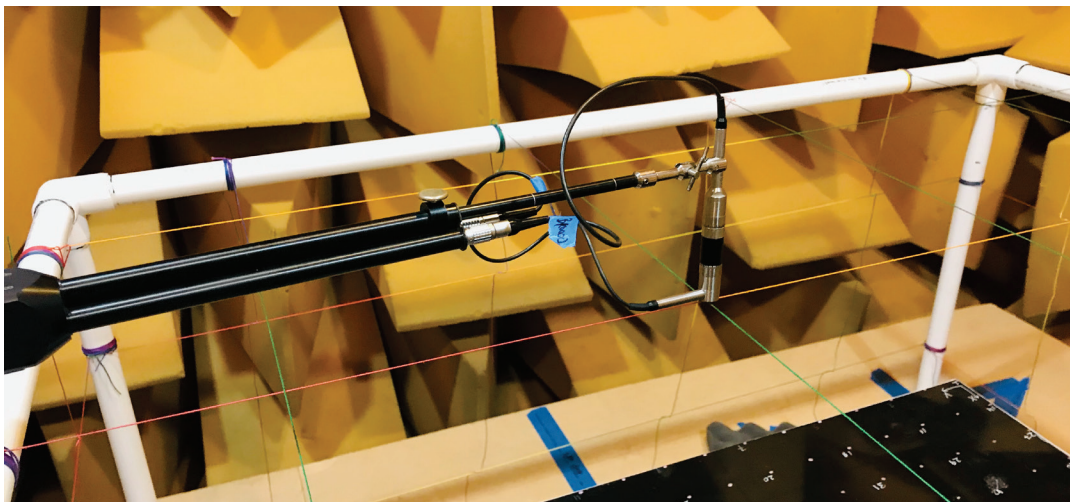


Figure 3-33 GRAS Intensity probe with 25 mm spacer

The data acquisition parameters and all other details related to the test are provided in Table 3-4

Table 3-4 Details of data acquisition parameters and the input signal for shaker

Parameter	Value
Software used	LMS Test.Lab Spectral Testing
Frequency resolution (Δf)	0.25 Hz
Acquisition time	4 seconds
Bandwidth	2048 Hz
Number of averages	40
Window on reference channel	Hanning
Window on response channels	Hanning
Shaker input signal	White Gaussian noise – 0.2 V RMS
Signal type	Burst random
Bandpass filter on input signal	10 Hz to 1024 Hz
Spacer used for GRAS intensity probe	25 mm

3.4.2 Input force participation

The response recorded in the intensity probe microphones depends upon the sound radiated from the test surface, which itself depends upon the input force. For ease of calculations, the analytical predictions assumed an input force of one Newton throughout the entire frequency band, but this was not the case for the experimental data. To avoid any complications in the processing due to this, the force contribution was removed from the experimental data by using Frequency Response Functions (FRFs) instead of the measured sound pressure response.

FRFs of the microphones are given by pressure response recorded by the mics per unit force, which means that the FRFs are the response of the structure for an input force of one Newton, assuming the structure is linear. Building on this idea, all the calculations for intensity using experimental data were performed using FRFs instead of the measured sound pressure response.

3.4.3 Comparison of results

Before discussing the comparison of analytical and experimental results, it is important to talk about the limitations of the experimental test set-up. The test was performed in an anechoic chamber and based on the design of this chamber, it is only good for frequencies higher than 125 Hz, approximately. Therefore, a good comparison of experimental and analytical data below 125 Hz OTO was not expected.

In this section, we take a look at the intensity heat maps of the test plate and compare the analytical and experimental OTO-based sound power levels.

3.4.3.1 Intensity heat maps

Figure 3-34 to Figure 3-41 show the intensity heat maps generated from actual measurements for OTO bands ranging from 160 Hz to 800 Hz. The plots are made based on the measurement locations represented with black-colored dots in Figure 3-31.

The purpose to present these intensity heat maps is to show the quality and consistency of measurement data and to confirm that as frequency goes up, it is expected to see an increased number of wavelengths for the same-sized surface. For example, 630 Hz and 800 Hz have about two wavelengths on the top measurement surface, as compared to the lower OTO bands that only have close to one wavelength. This is because of the fact that as frequency goes up, wavelength decreases and wavenumber increases, thus generating more number of wavelengths for the same surface area.

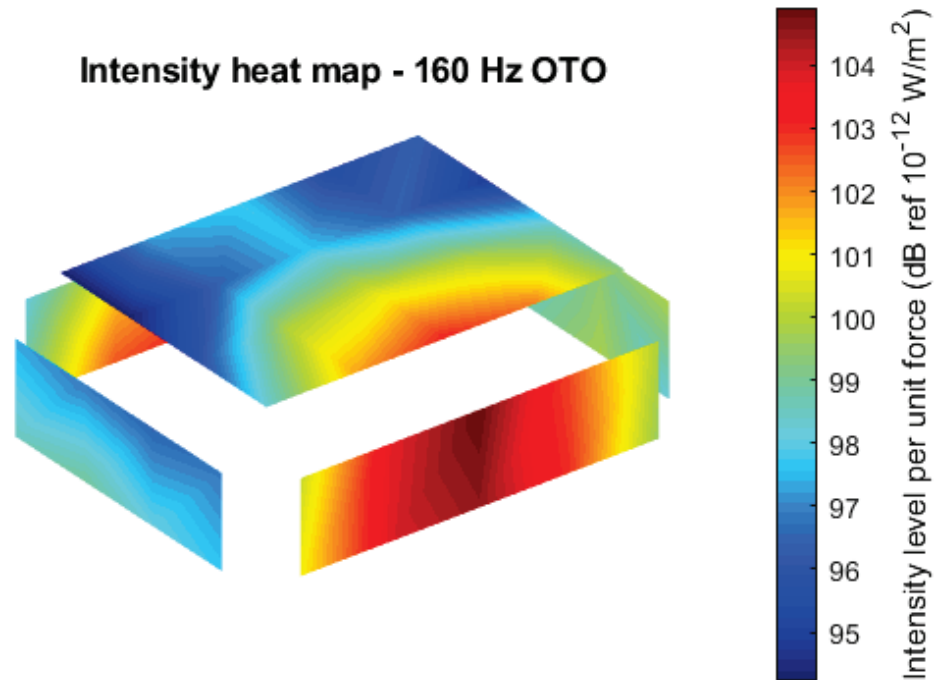


Figure 3-34 Intensity heat map - 160 Hz OTO

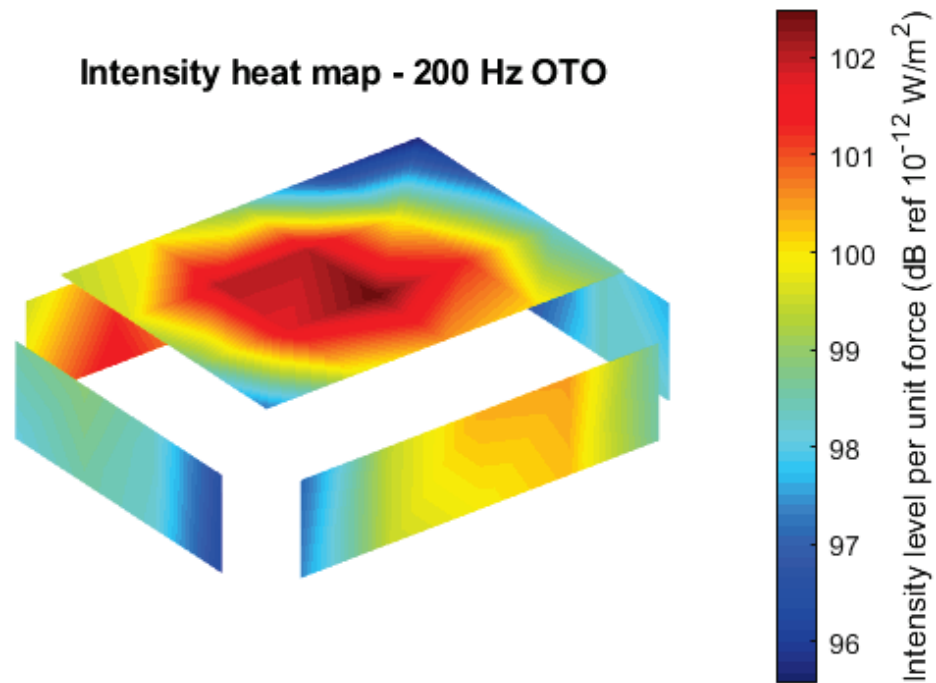


Figure 3-35 Intensity heat map - 200 Hz OTO

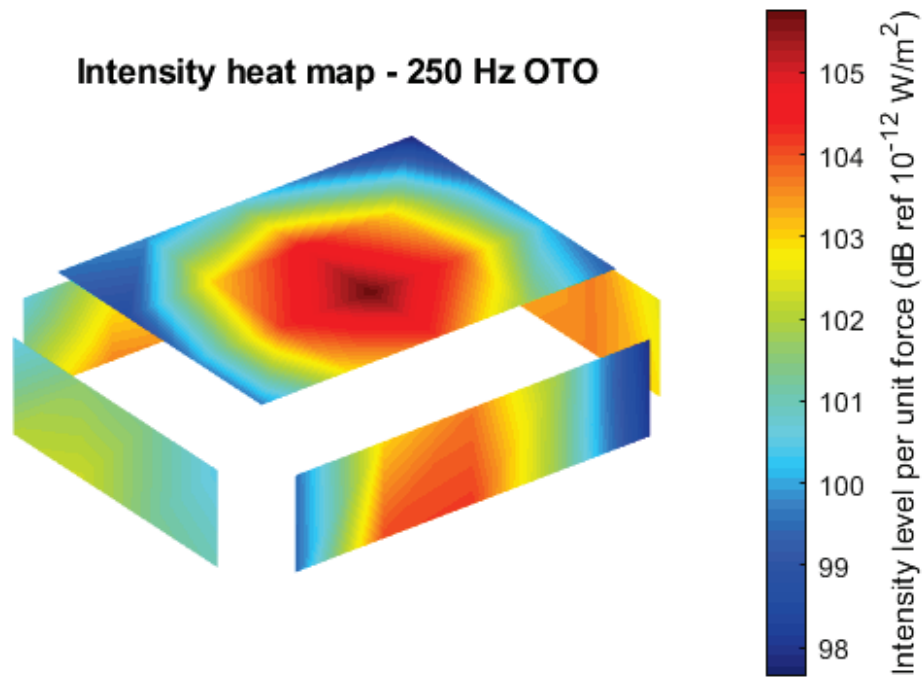


Figure 3-36 Intensity heat map - 250 Hz OTO

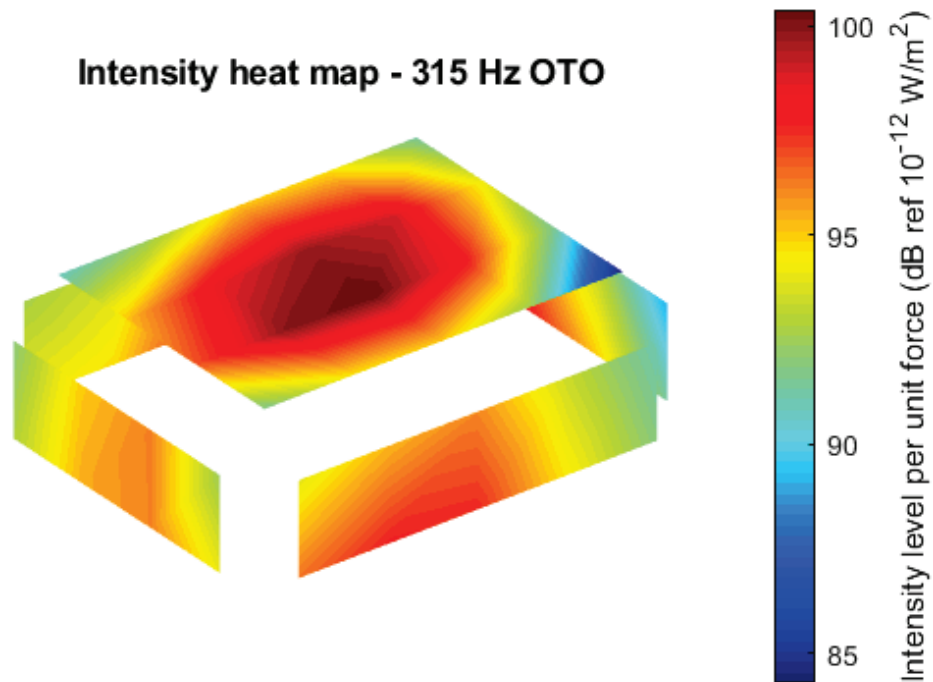


Figure 3-37 Intensity heat map - 315 Hz OTO

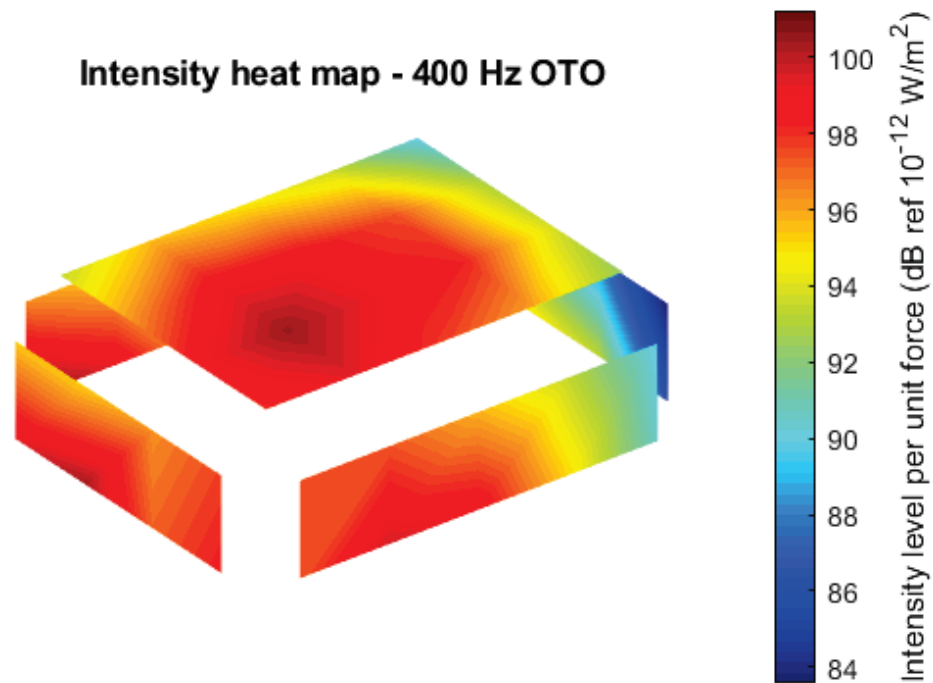


Figure 3-38 Intensity heat map - 400 Hz OTO

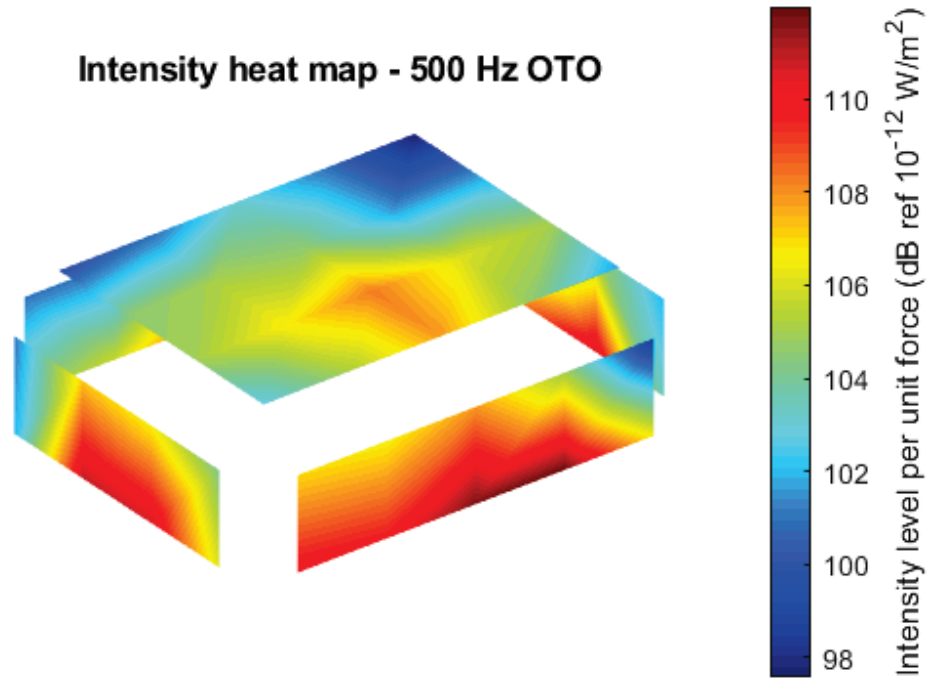


Figure 3-39 Intensity heat map - 500 Hz OTO

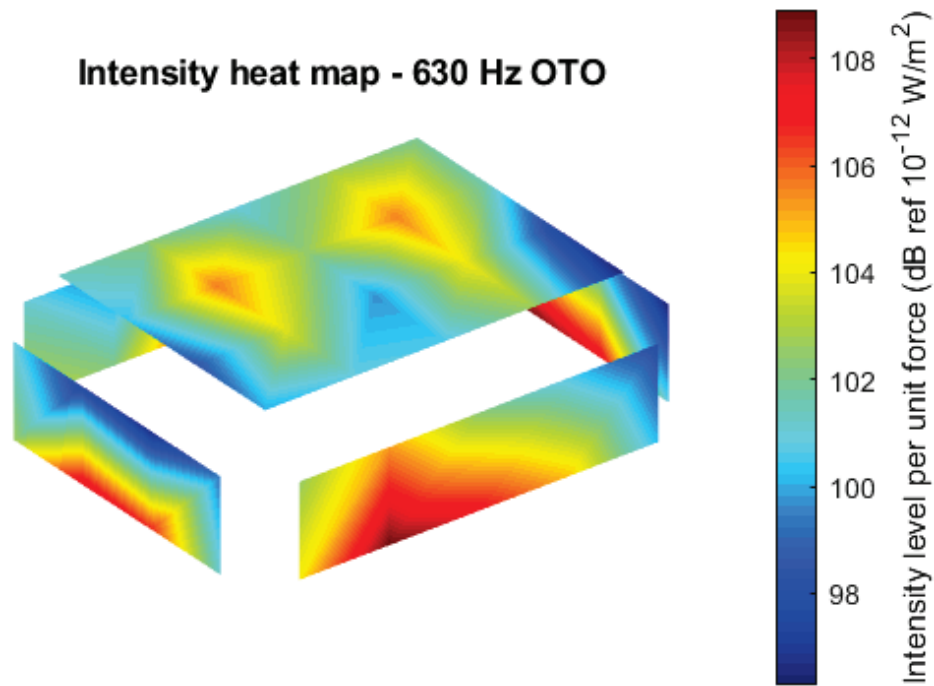


Figure 3-40 Intensity heat map - 630 Hz OTO

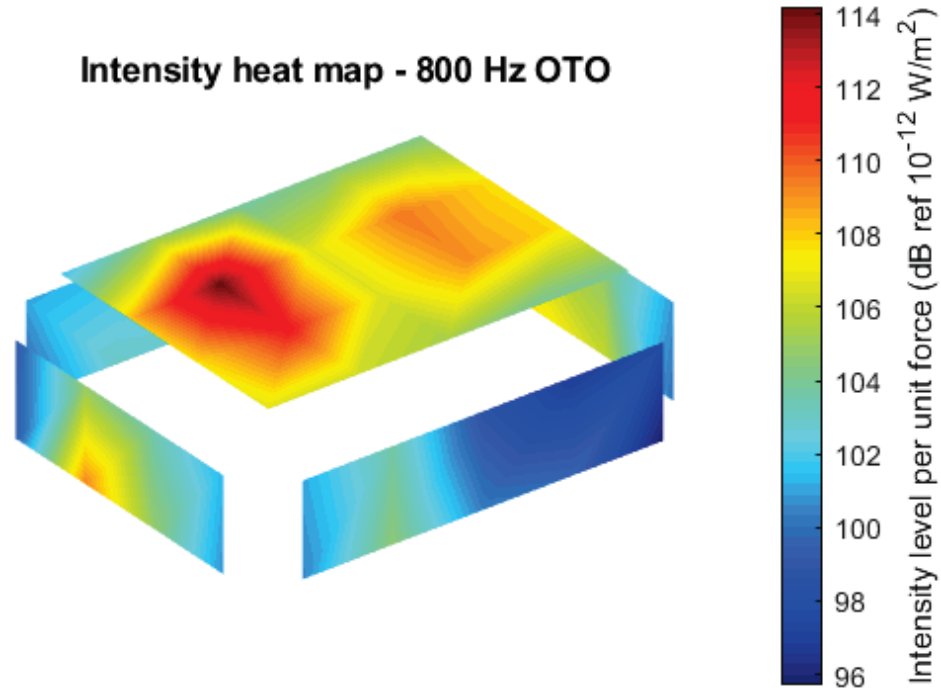


Figure 3-41 Intensity heat map - 800 Hz OTO

3.4.3.2 Sound power level comparison

The comparison of analytical predictions and experimental results is presented in Figure 3-43. The blue-colored bars are the analytical data, orange colored bars are experimental data, and the yellow colored bars represent how the analytical predictions under- or over-estimates the experimental results.

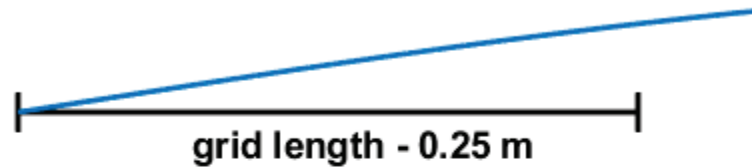
The comparison for the OTO bands below 125 Hz is not good. This is because of the limitations of the anechoic chamber, as discussed in Section 3.4.3. Some of the extraneous energy was canceling the acoustic energy flowing out from the structure at the measurement grid, thus reducing the intensity values measured by the probe microphones.

For bands ranging from 160 Hz to 400 Hz, the analytical data compares well with the experimental data (within 1-2 dB) but this is not the case for high-frequency OTO bands (500 Hz and above). This poor comparison in high-frequency OTO bands is due to the limitation of the measurement grids.

Recall from Section 3.4.1 that the intensity measurement grids have an area of 0.25×0.25 m². As we go higher up in frequency, the number of wavelengths per grid unit length increases, also increasing the uncertainty in measurements. Figure 3-42 shows the

portion of wavelength covered over the measurement grid length for 160 Hz and 800 Hz frequencies. For lower frequencies (160 Hz), the variation in SPL values over the grid length is lesser as compared to higher frequencies (800 Hz). Therefore, the grid spacing used for this experiment works well for low- to mid-frequencies but not for higher frequencies. To characterize the response of these higher frequencies, a finer grid should be used.

160 Hz over the measurement grid length



800 Hz over the measurement grid length

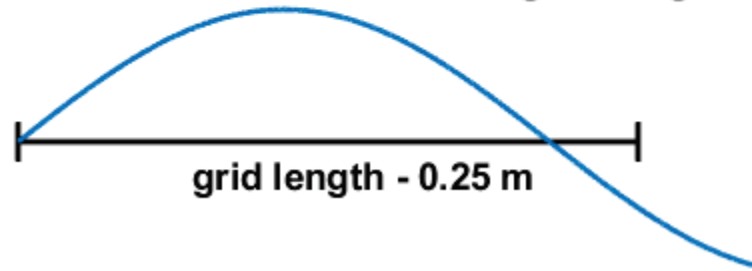


Figure 3-42 The portion of wavelength covered over the length of the test grid for 160 Hz and 800 Hz. Note that the measurement uncertainty is higher for higher frequencies

Another reason for the differences between analytical and experimental data was experimental errors, potentially caused by the following three reasons:

1. The concrete base has some modal participation over the frequency range of excitation (recall Section 3.2.2) and these modes of the concrete base also radiate some sound, which is not considered for the analytical sound prediction model.
2. Any inefficiency in blocking the sound radiating from the bottom face of the test plate with foam may cause the experimental levels to be higher than analytical predictions.
3. An imperfect assembly of the shaker to the test plate (error in controlling the exact location of the force input and the stinger angle for the shaker) would create an error while comparing analytical and experimental data.

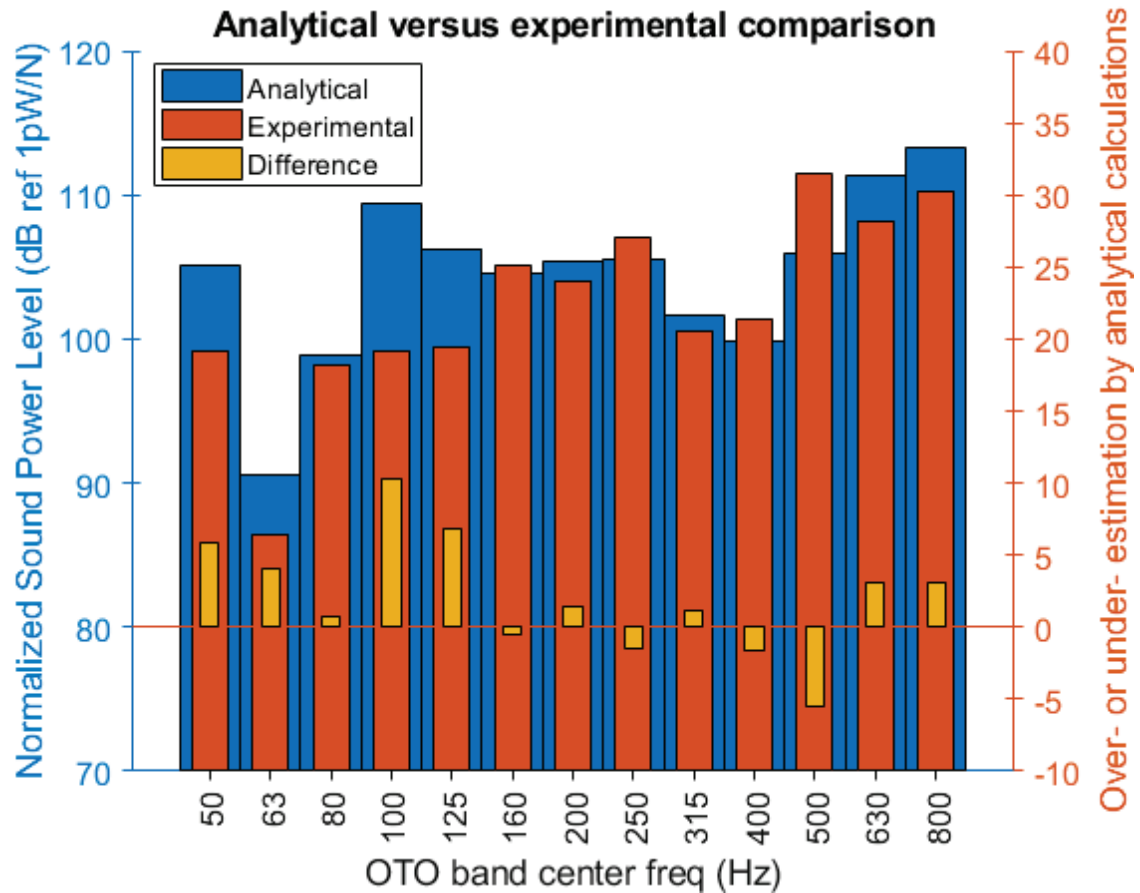


Figure 3-43 Comparison of analytical and experimental sound power radiation. Note that OTO bands 160 Hz to 400 Hz are expected to be more accurate than outlying OTO bands

3.5 Testing a new, unknown assembly

As a final step for the validation of the proposed method, the approach was used to characterize the room contribution and remove it during post-processing for a new, unknown assembly in the reverberation chamber. Think of this new, unknown assembly as the actual floor/ceiling assembly to be tested in the IIC labs for sound power levels. In this scenario, the existing ABS plastic assembly works as the “reference” calibration assembly.

To show that the proposed comparison method can characterize the true sound power of the new, unknown assembly, it is required to understand what this true sound power is. In this section, we discuss the details of this new, unknown assembly, anechoic chamber testing to obtain reference sound power levels, testing in the reverberation chamber, and calculations and final remarks.

3.5.1 Details of the new assembly

To keep things simple, a rectangular plate cut out of 0.13 in (3.3 mm) hardboard was used as the new, unknown assembly. The length and breadth of this hardboard were same as the existing ABS assembly (30 in X 19 in, or, 762 mm X 482.6 mm) so that both of these excite similar acoustic room modes. The hardboard plate is shown in Figure 3-44.

3.5.2 True sound power measured in the anechoic chamber

The true sound power of the hardboard plate could either be obtained using analytical calculations or experimental tests. Given the complications of the material properties, making analytical predictions would be difficult. Therefore, the true sound power of the hardboard plate was obtained using experimental tests.

The hardboard plate was mounted with free-free boundary conditions using foam on all four sides and a discrete point intensity test was performed for 28 grids with a grid size of $0.5 \times 0.25 \text{ m}^2$. The base was blocked off with foam to simulate the infinite baffle conditions, as shown in Figure 3-44. The details of transducers and data acquisition parameters are the same as those mentioned in Section 3.4.1, with the exception of the shaker input signal of 0.18 V instead of 0.2 V. The input signal levels were lowered because of the limitations of the bond between the hardboard plate and the shaker.

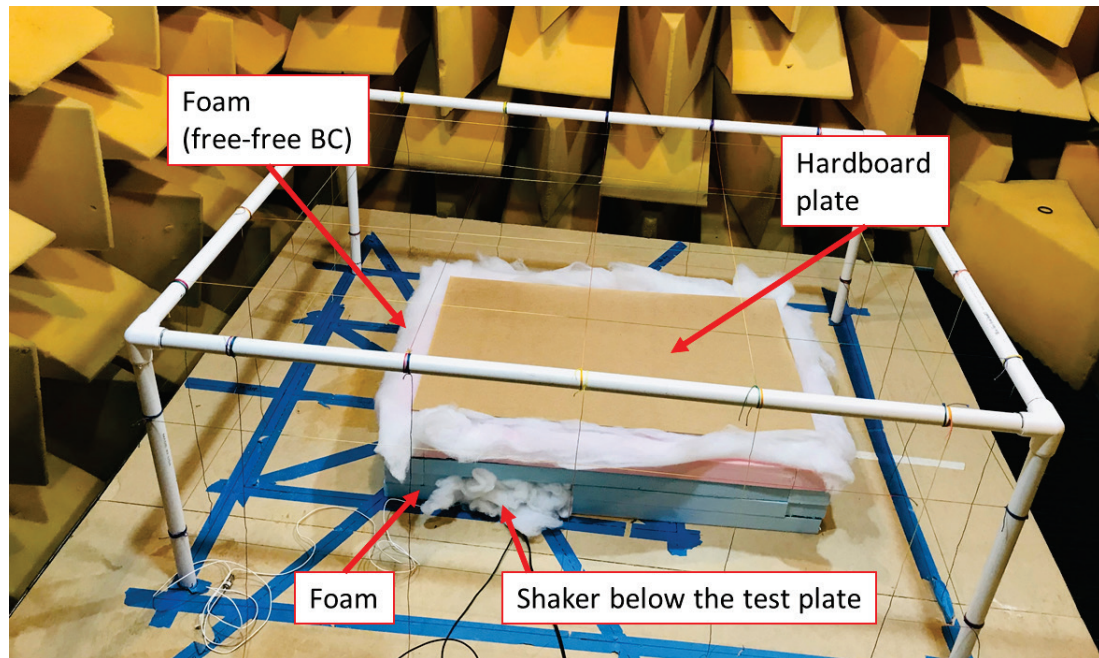


Figure 3-44 Discrete point intensity test for the new assembly. Input shaker is below the structure, cannot be seen in the picture

3.5.3 Testing the assemblies in the reverberation chamber

The ABS assembly, or, the reference calibration source was tested in the reverberation chamber with two random incidence microphones kept at different locations in the room (highlighted with red), shown in Figure 3-45. The model numbers of these two microphones are PCB 378B20 SN 118672, and PCB 378B20 118673. The data acquisition parameters are the same as those mentioned in Table 3-4, with the exception of a 0.18V shaker input signal, instead of 0.2V, and a random noise signal, instead of burst random.

The ABS assembly was then replaced with the hardboard assembly (or, the floor/ceiling assembly for IIC tests) and the same experiment was repeated, without changing the microphone locations in the room.

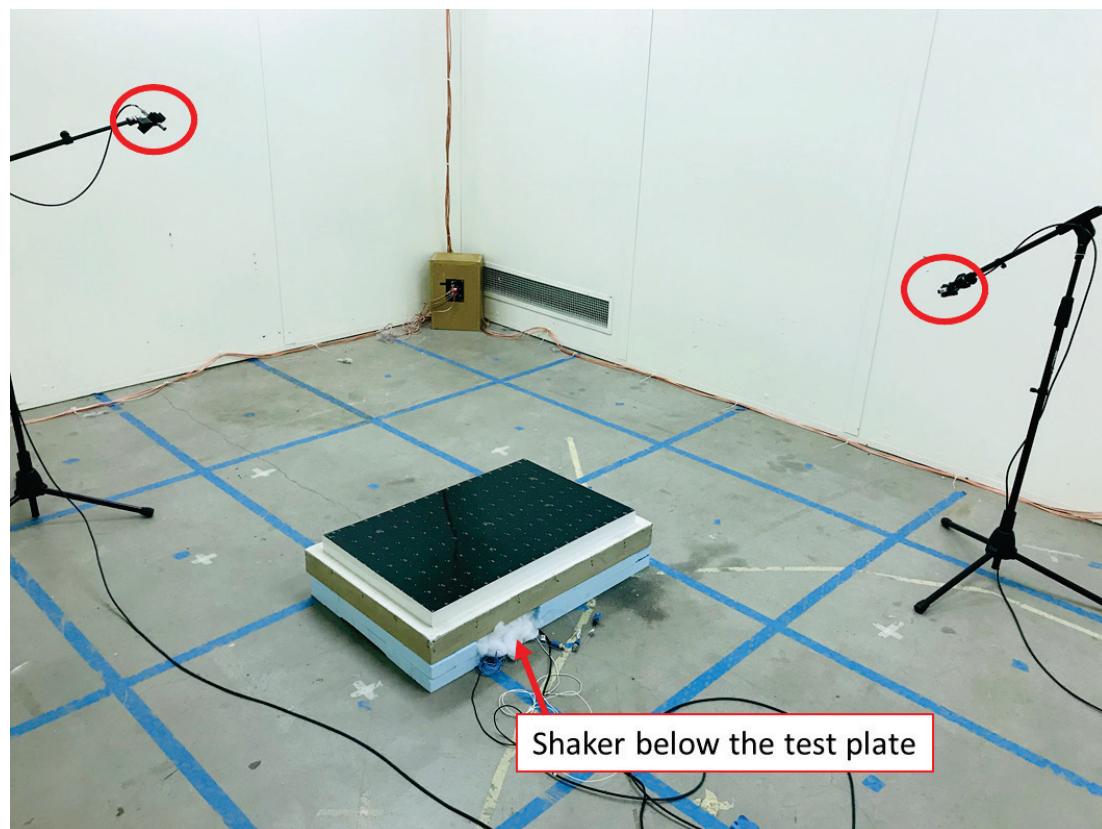


Figure 3-45 Test of ABS assembly in the reverberation room. Input shaker is below the structure, cannot be seen in the picture

3.5.4 Calculations and final remarks

Recall Section 3.4.2, FRFs are used for all the calculations in this section, instead of the measured response. Also, recall Section 2.2 for the calculations of the “Calibration Factor” (CF) used to characterize the room contribution.

The analytical predictions and experimental results for the existing ABS plate were used to calculate two sets of CFs, per Equation 2-2 (Analytical CF, or, AN CF, and Experimental CF, or EX CF). The sound pressure level response of the new hardboard assembly was then converted to sound power using these two sets of CFs, per Equation 2-2.

Figure 3-46 shows the comparison of the processed sound power (using analytical and experimental CF) and the true sound power as measured independently in the anechoic chamber. The low-frequency bands (below 80 Hz) are not presented as they are outside the measurement range of the anechoic chamber used in this test.

For the analytical CF (AN CF), the proposed method works reasonably well for all OTO bands over 125 Hz, and the error is limited to about ± 5 dB, with the only exception of 800 Hz OTO band. The quality of comparison is improved when using the experimental CF (EX CF). The error for 160 – 400 Hz bands is limited to 1-2 dB and for 500 – 800 Hz, the error is limited to 5 dB. Higher error reported for high-frequency OTO bands is due to the limitation of the size of the measurement grid, as discussed in Section 3.4.3.2.

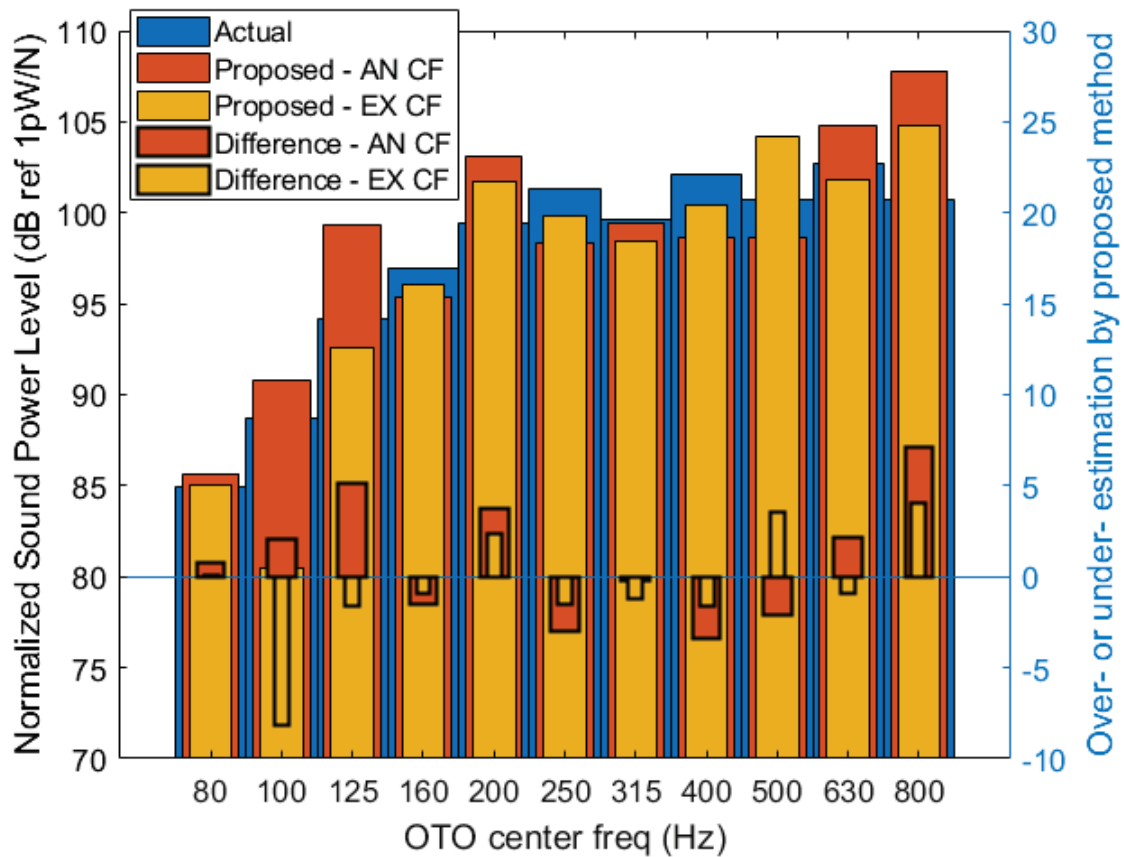


Figure 3-46 Comparison of the proposed method with the actual sound power of the test assembly

Another reason for the differences is the error related to the imperfect mounting of the shaker to the test plate. Since the reference ABS assembly is heavy, it was difficult to control the shaker mounting location and the stinger angle for the tests. A test was performed on two separate days by removing the shaker at the end of the first day and putting it back on the assembly before the second test and the measured SPL values are shown in Figure 3-47. There are some considerable differences in the SPL values between the two tests. By controlling the shaker mount and stinger angle, we expect a better correlation between the results.

In general, the EX CF method gets closer to the true sound power, as compared to the AN CF method.

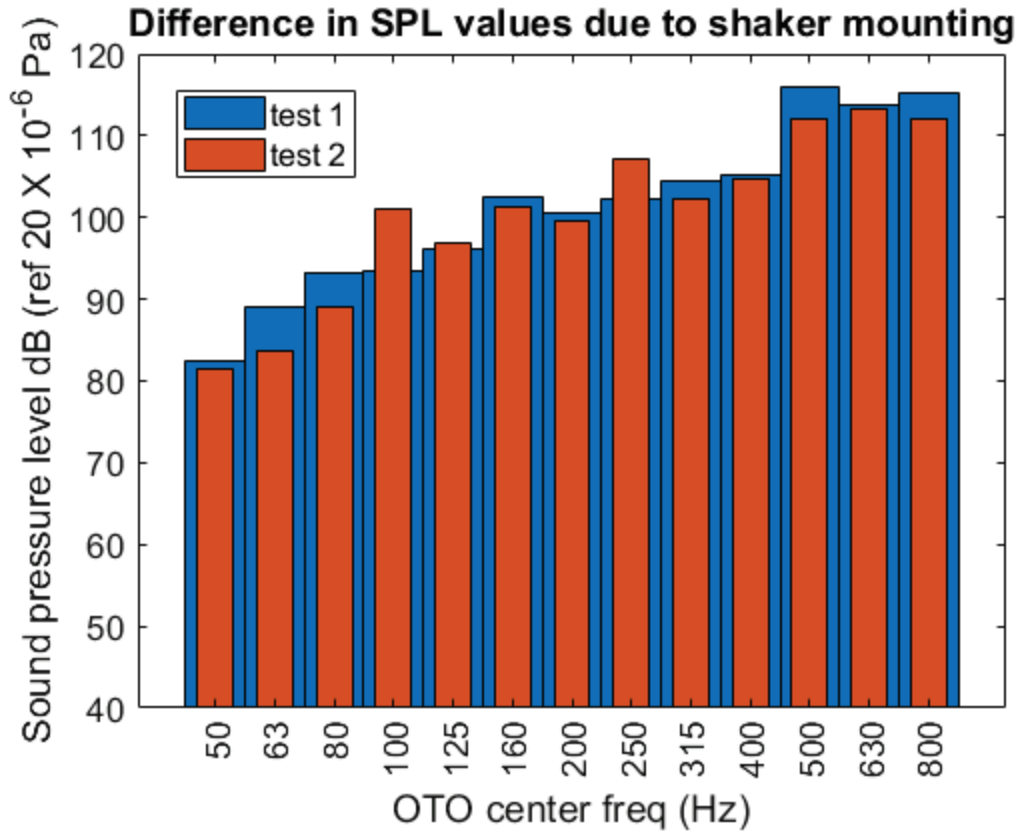


Figure 3-47 Difference in results due to imperfect shaker mounting

4 Guidelines to implement the proposed method

In general, the proposed comparison method works well to characterize the true sound power of the source in the reverberation chamber. This chapter presents a step-by-step procedure to be followed by the IIC test labs to implement the proposed method with minimum efforts and/or investment for testing floor/ceiling assemblies.

As a reminder from Section 2.2, a “calibration source” with known sound power is used to calculate the room contribution on the data. There are two ways to obtain this “known” sound power for any given material: Analytical predictions versus experimental measurements. In this section, we discuss these two methods and go over a step – by – step guide of obtaining the calibration factor of the room and using this to obtain an improved sound power based method to characterize floor/ceiling assemblies. We also discuss the importance of modal density of the reference assembly and computing the IIC rating with sound power values.

4.1 Analytical method

Any homogeneous, isotropic material could be cut to the size of the aperture in the test room, mounted with the simply supported boundary conditions using the method suggested by Olivier et al [17] or this report, and the equations mentioned in Section 2.2 could be used to analytically predict the sound power radiation from the calibration source. Once the analytical sound power radiation is predicted, use these values to follow the step – by – step guide mentioned in Section 4.4.

4.2 Experimental method

For the experimental method track, any material of the same overall size as the floor/ceiling assembly could be used as a calibration source. This gets rid of the requirement of a homogeneous, isotropic material. This means that the test labs could make their own reference structures based on the available resources, regardless of any joints or any other design complications. This method is, therefore, a more cost-effective solution, as compared to the homogenous, isotropic assembly used for analytical predictions.

This (potentially) complicated and cost-effective structure could be tested for its sound power using standard measurement methods and tapping machine as the input source. Some examples are, sound power using intensity test in an anechoic chamber (built for lower frequencies), sound power in an anechoic chamber using microphone array and hemi-anechoic method, sound power using signal separation techniques in reverberation chambers, etc. These may be expensive but if done once for any assembly, the sound power level values can be used as long as the structure and the boundary conditions are

unchanged. Once these sound power level values are obtained, follow the step – by – step guide mentioned in Section 4.4.

4.3 Importance of modal density of the reference assembly

An important consideration while choosing the reference assembly is the structural modal density in the frequency OTO bands under study. In order to make a reliable SPL measurement in the testing chamber, the structure should have sufficient sound radiation above the noise floor. A structure has high sound radiation when it is undergoing resonance. Therefore, it is important to ensure that the reference assembly is modally dense in the frequency bands under consideration, so that enough sound is radiated in the IIC testing room.

For the analytical track, a calculation is done for an Aluminum plate with SS boundary conditions using [12]

$$\omega_{mn} = \sqrt{\frac{D}{\rho h} \left[\left(\frac{m\pi}{l} \right)^2 + \left(\frac{n\pi}{b} \right)^2 \right]} \quad (4-1)$$

The plate with dimensions 12.5 ft. X 10 ft. X 0.03 ft. (3.81 m X 3.05m X 0.009 m) is used as reference and the first natural frequency comes out as approximately 5 Hz. For some of the low-frequency OTO bands important for the study of the performance of floor/ ceiling assemblies, the number of modes are represented in Table 4-1. This sized Aluminum panel is modally dense for OTO bands as low as 50 Hz as it fulfills the requirement of a minimum of three modes in the OTO band under consideration.

Table 4-1 Number of modes in OTO bands ranging from 40 Hz to 125 Hz for a 12.5 ft. X 10 ft. X 0.03 ft. Aluminum panel with SS boundary conditions

OTO band (Hz)	Number of modes
40	2
50	3
63	4
80	6
100	6
125	8

For the experimental track, the labs should use the tapping machine to generate an input force in the reference assembly and mount some accelerometers to look at the modal response in the OTO bands under consideration. If the test assembly has a minimum of three modes in any OTO band, it fulfills the modally dense requirement and thus, can be used as a reference assembly for the proposed method.

4.4 Common procedure – regardless of the basis of the method

Once the sound power level values of a calibration sample are known, use the following step – by – step guide to obtaining a repeatable and reproducible test method for IIC tests.

1. Mount the calibration assembly with controlled boundary conditions in the aperture available in IIC test chambers, instead of the floor/ceiling assembly.
2. Use the tapping machine to give an input force to the calibration assembly, in-keeping with the ASTM test standards [4], thus getting rid of the difference in force input location issue highlighted in Figure 3-47.
3. Measure the response by averaging data using multiple stationary microphones or a single microphone on a rotating boom.
4. Compare the measured sound pressure levels to the analytically calculated or experimentally measured sound power levels and obtain the calibration factor using Equation 2-2.
5. Replace the calibration assembly with the actual assembly without changing the microphone(s) location(s).
6. Use the tapping machine to generate input force and measure the sound pressure level response.
7. Use the calibration factor to obtain sound power levels for the floor/ceiling assembly.

This sound power level response would be repeatable and reproducible, provided that the microphone(s) is used at the same location(s) as for the calibration step and the room has not changed since the calibration (for example, addition or removal of any objects in the room may affect the absorption or reflection of sound). Every lab would have a different set of calibration factors for different microphone locations but by controlling these locations, the reproducibility of the IIC results could be improved for these labs.

4.5 Computing IIC rating with sound power

The reference contour used for calculating the IIC rating (Figure 2-1) is for the sound pressure level measurements, not sound power. The reference contours for sound power level measurements should be developed in collaboration with the ASTM committee members, IIC test labs, and floor/ceiling industry professionals. This needs some future work but it is easy to incorporate this method for low-frequency bands.

It is interesting to note that this reference contour is essentially a straight line for OTO bands ranging from 100 Hz to 315 Hz. For these low-frequency bands, an overall sound power can be calculated by linearly adding the sound power level response and this overall response dictates the performance of the floor/ceiling assembly. A high overall sound power level means that the assembly would not perform well, and vice versa.

5 Conclusions and future scope

The proposed comparison technique based method is able to characterize, and remove the effects of non-diffuse acoustic room contribution in non-diffuse low-frequency one-third octave bands using a reference calibration assembly and controlling the receiver (microphone) location. This can be done for various labs that test the floor/ceiling assemblies to obtain a reproducible test method to characterize the floor/ceiling assemblies. Through this report, we propose two ways of improving the reproducibility issues with the IIC test method: measure sound power instead of sound pressure, since it is a property of the source and not the path (the room), and use a reference assembly to obtain a reliable sound power measurement of the test assembly in non-diffuse field.

Sound pressure levels recorded using the microphone(s) have the path content and therefore, using these values to rank-order different floor/ceiling assemblies would give biased results. Hence, the need is to shift from a source-path based quantity to a source based quantity, such as sound power. With sound power measurements of different assemblies, we can obtain a true characteristic of the assembly itself and not the measurement room and we can use this information to rank-order different assemblies. With the existing measurement method, it is impossible to obtain sound power data from sound pressure levels measured by the microphones but the proposed method makes this switch using a reference assembly, even for non-diffuse fields.

Another advantage of the proposed method is that it is no longer required to calculate the absorption of the room since the calibration values are directly calculated for a microphone location. This gets rid of the disadvantages of using the time decay method to measure sound absorption and the differences in the location of test speakers and actual assembly in the testing room.

The proposed method gets rid of some of the major limitations associated with the measurement process defined in the ASTM standard [3], as highlighted in Section 1.2. This method should, therefore, be included as a part of the standard, as an improvement. In addition to the IIC test standard, all the other ASTM test standards that measure sound in non-diffuse fields are positively affected by the proposed method, such as ASTM E90 [18], E336 [19], and C423 [20].

The move from sound pressure based measurements to sound power based measurements for the ASTM standards requires development of a new reference contour for the OTO bands under consideration. This needs efforts from the members of the ASTM E33 committee on Building and Environmental Acoustics. Testing labs would be required to test a range of floor/ceiling assemblies with the proposed method to develop a database and some statistical methods should be applied to define the reference contour that would be used for sound power based measurements.

6 Reference List

- [1] F. Ljunggren, C. Simmons, and K. Hagberg, "Correlation between sound insulation and occupants' perception—Proposal of alternative single number rating of impact sound," *Applied Acoustics*, vol. 85, pp. 57-68, 2014.
- [2] W. E. Blazier Jr and R. B. DuPree, "Investigation of low-frequency footfall noise in wood-frame, multifamily building construction," *The Journal of the Acoustical Society of America*, vol. 96, no. 3, pp. 1521-1532, 1994.
- [3] *E989-06 Standard Classification for Determination of Impact Insulation Class (IIC)*, 2012.
- [4] *E492-09 Standard Test Method for Laboratory Measurement of Impact Sound Transmission Through Floor-Ceiling Assemblies Using the Tapping Machine*, 2016.
- [5] T. Mariner and H. Hehmann, "Impact-Noise Rating of Various Floors," *The Journal of the Acoustical Society of America*, vol. 41, no. 1, pp. 206-214, 1967.
- [6] J. R. Nordstedt, "Comparison between different methods for impact testing of floors," *The Journal of the Acoustical Society of America*, vol. 65, no. 2, pp. 418-424, 1979.
- [7] D. Olynyk and T. Northwood, "Subjective Judgments of Footstep-Noise Transmission through Floors," *The Journal of the Acoustical Society of America*, vol. 38, no. 6, pp. 1035-1039, 1965.
- [8] R. Öqvist, F. Ljunggren, and R. Johnsson, "Walking sound annoyance vs. impact sound insulation from 20 Hz," *Applied Acoustics*, vol. 135, pp. 1-7, 2018.
- [9] J. J. LoVerde and D. W. Dong, "A dual-rating method for evaluating impact noise isolation of floor-ceiling assemblies," *The Journal of the Acoustical Society of America*, vol. 141, no. 1, pp. 428-440, 2017.
- [10] A. Barnard, S. Girdhar, M. Penhale, and C. Widder, "Evaluation of Receiving Room Diffusivity and the Effect on Low Frequency Impact Insulation Class," *INTER-NOISE and NOISE-CON Congress and Conference Proceedings*, vol. 258, no. 2, pp. 5695-5706, // 2018.
- [11] *JI400 - Laboratory Measurement of the Airborne Sound Barrier Performance of Flat Materials and Assemblies*, 2010.

- [12] S. A. Hambric, S. H. Sung, and D. J. Nefske, *Engineering Vibroacoustic Analysis: Methods and Applications*. John Wiley & Sons, 2016.
- [13] C. Wallace, "Radiation resistance of a rectangular panel," *The Journal of the Acoustical Society of America*, vol. 51, no. 3B, pp. 946-952, 1972.
- [14] G. Squicciarini, D. Thompson, and R. Corradi, "The effect of different combinations of boundary conditions on the average radiation efficiency of rectangular plates," *Journal of Sound and Vibration*, vol. 333, no. 17, pp. 3931-3948, 2014.
- [15] F. J. Fahy and P. Gardonio, *Sound and structural vibration: radiation, transmission and response*. Elsevier, 2007.
- [16] F. J. Fahy, "Measurement of acoustic intensity using the cross-spectral density of two microphone signals," *The Journal of the Acoustical Society of America*, vol. 62, no. 4, pp. 1057-1059, 1977.
- [17] O. Robin, J.-D. Chazot, R. Boulandet, M. Michau, A. Berry, and N. Atalla, "A plane and thin panel with representative simply supported boundary conditions for laboratory vibroacoustic tests," *Acta Acustica united with Acustica*, vol. 102, no. 1, pp. 170-182, 2016.
- [18] *E90-09 Standard Test Method for Laboratory Measurement of Airborne Sound Transmission Loss of Building Partitions and Elements*, 2016.
- [19] *E336-17 Standard Test Method for Measurement of Airborne Sound Attenuation between Rooms in Buildings*.
- [20] *C423-17 Standard Test Method for Sound Absorption and Sound Absorption Coefficients by the Reverberation Room Method*.
- [21] *9614-1 Acoustics—Determination of sound power levels of noise sources using sound intensity: Part 1*, 1993.

A Measurement uncertainty

The measurement uncertainty related with the sound intensity test as explained in 3.4.1 is characterized using three field indicators defined in the ISO 9614 – 1 [21] standard (F2, F3, and F4) for three different grades: precision, engineering, and survey. The calculations and comparison for these indicators are discussed in this appendix section.

A.1 Surface pressure-intensity indicator (F2)

The surface pressure-intensity indicator (F2) should be less than the dynamic capability index (L_d) for the measurement grid to qualify for sound power measurement using intensity values. This dynamic capability index is calculated using the bias error (based on precision, engineering, or survey grade) subtracted from the pressure-residual index of the intensity probe. F2 indicator is calculated using the averaged surface pressure and averaged unsigned intensity values for each OTO frequency band. Figure A-1 shows a comparison of F2 indicator with precision grade dynamic capability index and the requirement for F2 indicator is met.

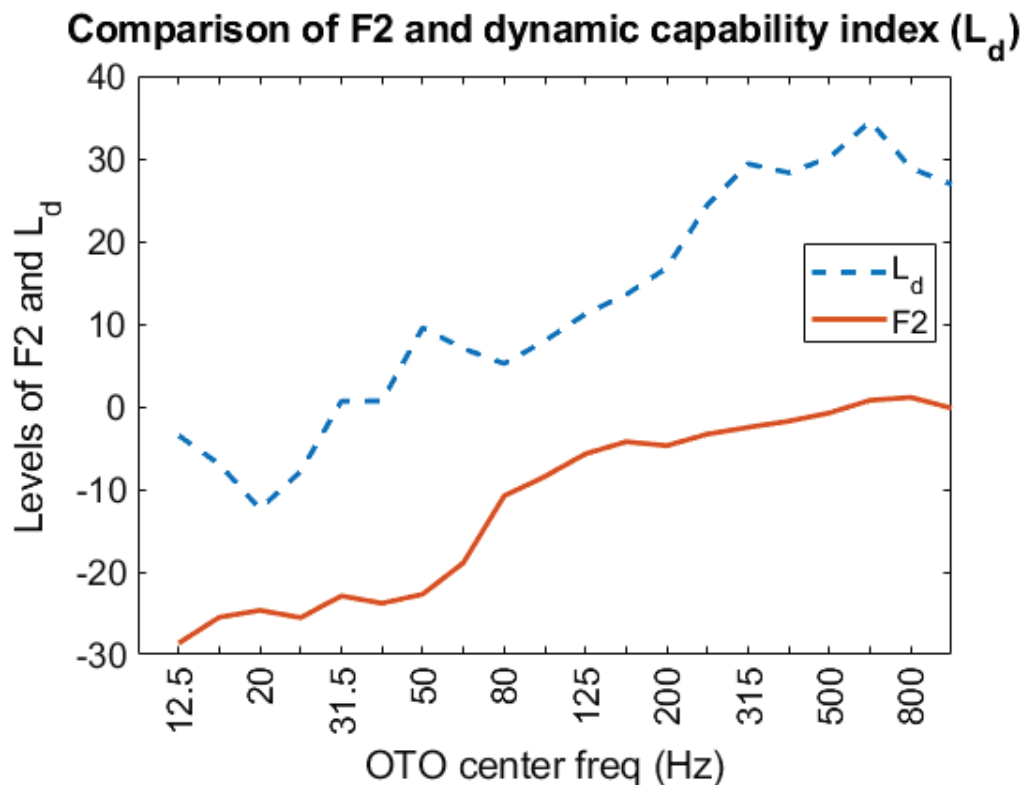


Figure A-1 F2 field indicator is lesser than the dynamic capability index (L_d)

A.2 Negative partial power indicator (F3)

Similar to the F2 indicator, the negative partial power indicator (F3) should be less than the dynamic capability index for the OTO bands under study for the measurement grid to qualify for sound power measurements using intensity method and Figure A-2 proves this condition to be true when compared with precision grade dynamic capability index. F3 indicator is calculated using the averaged surface pressure and averaged signed intensity values for each OTO frequency band.

In addition to this, the ISO standards also uses the difference between F3 and F2 to check the effect of extraneous noise on the measured values. If $F3 - F2 > 3$ dB, it may indicate a presence of a strongly directional extraneous noise source affecting the test measurements. This difference is represented in Figure A-3 as the difference between F3 and F2 values is less than 3 dB for OTO bands higher than 100 Hz. This again shows that the anechoic chamber used to perform the intensity test is not able to block extraneous noise for frequencies below 100 Hz.

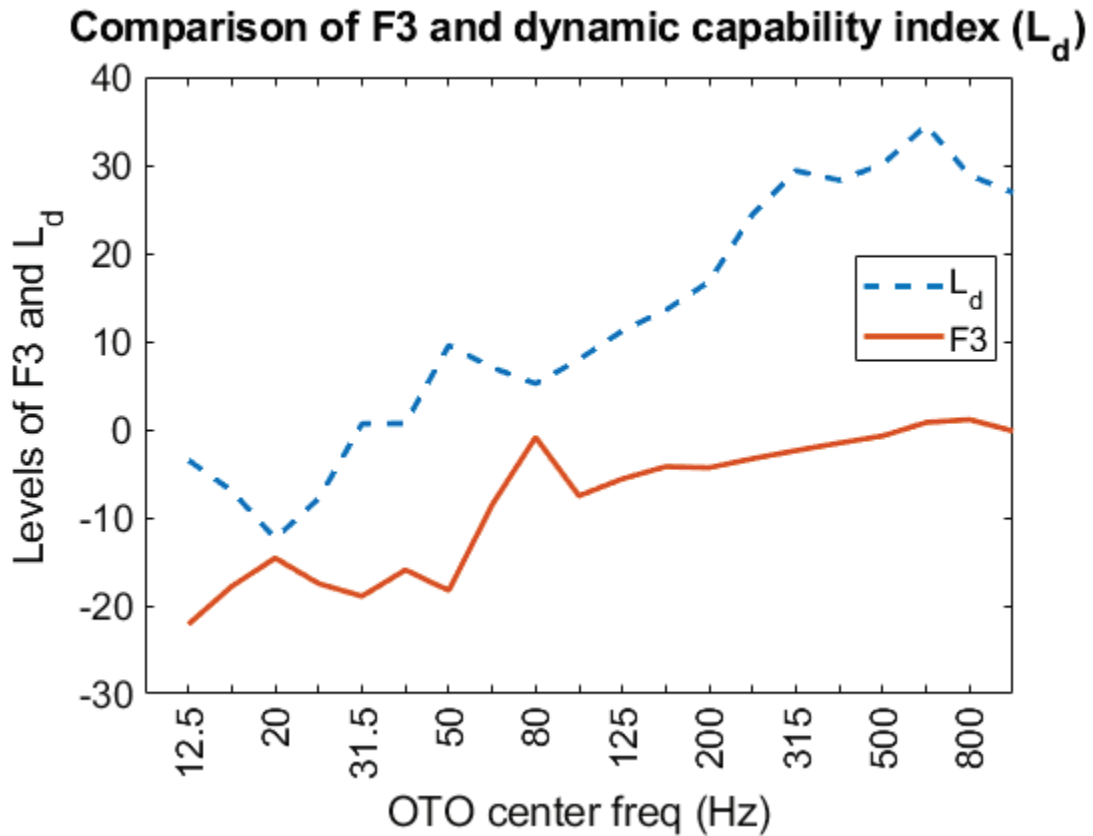


Figure A-2 F3 field indicator compared with dynamic capability index (L_d) for all OTO bands under consideration

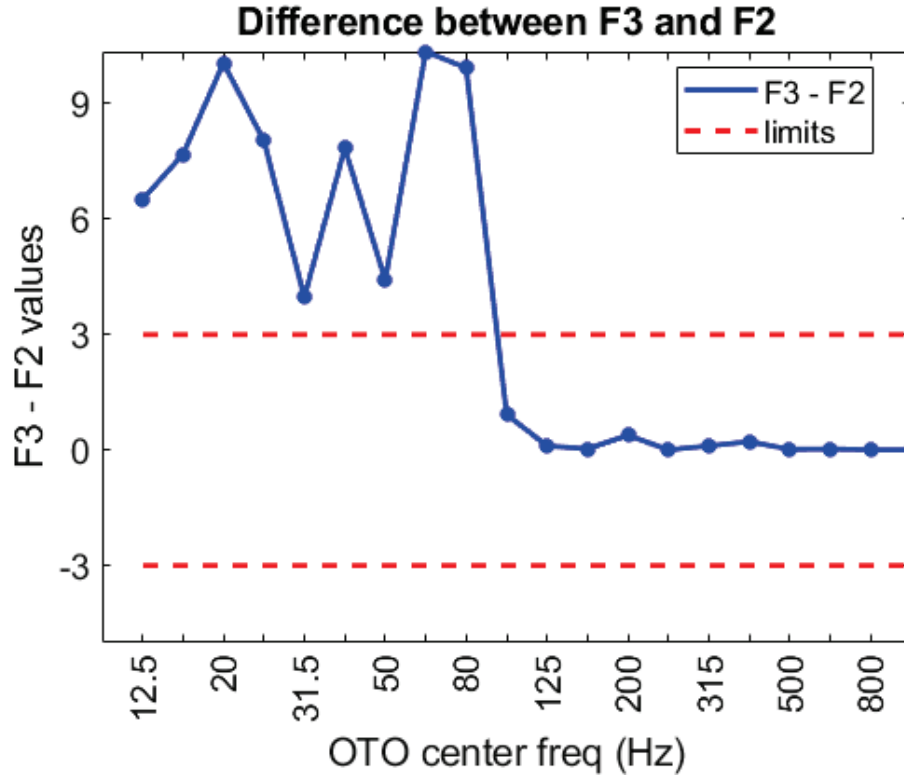


Figure A-3 F3-F2 less than 3dB for OTO bands higher than 100 Hz

A.3 Field non-uniformity indicator (F4)

The field non-uniformity indicator (F4) checks whether the measurement array chosen is adequate for to calculate sound power for the given source within the allowable uncertainty or not. The indicator uses the intensity values measured at each measurement location and compares this with the overall averaged intensity values in each measurement OTO band. This is used to characterize non-uniformity in the sound radiated by the test structure. For the intensity test to give reliable values, the value of constant “C”, given by the number of measurement locations divided by the square of F4 indicator (refer [21]) should be higher than the standard deviation grade required (precision grade, engineering grade, or survey grade). It can be observed from Figure A-4 that this value of constant “C” is greater than the precision grade for all OTO bands higher than 31.5 Hz, other than 800 Hz, where the value is higher than the engineering grade. This shows that the measurement grid used for the intensity test is adequate, according to the ISO standard requirements.

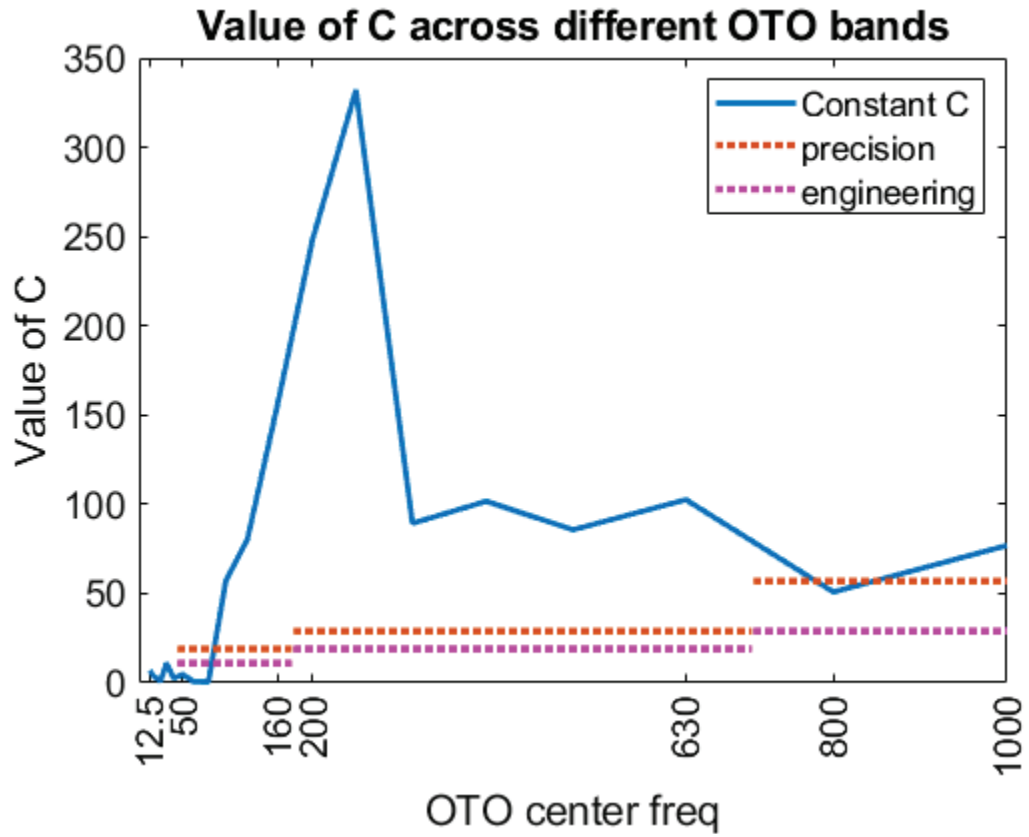


Figure A-4 Value of factor C calculated using F4 field indicator compared with standard deviation grades

B Copyright documentation

B.1 Copyright permission for re-use of Figure 1-2

3/4/2019

Michigan Technological University Mail - Tapping Machine Photos



Sunit Girdhar [REDACTED]

Tapping Machine Photos

3 messages

Paul Jansen [REDACTED]
To: [REDACTED]
Cc: Carey Widder [REDACTED]

Mon, Feb 4, 2019 at 10:18 AM

Sunit,

Please find a selection of tapping machine photos attached via zip folder.

Media usage authorized exclusively for Sunit Girdhar by Carey Widder.

[REDACTED]

Regards,

Paul Jansen

[REDACTED]
[REDACTED]
[REDACTED]
[REDACTED]
[REDACTED]
[REDACTED]
[REDACTED]
[REDACTED]

Tapper Photos.zip
9385K

[REDACTED] [REDACTED]
[REDACTED]
[REDACTED]

[REDACTED] 1/2

3/4/2019

Michigan Technological University Mail - Tapping Machine Photos

[REDACTED]
[REDACTED]
[REDACTED]

Carey Widder [REDACTED]
To: Sunit Girdhar [REDACTED]
Cc: Paul Jansen [REDACTED]

Mon, Feb 4, 2019 at 1:04 PM

Confirmed. Thanks to Paul. [REDACTED]
[REDACTED]

B.2 Copyright permission for Figure 1-3

3/8/2019 RightsLink Printable License

1/4

ASTM INTERNATIONAL LICENSE TERMS AND CONDITIONS

Mar 08, 2019

This Agreement between Michigan Technological University -- Sunit Girdhar ("You") and

ASTM International ("ASTM International") consists of your license details and the terms

and conditions provided by ASTM International and Copyright Clearance Center.

License Number 4544330296084

License date Mar 08, 2019

Licensed Content

Publisher

ASTM International

Licensed Content

Publication

ASTM Standard

Licensed Content Title ASTM E492-09(2016)e1 Standard Test Method for Laboratory Measurement of Impact Sound Transmission Through Floor-Ceiling Assemblies Using the Tapping Machine

Licensed Content Date Apr 1, 2016

Type of Use Thesis/Dissertation

Requestor type Academic institution

Format Electronic

Portion image/photo

Number of images/photos requested

1

Rights for Main product

Duration of use Life of current edition

Creation of copies for the

disabled

no
With minor editing
privileges
no
For distribution to Worldwide
In the following
language(s)
Original language of publication
With incidental
promotional use
no
The lifetime unit quantity
of new product
0 to 499
Order reference number N/A
Title Improved low-frequency Impact Insulation Class measurements using
comparison techniques
Institution name Michigan Technological University
Expected presentation
date
Apr 2019
Order reference number N/A
Portions Figure 1 (Tapping machine position on a floor with structural members)
Requestor Location Michigan Technological University
3/8/2019 RightsLink Printable License
2/4
1400 Townsend Dr
HOUGHTON, MI 49931
United States
Attn: Michigan Technological University
Billing Type Invoice
Billing Address Michigan Technological University
1400 Townsend Dr
HOUGHTON, MI 49931
United States
Attn: Michigan Technological University
Total 0.00 USD
Terms and Conditions

Permissions Terms & Conditions

Introduction

The publisher for this copyrighted material is ASTM International ("ASTM"). By clicking "accept" in connection with completing this licensing transaction, you ("Licensee") agree that the following terms and conditions apply to this transaction (along with the Billing and Payment terms and conditions established by Copyright Clearance Center, Inc. ("CCC"), at the time that Licensee opened your CCC account.

Limited License:

ASTM hereby grants to Licensee a non-exclusive license to use this material. Licenses are

for one-time use only with a maximum distribution equal to the number that Licensee identified in the licensing process. No emailing of ASTM documents is permitted.

Licenses

are for reproduction rights only and do not include a copy of the material.

It is the Licensee's responsibility to ensure that the material is original to ASTM's and does

not contain the proprietary rights of another person or entity.

Altering/Modifying Material: Not Permitted

Licensee may not alter or modify the material in any manner. Licensee may not translate the

material into another language.

Reservation of Rights:

ASTM reserves all rights not specifically granted in the combination of (i) the license details

provided by Licensee and accepted in the course of this licensing transaction, (ii) these terms

and conditions and (iii) CCC's Billing and Payment terms and conditions.

License Contingent on Payment:

While Licensee may exercise the rights licensed immediately upon issuance of the license at

the end of the licensing process for the transaction, provided that Licensee have disclosed complete and accurate details of your proposed use, no license is finally effective unless and

until full payment is received from Licensee (either by ASTM or by CCC) as provided in CCC's Billing and Payment terms and conditions. If full payment is not received on a timely

basis, then any license preliminarily granted shall be deemed automatically revoked and shall be void as if never granted. Further, in the event that Licensee breach any of these terms and conditions or any of CCC's Billing and Payment terms and conditions, the license

is automatically revoked and shall be void as if never granted. Use of materials as described

in a revoked license, as well as any use of the materials beyond the scope of an unrevoked

license, may constitute copyright infringement and ASTM reserves the right to take any and

all action to protect its copyright in the materials.

Copyright Notice:

Licensee must include the following copyright and permission notice in connection with any

reproduction of the licensed material: "Reproduced, with permission from [FULL

3/8/2019 RightsLink Printable License

3/4

CITATION], copyright ASTM International, 100 Barr Harbor Drive, West Conshohocken, PA 19428."

Disclaimer of Warranty:

Unless specified in this license, all express or implied conditions, representations and warranties, including any implied warranty of merchantability, fitness for a particular purpose or non-infringement are disclaimed, except to the extent that these disclaimers are held to be legally invalid.

Verification:

ASTM has the right to verify compliance with this license, at its expense, and at any time during the course of normal business hours. To do so, ASTM will engage an independent consultant, subject to a confidentiality agreement, to review your use of ASTM's material.

Licensee agrees to permit access to its information and computer systems for this purpose.

Verification will take place upon no less than 15 days notice, during normal business hours

and in a manner that does not interfere unreasonably with Licensee's operations. If verification reveals unlicensed or prohibited use of the ASTM material, Licensee agrees to

reimburse ASTM for the costs incurred in verification and reimburse ASTM for any unlicensed/prohibited uses. By invoking this procedure, ASTM does not waive any of its rights to enforce this Agreement or to protect its intellectual property by any other means permitted by law.

Limitation of Liability:

To the extent not prohibited by law, in no event will ASTM and CCC be liable for any loss, damage, lost data or for special, indirect, consequential or punitive damages, however caused regardless of the theory of liability, arising out of or related to the use of ASTM material. In no event will ASTM's and CCC's liability exceed the amount paid by Licensee under this License Agreement.

No Transfer of License:

This license is personal to you and may not be sublicensed, assigned, or transferred by you to any other person without publisher's written permission.

Governing Law, Venue, and Jurisdiction:

This license shall be interpreted and construed in accordance with the laws of the Commonwealth of Pennsylvania. Licensee agrees to submit to jurisdiction and venue in the

state and federal courts of Pennsylvania for any dispute which may arise under this license.

Licensee also agrees to waive any claim of immunity it may possess.

Integration

ASTM hereby objects to any terms contained in any purchase order, acknowledgment, check

endorsement or other writing prepared by Licensee, which terms are inconsistent with these

terms and conditions or CCC's Billing and Payment terms and conditions. These terms and

conditions, together with CCC's Billing and Payment terms and conditions (which are incorporated herein), comprise the entire agreement between Licensee and ASTM

International (and CCC) concerning this licensing transaction. In the event of any conflict between your obligations established by these terms and conditions and those established by

CCC's Billing and Payment terms and conditions, these terms and conditions shall control.

No modification of this license will be binding, unless in writing and signed by an authorized representative of each party (or, in the case of ASTM, by CCC on ASTM's behalf).

Licensee acknowledges and agrees that the adoption, enactment, reference, or incorporation

of any of the ASTM material by any government or agency has not and will not effect, transfer, modify or alter the ASTM Rights in the ASTM materials in any way.

There are additional terms and conditions, established by Copyright Clearance Center, Inc.

("CCC") as the administrator of this licensing service that relate to billing and payment for

licenses provided through this service. Those terms and conditions apply to each transaction

as if they were restated here. As a user of this service, you agreed to those terms and

3/8/2019 RightsLink Printable License

4/4

conditions at the time that you established your account, and you may see them again at any

time at <http://myaccount.copyright.com>.

Content Services:

Subject to these terms of use, any terms set forth on the particular order, and payment of the

applicable fee, Licensee may make the following uses of the ordered materials:

Content Rental: Licensee may access and view a single electronic copy of the materials ordered for the time period designated at the time the order is placed. Access to the materials

will be provided through a dedicated content viewer or other portal, and access will be discontinued upon expiration of the designated time period. An order for Content Rental does not include any rights to print, download, save, create additional copies, to distribute or

to reuse in any way the full text or parts of the materials.

The materials may be accessed and used only by the person who placed the Order or the person on whose behalf the order was placed and only in accordance with the terms included

in the particular order.

Licensee acknowledges and agrees that the adoption, enactment, reference, or incorporation

of any of the ASTM material by any government or agency has not and will not effect, transfer, modify or alter the ASTM Rights in the ASTM materials in any way.

There are additional terms and conditions, established by Copyright Clearance Center, Inc.

("CCC") as the administrator of this licensing service that relate to billing and payment for

licenses provided through this service. Those terms and conditions apply to each transaction

as if they were restated here. As a user of this service, you agreed to those terms and conditions at the time that you established your account, and you may see them again at any

time at <http://myaccount.copyright.com>.

Other Terms and Conditions:

v1.1

Questions? customercare@copyright.com or +1-855-239-3415 (toll free in the US) or

+1-978-646-2777.

B.3 Copyright permission for re-use of Figure 1-4

3/4/2019

Michigan Technological University Mail - RE: [External]_Picture of a diffuser in the reverb. chamber for my graduate report



Michigan Tech

[Redacted]

RE: [External]_Picture of a diffuser in the reverb. chamber for my graduate report

4 messages

Wolfram, Eric P

To: Sunit Girdhar

Mon, Mar 4, 2019 at 3:01 PM

Hello Sunit,

Attached are some photos of ours. Our labs isn't super photogenic, but I hope these are helpful. The brown convex diffusers are used in the receive room of our floor/ceiling lab.

-Eric Wolfram
Laboratory Manager

Riverbank Acoustical Laboratories™



From: Sunit Girdhar

Sent: Friday, March 01, 2019 3:00 PM

To: Wolfram, Eric P

Subject: [External]_Picture of a diffuser in the reverb. chamber for my graduate report

Hi Eric,

Hope you are doing great!



My graduate project here at Michigan Tech closely relates to the IIC test method and how can we improve repeatability with this method.

for my final report submission, I am including some information about the diffusers we use in the reverberation chambers to create a more diffuse field. I have already written about it but I sincerely feel that a picture would go a long way in addition to the text I have. Would you be able to share a couple of pictures of the diffusers you have in the reverberation room in your lab?



1/4

3/4/2019

Michigan Technological University Mail - RE: [External]_Picture of a diffuser in the reverb. chamber for my graduate report

I would also like to mention that since I will use this picture in my report, I need to show the copyright permissions. I would really appreciate it if you just mentioned in your reply that I have your permission to use these pictures in my report.

Thank you!

Best regards,
Sunit Girdhar

Wolfram, Eric P
To: Sunit Girdhar

Mon, Mar 4, 2019 at 3:02 PM

3/4/2019

Michigan Technological University Mail - RE: [External]_Picture of a diffuser in the reverb. chamber for my graduate report

Sunit,

I took the photos and you have permission to use them for your presentation.

-Eric Wolfram
Laboratory Manager

Riverbank Acoustical Laboratories™



B.4 Copyright permission for re-use of Figure 1-5



Michigan Tech

Sunit Girdhar [REDACTED]

Internoise proceedings reprint permission

5 messages

Sunit Girdhar [REDACTED]

Mon, Apr 8, 2019 at 4:56 PM

To: Andrew Barnard [REDACTED]

[REDACTED]

[REDACTED]

[REDACTED]

[REDACTED]

Andrew Barnard [REDACTED]

Mon, Apr 8, 2019 at 6:03 PM

To: Sunit Girdhar [REDACTED], Gordon Ebbitt [REDACTED]

Gordon,

My student, Sunit, would like to use an InterNoise proceedings figure in his MS thesis. I'm putting him in contact with you for permission. Thanks,

Andrew

[Quoted text hidden]

Sunit Girdhar [REDACTED]

Mon, Apr 8, 2019 at 6:12 PM

To: Gordon Ebbitt [REDACTED]

Cc: Andrew Barnard [REDACTED]

Hi Gordon,

Hope you are doing great!

I wish to re-use Figure 1 from IN 2213 paper presented during Internoise 2018 conference (here's the citation: Barnard, Andrew, et al. "Evaluation of receiving room diffusivity and the effect on low-frequency impact insulation class." *INTER-NOISE and NOISE CON Congress and Conference Proceedings*. Vol. 258. No. 2. Institute of Noise Control Engineering, 2018)

Please give me permission to re-use the figure.

Thank you!

Best,
Sunit

[Quoted text hidden]

Gordon Ebbitt [REDACTED]

Mon, Apr 8, 2019 at 10:24 PM

To: Sunit Girdhar [REDACTED]

Cc: Andrew Barnard [REDACTED]

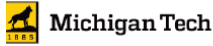
Hi Sunit,

Permission is granted. Good luck with your thesis.

Real regards,
Gordon

Sent from my iPhone

B.5 Copyright permission for re-use of Figure 3-2



Sunit Girdhar [REDACTED]

WG: Reprint Permission Request

2 messages

Badelt, Brigitte [REDACTED]
To: [REDACTED]

Thu, Feb 7, 2019 at 6:04 AM

Dear Mr. Girdhar,

Thank you for your permission request enclosed below. We don't object if you include the named figure in your master graduate project report at Michigan Technological University. Please provide exact reference to the source.

Best regards

Brigitte Badelt

Permissions

[REDACTED]

[REDACTED]

[REDACTED]

[REDACTED]

[REDACTED]

This e-mail is confidential and is intended solely for use by the individual to whom it is addressed. Access to this e-mail by anyone else is unauthorized. If you are not the intended recipient, please notify the sender immediately and delete this e-mail and any copies of it from your computer system. Please be advised that if you have received this mail in error, any use, dissemination, forwarding, printing or copying of it is strictly prohibited.

[REDACTED]
Gesendet: Mittwoch, 6. Februar 2019 04:22

An: Badelt, Brigitte
Betreff: Reprint Permission Request

Title Mr.
First Name Sunit
Last Name Girdhar
E-mail [REDACTED]
Position Graduate Student Assistant

Institute/Company Michigan Technological University

an article tentatively entitled N/A

to be published in N/A

Journal title N/A

Book title N/A

Publisher N/A

Author Robin, O., Chazot, J. D., Boulandet, R., Michau, M., Berry, A., & Atalla, N.

Title A plane and thin panel with representative simply supported boundary conditions for laboratory vibroacoustic tests

Journal Acta Acustica united with Acustica

Vol. 102(1)

Figure(s) / table(s) / text quotation(s) Figure 6. Assembly plan

Page 176

Publisher Acta Acustica united with Acustica

Year of 2016

publication

Remarks I want a part of this figure (not the full figure) for my graduate project report (master's) which would be published by my university sometime this May. Please let me know if you have any additional questions

Captcha ralqk

Privacy Policy Text By submitting this contact form I agree that Hirzel Verlag may use my personal data as given in the input mask for the purpose of getting in contact with me and responding to my enquiry. This permission can be revoked at any time by mail to service@hirzel.de.

Privacy Policy I have read and accept the Publisher's Data Use Privacy Policy.

C MATLAB codes for analytical calculations

C.1 Main body

```
clear; clc;
format compact; format short g

%% Defining the material properties for ABS plastic
% ABS plastic - McMaster-Carr

Lx = convlength(30,'in','m'); % length
Ly = convlength(19,'in','m'); % width
h = convlength(0.125,'in','m'); % thickness

E = convpres(327000, 'psi', 'Pa'); % psi to Pa, Young's modulus
loss = 0.0137; % loss factor, experimental
pois = 0.35; %Poisson's ratio
compE = E*(1+1i*loss);
rho = 1.03*1000; % Density, kg/m3
compD = (compE*h^3)/(12*(1-(pois^2))); % complex bending stiffness
E = compE; D = compD;
clear compE compD

%% Assuming the number of modes to study
mmax = 20; nmax = 20; % 20 X 20 modes to be studied

%% Natural frequency
% Calculating a matrix of natural frequencies
omega = zeros(mmax,nmax);
kmn = zeros(mmax,nmax); %Wavenumber
for ii = 1:mmax % modes in 'm'
    for jj = 1:nmax % modes in 'n'
        omega(ii,jj) = sqrt((D/(rho*h))*(((ii*pi())/Lx)^2 + ...
            ((jj*pi())/Ly)^2));
        kmn(ii,jj) = sqrt(((ii*pi())/Lx)^2 + ((jj*pi())/Ly)^2);
    end
end
clear ii jj
% Sorting the natural frequencies
omega_sort = zeros(size(omega,1)*size(omega,2),4);
omega_sort(:,1) = omega(:); omega_sort(:,4) = kmn(:);
temp = 0;
for ii = 1:nmax
    for jj = 1:mmax
        omega_sort(temp+jj,2) = jj;
        omega_sort(temp+jj,3) = ii;
    end
    temp = temp+jj;
end
wmn_kmn = sortrows(omega_sort);
clear temp ii jj omega_sort omega
```

```

% Frequency in Hz
freq_kmn = real(wmn_kmn); % taking only the real part of natural
frequency
freq_kmn(:,1) = freq_kmn(:,1)/(2*pi); % natural frequencies in Hz
% Modal density in different OTO bands
freq_center = octave_bands(100,5000); % studying 100 Hz to 5000 Hz OTO
modal_den = zeros(18,2);
modal_den(:,1) = freq_center(:,2);
for ii = 1:length(freq_kmn)
    for jj = 1:length(freq_center)
        if(freq_kmn(ii,1)>=freq_center(jj,1)&&...
            (freq_kmn(ii,1)<=freq_center(jj,3))
            modal_den(jj,2) = modal_den(jj,2) + 1;
        end
    end
end
clear ii jj
% Modes in 250 Hz OTO - for mode shapes
temp = zeros(1,1);
band_idx = freq_center(:,2) == 250;
freq_study = freq_center(band_idx,:);
for ii = 1:length(freq_kmn)

if(freq_kmn(ii,1)>=freq_study(1,1)&&(freq_kmn(ii,1)<=freq_study(1,3))
    temp(modal_den,1) = freq_kmn(ii,1);
    temp(modal_den,2) = freq_kmn(ii,2);
    temp(modal_den,3) = freq_kmn(ii,3);
end

end
modes_in_band = temp;
clear ii jj temp band_idx freq_study

%% Mode shapes
x_grid = 19; y_grid = 13; % Number of points in x, and y- direction
% Plot the mode shapes
[mode_s] = mode_shapes(Lx,Ly,modes_in_band,x_grid,y_grid);

%% Mobility
% Matrix of input locations - consider point 1 as (0,0)
x_act = linspace(0,Lx,x_grid); y_act = linspace(0,Ly,y_grid);
[input_X,input_Y] = meshgrid(x_act,y_act);
grid_loc = zeros(x_grid*y_grid,3);
grid_loc(:,1) = 1:x_grid*y_grid;
grid_loc(:,2) = reshape(input_X,[],1);
grid_loc(:,3) = reshape(input_Y,[],1);
clear x_act y_act input_X input_Y
acc_loc = grid_loc([101, 124, 190, 212],:);
delta_f = 0.25; % assumption
bandwidth = 1024; % assumption
freq = (0:delta_f:bandwidth)'; % frequency vector
% Drive point mobility (all 4 response locations)

```

```

drive_mob = zeros(length(freq),size(acc_loc,1)); % initialize the
variable
for ii = 1:size(acc_loc,1)
    [drive_mob(:,ii),mob_inf] = mobility_function(freq, ...
        wmn_kmn,acc_loc(ii,2),acc_loc(ii,3),acc_loc(ii,2), ...
        acc_loc(ii,3),Lx,Ly,h,rho,D);
end
% Surface averaged mobility
surf_mob = zeros(length(freq),length(acc_loc),length(grid_loc));
for ii = 1:size(acc_loc,1)
    for jj = 1:length(grid_loc)
        surf_mob(:,ii,jj) = abs(mobility_function(freq, ...
            wmn_kmn,acc_loc(ii,2),acc_loc(ii,3),grid_loc(jj,2), ...
            grid_loc(jj,3),Lx,Ly,h,rho,D));
    end
end
% Average of the surface mobility
surf_avg_mob = mean(surf_mob,3);

%% Sound power comparison
% Need a new grid with the center of the plate as (0,0)
x_act = linspace(-Lx/2,Lx/2,x_grid); y_act = linspace(-
Ly/2,Ly/2,y_grid);
del_x = x_act(2)-x_act(1);del_y = y_act(2)-y_act(1); % grid spacing
[input_X,input_Y] = meshgrid(x_act,y_act);
grid_loc = zeros(x_grid*y_grid,3); % Making a new grid matrix
grid_loc(:,1) = 1:x_grid*y_grid;
grid_loc(:,2) = reshape(input_X,[],1);
grid_loc(:,3) = reshape(input_Y,[],1);
clear x_act y_act input_X input_Y
% Shaker input at point 100
input_loc(:) = grid_loc(100,:);
[power,power_total,power_an_W] = sound_power(Lx,Ly,wmn_kmn,freq,...
    grid_loc,input_loc,h,rho,D,del_x,del_y);

```

C.2 Function: mode_shapes

```

function [mode_s] = mode_shapes(Lx,Ly,modes_in_band,x_grid,y_grid)
m = modes_in_band(:,2);
n = modes_in_band(:,3);
freq = modes_in_band(:,1);
x = linspace(0,Lx,x_grid); y = linspace(0,Ly,y_grid); % actual meas.
grid
[X,Y] = meshgrid(x,y);
mode_s = zeros(length(y),length(x),length(freq));

for ii = 1:length(freq)
    mode_s(:, :, ii) = sin(m(ii)*pi()*X/Lx).*sin(n(ii)*pi()*Y/Ly);
end
clear ii;
% Figure out how to plot the graphs
temp = length(freq);

```

```

temp2 = mod(temp,2);
if(temp2) == 1
    sub_x = temp + 1;
else
    sub_x = temp;
end

```

C.3 Function: mobility_function

```

function [mob,mob_inf] =
mobility_function(f,wmn_kmn,x0,y0,x,y,l,b,h,rho,D)
modal_mass = ((l*b*h)*rho)/4;
mob_inf = 1/(8*(sqrt(abs(D)*rho*h))); % Infinite plate mobility
mob = zeros(size(f));
w = 2*pi()*.*f;
M = wmn_kmn(:,2); N = wmn_kmn(:,3);
modal_coeff = li/modal_mass.*sin(M*pi()*x0/l).*sin(N*pi()*y0/b).* ...
    sin(M*pi()*x/l).*sin(N*pi()*y/b);
for ii = 1:length(f)
    denom = wmn_kmn(:,1).^2 - w(ii).^2;
    mob(ii) = sum(w(ii).*(modal_coeff./denom));
end

```

C.4 Function: sound_power

```

function [power,power_total_Lw,power_total] =
sound_power(Lx,Ly,wmn_kmn,freq,grid_loc,input_loc,h,rho,D,del_x,del_y)
% Force assumed as one Newton throughout the measurement bandwidth
rho_air = 1.225; % kg/m3, density of air
c_air = 343; % m/s, speed of sound at 20 deg
omega = 2*pi*freq;
k_air = omega./c_air;
% Co-ordinates for a spherical quadrant for calculations
[phi,theta,~,dphi,dtheta] = spherical_meas_grid_meshgrid;
grid_sph = zeros(size(phi,1)*size(phi,2),3);
grid_sph(:,1) = reshape(phi,[],1);
grid_sph(:,2) = reshape(theta,[],1);
grid_sph(:,3) = 10*ones(length(grid_sph),1);
% The top center point is being repeated over and over, so get rid of
that
index = find(grid_sph(:,2) == 0);
index = index(2:end);
grid_sph(index,:) = [];
% Calculate power
power = zeros(length(freq),length(wmn_kmn));
for ii = 1:length(wmn_kmn) % for every mode
    surf_mob = zeros(length(freq),length(grid_loc));
    for jj = 1:length(grid_loc)
        surf_mob(:,jj) = (mobility_function(freq, ...
            wmn_kmn(ii,:),input_loc(1,2),input_loc(1,3),grid_loc(jj,2), ...
            grid_loc(jj,3),Lx,Ly,h,rho,D));
    end
end

```

```

clear jj
temp = conj(surf_mob).*surf_mob; % mobility autopower
temp = sum(temp,2)*del_x*del_y;
u_mean_sq = (4/(Lx*Ly))*temp; % Integration - formula in textbooks
and papers
clear temp
coeff = 8*rho_air*c_air*u_mean_sq.*((k_air.*Lx.*Ly)./...
    (pi()^3*wmn_kmn(ii,2)*wmn_kmn(ii,3))).^2; % 8 because of 1/8 of
a sphere instead of hemisphere
m = wmn_kmn(ii,2); n = wmn_kmn(ii,3);
% Define alpha and beta (with new k_air)
mid = zeros(length(freq),length(grid_sph));
for jj = 1:length(grid_sph)
    alpha =
abs(wmn_kmn(ii,1)/c_air).*Lx*sin(grid_sph(jj,2)).*cos(grid_sph(jj,1));
    beta =
abs(wmn_kmn(ii,1)/c_air).*Ly*sin(grid_sph(jj,2)).*sin(grid_sph(jj,1));
    denom = (((alpha./(m*pi())).^2-1).*((beta./(n*pi())).^2-1));
    if(mod(m,2) == 0 % even number
        mid(:,jj) = (sin(alpha/2));
    else % odd number
        mid(:,jj) = (cos(alpha/2));
    end
    if(mod(n,2) == 0 % even number
        mid(:,jj) = mid(:,jj).*(sin(beta/2));
    else % odd number
        mid(:,jj) = mid(:,jj).*(cos(beta/2));
    end
    mid(:,jj) =
((mid(:,jj)./denom).^2)*sin(grid_sph(jj,2))*dphi*dtheta;
end
power(:,ii) = coeff.*sum(mid,2);
end
clear ii jj
power_total = sum(power,2); % In an infinite rigid baffle
power = 10*log10(power./10^-12);
power_total_Lw = 10*log10(power_total./10^-12);

```